CANCELLOUS BONE ADAPTATION TO NON-INVASIVE MECHANICAL LOADING IN THE MURINE TIBIA

by Maureen Ellen Lynch

CANCELLOUS BONE ADAPTATION TO NON-INVASIVE MECHANICAL LOADING IN THE MURINE TIBIA

A Dissertation

Presented to the Faculty of the Graduate School

of Cornell University

in Partial Fulfillment of the Requirements for the Degree of

Doctor of Philosophy

by

Maureen Ellen Lynch

August 2010

CANCELLOUS BONE ADAPTATION TO NON-INVASIVE MECHANICAL LOADING IN THE MURINE TIBIA

Maureen Ellen Lynch, Ph.D.

Cornell University 2010

Osteoporosis causes over 2 million skeletal fractures every year in people 50 years of age or older. Fractures predominantly happen at corticocancellous sites, such as the hip and spine. Due to lower accrual of bone mass during growth and rapid bone loss following menopause, 71% of these fractures occur in women. Mechanical loading, which stimulates bone formation, is a potential anabolic therapy for pathological bone loss. Determining the parameters of mechanical loading that stimulate osteogenesis in cancellous bone is critical for harnessing the therapeutic potential of mechanical stimuli. In this thesis, the effects of sex, aging, and estrogen deficiency on the adaptive response of cancellous bone were examined using in vivo tibial compression applied to mice.

The effect of sex on the cancellous adaptive response to tibial loading was investigated in growing mice. The magnitude of peak applied loads that corresponded to +1200 με at the tibial mid-shaft was determined to be -11.5 N in both males and females from in vivo strain gauging. This peak load resulted in similar peak cancellous tissue strains of ~-2400 με in females and ~-2100 με. Following 2 weeks of tibial compression, male and female mice increased cancellous bone mass 73% in the proximal tibia, primarily through increased trabecular thickening (+75%). Tissue mineral density increased 18% and trabecular separation decreased 19% as well. As a result of adaptation, the proportion of the applied load carried by the cancellous compartment, rather than by the cortical shell, increased. In addition, the metaphyseal

stiffness of the loaded limbs was greater than in control limbs. None of these loading-induced changes differed by sex.

Next, the effect of aging on the cancellous adaptive response was investigated in adult, osteopenic female mice, and this response was compared to that observed previously in growing mice. We applied the same peak compressive loads (-11.3 N) to one group of adult female mice (Load-Matched), which corresponded to +2200 με mid-diaphyseal strains and peak cancellous tissue strains of -2257 με. We applied the same peak mid-diaphyseal strains (+1200 με) to a second group of adult female mice (Strain-Matched), engendered by -5.9 N peak applied load, which corresponded to peak cancellous tissue strains of -1112 με. In the LM group, cancellous bone mass increased 49% through increased trabecular thickening (+64%), and cortical mass increased 41% through medullary contraction (-19%). These adaptive changes increased the metaphyseal stiffness of loaded limbs relative to control limbs (I_{MAX} +88%, I_{MIN} +54%). No adaptive response was observed in the SM group. The response in the cancellous compartment was reduced relative to that observed in growing mice. However, tibial loading recovered age-related loss to levels equivalent to control limbs of young animals, supporting the use of mechanical loading as a therapeutic intervention against osteoporotic fractures. In contrast, the response in the cortical compartment was enhanced relative to that in young mice. While both young and adult mice similarly increased I_{MAX} and cortical area, adult mice underwent enhanced medullary contraction.

Finally, tibial compression was applied to osteopenic, estrogen-deficient adult female mice to demonstrate that mechanical loading can stimulate cancellous bone formation following estrogen withdrawal. Loading was applied immediately following ovariectomy (OVX) or sham (Sham) surgery and lasted 1, 2, and 6 weeks to characterize the adaptive response over time. Estrogen deficiency did not inhibit the

adaptive response of cancellous bone in adult females. After 6 weeks of loading, cancellous bone mass increased similarly in Sham and OVX groups. Cancellous bone mass exhibited a bimodal change with loading due to the different effects of loading and estrogen deficiency, acting at different rates, on cancellous architecture. Loading primarily increased trabecular thickness while estrogen deficiency primarily increased separation. No differences in the control limbs between Sham and OVX groups were observed within the 6 week time period.

In summary, tibial compression elicited a robust anabolic response in cancellous bone, which increased mass in growing young male and female mice, and in osteopenic and estrogen deficient adult female mice. Cancellous mass occurred primarily through trabecular thickening and resulted in an overall stiffer tibia metaphysis. Tibial compression recovered age-related bone loss in osteopenic adult female mice to levels equivalent to the control limbs of young mice, even following estrogen withdrawal. These results demonstrate that mechanical loading can be targeted to corticocancellous sites to increase bone mass, improve structural integrity, and reduce risk for fracture. Additionally, these results demonstrate that mechanical loading can be implemented as a preventative measure, either in growing children, or pre- and peri-menopausal women, to increase peak bone mass and reduce risk of fracture.

BIOGRAPHICAL SKETCH

Maureen Ellen Lynch was born, 4th in a family of 8 children, in Columbia, South Carolina. She graduated as valedictorian from Cardinal Newman High School in 2000. In 2005, she graduated cum laude with honors from Clemson University with a Bachelor of Science degree in Mechanical Engineering and a minor in Bioengineering. While at Clemson, she participated in NSF's Biomaterials and Bioinformatics Summer Institute and received an NIH Mini-grant. She was inducted into Pi Tau Sigma, for whom she served as Fundraising Chair, and Tau Beta Pi. She also played for the Clemson Club Volleyball team for 5 years and coached U11 and U12 girls' volleyball. In 2008, she received her Master of Science degree in Mechanical Engineering at Cornell University. In July 2010, she received her Doctorate of Philosophy degree in Mechanical Engineering with a minor in Physiology at Cornell University. While at Cornell, she received an NSF Graduate Research Fellowship. She volunteered extensively, most notably for Expanding Your Horizons for 5 years by serving as Workshop Leader and Conference Chair. She also served as TA Trainer and TA Fellow for the Office of Engineering Learning Initiatives.

I dedicate this work to my mom.

ACKNOWLEDGEMENTS

My funding sources provided the financial support for this work, without which this work would not be possible. I acknowledge the NSF, who provided me with a 3-yr Graduate Research Fellowship. I acknowledge the NIH for their extensive support: R01-AG028664, P30-AR46121, F32-AR054676, and S10-RR024547.

Many people have given me their support, both technical and non-technical, during my graduate years and I am forever grateful to them all.

I would like to thank my committee members Dr. Pat Johnson and Dr. Tim Wright for all of their assistance with my work and my career. I want to give special thanks to thank Dr. Marjolein van der Meulen, my committee chair, for being an exceptionally gifted mentor, scientist, and role model. She has been, and continues to be, an incredible inspiration for me.

I could not have successfully completed my experiments without extensive assistance from others. I acknowledge the work and support Judy Thoroughman and Marcia Sawyer provided, without which grad school would have been infinitely more difficult. They keep this place running! I would like to thank Dan Walsh, Tommy Schmicker, Sarah Yagerman, Ken Stern, Frank Ko, Russ Main, Dan Brooks, Siddarth Pathi, and Kirsten Stoner for all of their participation in my numerous loading studies. I would like to thank the excellent staff at the Cornell Center for Animal Resources and Education, especially Brenda Collins, Dr. Wendy Williams, Dr. Kirk Maher, Dave Collins, Kevin Yager, and Christine Peterson. I would also like to thank Lindsey Trevino and Mila Kundu of Dr. Johnson's lab for their help with RIAs and Damien Ladier for his histomorphometric analysis. Finally, I would like to extend many thanks Jeff Meganck, Paul Picot, Lyudmila Lukashova, Kostas Verdelis, and Rhima Coleman for their assistance in microCT analysis.

I was fortunate to have indispensable and very talented sources of feedback and support from several key peer groups. My group mates, both current and former, were an especially valuable source of feedback and support: Eve Donnelly, Chris Fritton, Frank Ko, Amy Orlansky, Tee Pamon, Theresa Galie, Bassem Ghali, Dan Brooks, Kirk Gunsallus, Simranjit Singh, Jayme Burket, Garry Brock, and Dan Chen. I especially thank Jacque Cole and Russ Main for their advice, mentoring, and friendship. Members of the Biomechanics Seminar, especially: Jeff Ballyns, Robby Bowles, Satish Degala, Jason Long, Garry Hayeck, Tunde Babalola, and Veronica Santos. My colleagues at HSS: Lyudmila Lukashova, Kostas Verdelis, Rhima Coleman, Jocelyn Beach, Natalie Kelly, Kate Meyers, Carl Imhauser, Dr. Bostrom, Dr. Padgett, Dr. Lane, and Dr. Adele Boskey. My Cornell office mates and friends: Shan Mohiddiun, Michael Sherback, Trey Riddle, Katie and Jon Schoenburg, Terry McLoughlin, Ben Hawkins, Bernardo Cordovez, Justin Atchison, Jay Schuren, Vishal Tandon, Edgar Cuiji, Brett Streetman, Michele Carpenter, and John Ferguson.

Along the way, many faculty members have provided me with additional mentoring and career advice: Dr. Adele Boskey, Dr. Brian Kirby, Dr. Suzanne Maher, Dr. Don Bartel, Dr. Larry Bonassar, Dr. Hadas Kress-Gazit, and Dr. Mitch Schaffler.

I would not be here without the love and support from my family. My brothers, John and Michael, and sisters, Megan, Erin, Beth, Mary, and Anne Marie, will always be my best friends and biggest fans for life. My uncle Kenny, with whom I stayed many times in NYC, provided me with a friendly home during many long work days. My aunt Ag continues to be my beloved guide in this life, to whom I know I can always turn (because I always do!). My Ithaca family, Erika Johnson, Grace Kim, and Natalie Galley, my closest companions, from whom I received unwavering love, support, encouragement, and the bond of genuine friendship. Rob MacCurdy, for

whom I do not have the verbal prowess to adequately express my love, gratitude, admiration, and so much more, I can merely say thank you and I love you.

My biggest thanks are reserved for my parents. To you, who sacrificed so much to provide me with a superb education, who challenged me to live up to my full potential, and who instilled in me the self-confidence to achieve my goals, I owe everything.

TABLE OF CONTENTS

LIST OF FIGURES

LIST OF TABLES

CHAPTER 1

INTRODUCTION

1.1 Osteoporosis

Osteoporosis causes skeletal fractures in more than 2 million men and women over the age of 50 every year, with nearly $17 billion in associated costs [1]. The incidence and economic burden of this condition will only increase as the population ages. The U.S. population of persons over 65 years of age is projected to increase over 50% by 2025 to reach 71 million [2] with costs of osteoporosis-related fractures rising over $25 billion annually [1]. Therefore, designing and implementing both therapeutic and preventative strategies are critical to reducing costs associated with osteoporosis.

Osteoporosis is diagnosed based on the results of a bone mineral density (BMD) from a dual energy x-ray absorptiometry (DXA) scan. A portion of the patient's spine is scanned and the BMD measure is compared to a population of a young, healthy, white female population. The World Health Organization has defined an osteoporotic person as having a T-score, or standard deviation (SD), of -2.5 or lower relative to the mean BMD of this young population. An osteopenic person is defined as having a T-score between -1 and -2.5, and has reduced bone mass relative to this young population, but the risk for potential fractures are not as high as in osteoporotic patients.

Fractures associated with pathological bone loss occur predominantly at sites rich in cancellous bone, such as the spine, wrist, and hip (Fig. 1.1a). Cancellous bone is the porous bone found in vertebrae and at the ends of long bones. It is comprised of individual trabeculae that form a lattice network of rod- and plate-like struts with a porosity between 50-90%. Cancellous bone constitutes 20% of total skeletal bone mass [3]. Cortical bone is the denser bone found in the shaft of long bones and also

provides a protective shell around cancellous bone. Cortical bone has a porosity between 5-10%, considerably smaller than that of cancellous bone. Therefore, cancellous bone has much greater surface area. Consequently, bone turnover occurs more frequently in cancellous bone, despite its small volume within the skeleton (see ***1.2 Bone Remodeling***). Alterations to the turnover process can have substantial consequences on bone mass at these sites, as in the case of osteoporosis (Fig. 1.1b).

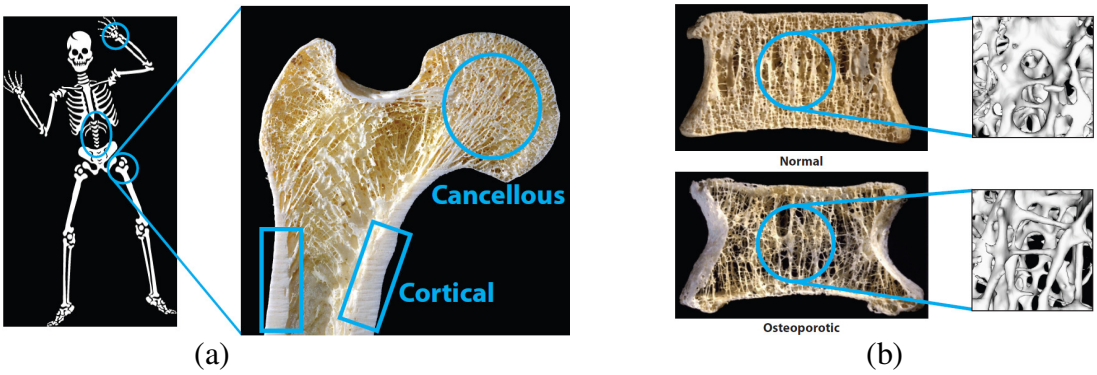

Figure 1.1 Locations within the human skeleton at greatest risk for osteoporotic fracture. (a) The wrist, spine, and hip (at left, in circles) are the most common sites of osteoporotic fracture. These sites contain a large amount of cancellous bone, which is porous bone (at center, in circle), while cortical bone (at center, in squares) is dense, compact bone. (b) Cross-sectional images (at right) from a normal (top) and an osteoporotic (bottom) vertebra [4], with associated representative micro-computed tomography scans (at right).

Women account for 71% of all osteoporotic fractures [1]. Women have lower peak bone mass than men and experience greater bone loss in adulthood (Fig. 1.2). Men attain 25% greater peak bone mass because they undergo 2 additional years of pre-pubertal growth and their pubertal growth spurt lasts 1 year longer than girls, both stages when bone remodeling and accrual rate are greatest [5]. In addition, women experience rapid bone loss associated with estrogen withdrawal at menopause. During this rapid phase, women can lose as much as 20% total bone mass in the first 5 years following menopause [6]. Combined, these two events leave women far more susceptible to fracture than men.

Both adult men and women undergo bone loss with aging (Fig. 1.2). Type I osteoporosis refers to the rapid phase of bone loss that occurs in women during and following menopause, and is caused by acute estrogen deficiency [7]. This early phase of bone loss lasts 5-10 years, then subsides. Type II osteoporosis refers to gradual, age-related bone loss that both men and women experience and is caused by chronic estrogen deficiency.

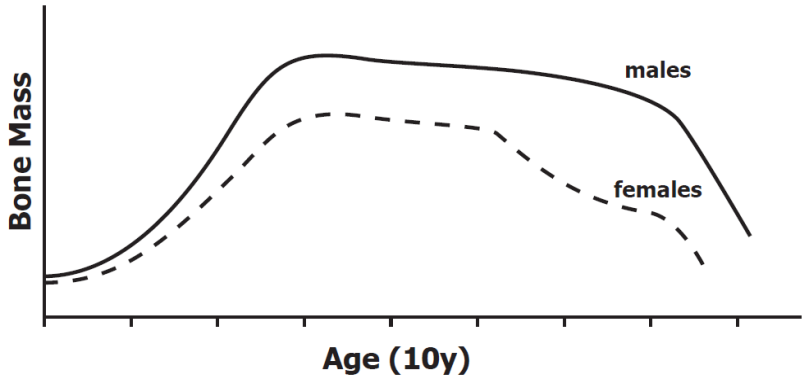

Figure 1.2 Schematic of bone mass over the lifetimes of men (solid line) and women (dashed line), illustrating the two phases of bone loss in adults. At approximately age 50, women undergo a transient period of rapid bone loss associated with menopause, called Type I osteoporosis. Eventually, this rapid phase ends. Both men and women experience a continual phase of age-related bone loss, called Type II osteoporosis. Because women consistently have lower bone mass than men and experience rapid bone loss at menopause, they are especially susceptible to fractures.

1.2 Bone Remodeling

The skeleton serves primarily as the structural support frame for our bodies. Bone is continuously remodeled through the interplay between osteoclasts, cells that resorb bone, and osteoblasts, cells that form bone (Fig. 1.3). Both osteoclasts and osteoblasts originate from precursor cells in bone marrow. Osteoclasts are multinucleated cells that derive from pluripotent hematopoietic cells of the macrophage lineage. Osteoblasts are mononuclear cells that derive from multipotent mesynchymal stem cells [8]. Together, these cells form basic multicellular units (BMUs), the cellular structure responsible for skeletal homeostasis. The purpose of

BMUs is to replace old bone, likely to prevent accumulation of microdamage that could lead to fracture [9]. Remodeling is an ongoing process with ~1 million BMUs turning over bone at any given time in healthy humans. The entire skeleton is remodeled approximately every 10 years [8].

Bone remodeling is a surface-based activity that occurs on four types of surfaces. Cortical surfaces include the periosteum, the endosteum, and intracortical surfaces along Haversian canals. Cancellous surfaces are simply the surfaces of individual trabeculae. Because cancellous bone has a high surface area to volume ratio, it is much more metabolically active than all the other surfaces.

Once the remodeling process is activated, bone lining cells, which are quiescent osteoblasts on the surface of bone, disappear and expose a suitable surface to which osteoclasts can attach. Once attached, osteoclasts initiate acidic degradation of bone, creating a tunnel (cortical bone) or a trench (cancellous bone) as they proceed forward. Once the resorption process is completed, osteoclasts undergo apoptosis. Next, osteoblasts begin re-filling the tunnel or trench with collagenous osteoid, which is eventually mineralized to form new bone. Osteoblasts that are buried within the bone matrix become osteocytes.

The remodeling process is mediated through a whole host of factors including, but not limited to:

Systemic Factors:

- Mechanical signals
- Estrogen and its receptors (ERs)
- Aging
- Genes
- Other systemic hormones (e.g. parathyroid hormone PTH)
- Diet

Local Factors:

- Proteins (especially nuclear factor-κβ RANK and its ligand RANKL, and osteoprotegerin OPG)
- Growth factors (e.g. bone morphogenetic proteins BMPs, transforming growth factor β TGF-β)

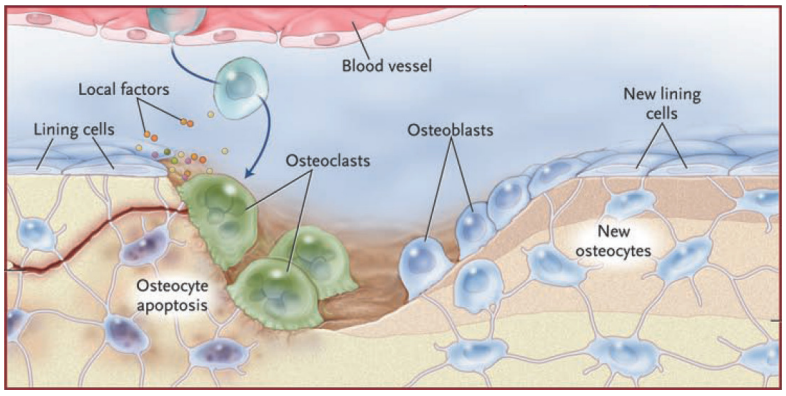

Figure 1.3 Graphic representation of the remodeling process. Osteoclasts are recruited from circulating blood and marrow, attach to the bone surface, and remove bone. After osteoclast apoptosis, osteoblasts lay down new bone in the same place. From [10].

With osteoporosis, the remodeling process becomes unbalanced, favoring osteoclast activity and resulting in a net bone loss. As stated previously, the majority of osteoporotic bone loss occurs at corticocancellous sites. Following menopause, bone resorption in women rapidly increases 90% while bone formation increases 45% and results in losses of 20-30% in cancellous bone, compared to only 5-10% in cortical bone [5, 6, 11]. Type I osteoporotic cancellous bone loss is characterized by perforation and eventual removal of individual trabeculae [12, 13]. Age-related bone loss occurs in both men and women, where similar amounts of bone are lost from cortical and cancellous compartments. Type II cancellous bone loss is characterized by gradual thinning of trabeculae [12, 13]. Because of the low volume fraction in cancellous bone, loss from this compartment is disproportionately detrimental to overall mechanical integrity, rendering it far more susceptible to fracture than cortical sites.

1.3 Effects of Estrogen Deficiency and Aging

Estrogen deficiency is hypothesized to be the underlying cause of both Type I and Type II osteoporosis [7, 14]. At the tissue level, estrogen acts to conserve bone

mass by suppressing BMU activation frequency. At the cell level, estrogen inhibits osteoclastogenesis and decreases osteoclast lifespan by promoting apoptosis. Estrogen also inhibits osteoblast and osteocyte apoptosis [5, 8]. Therefore, estrogen deficiency permits osteoclastogenesis and osteoblastogenesis and enhanced BMU activation frequency. Increased activation leads to an increased rate and occurrence of bone turnover. Furthermore, bone turnover becomes imbalanced, favoring resorption due to increased osteoclast lifespan concomitant with decreased osteoblast lifespan [8]. Overall, net erosion of bone mass occurs. These effects can be prevented or attenuated with estrogen administration [15] (see ***1.4 Therapies***).

Both adult men and women experience estrogen deficiency. Women undergo menopause, which is the sudden cessation of ovarian estrogen production. Because ovarian production accounts for over 95% of estrogen synthesis in females [5], the acute loss of estrogen production causes rapid bone loss. In men, synthesis of estrogen is also reduced with age and causes similar, but slower, bone loss (Fig. 1.2). In addition to altering bone homeostasis, reduction in estrogen also alters extraskeletal calcium metabolism by reducing $1,25(OH)_2D$ levels and calcium absorption in the gut, and increasing renal calcium wasting. Combined, these effects lead to secondary hyperparathyroidism. Additionally, the populations of cytokines, growth factors, etc. change with aging and also lead to decreased osteoblastogenesis and increased osteoclastogenesis. Estrogen receptors on the cell membranes of osteoclasts, osteoblasts, and osteocytes are thought to mediate the effects of estrogen. Dwindling populations of these receptors in bone cell membranes also contributes to the skeleton's reduced responsiveness to mechanical stimuli with aging [16].

1.4 Therapies: Anti-catabolic and Anabolic

Currently, virtually all therapies for osteoporosis and osteopenia are pharmacologic. Most therapies target osteoclast activity to reduce resorption and therefore are anti-catabolic or anti-resorptive. Bisphosphonates, such as alendronate and risondrate, are the most commonly used drug therapy. Bisphosphonates bind to the mineral crystals on bone surface, are ingested by osteoclasts, and inhibit osteoclast resorption. Administration of exogenous estrogen, called Hormone Replacement Therapy, is successful for attenuating bone loss, but is limited in use due to the associated risk for breast cancer. Selective estrogen receptor modulators (SERMs), such as raloxifene, were developed to address this issue. SERMs are estrogen agonists in bone tissue, but antagonists in breast tissue, and therefore attenuate bone turnover as well as reduce the risk of breast cancer [17].

While anti-catabolic therapies are successful at inhibiting bone loss and reducing fracture risk, finding ways to increase bone formation is important in a population that is already osteoporotic or osteopenic. Increasing bone formation can be achieved by: 1) increasing the pool of mature osteoblasts, through amplified precursor cell differentiation and replication [18] and 2) by increasing the activity of mature osteoblasts. To date, parathyroid hormone (PTH), teriparatide, is the only FDA-approved anabolic pharmacologic treatment. PTH increased vertebral BMD 8-9% and femoral BMD 3% after 21 months of daily administration, which reduced the incidence of fracture 65% and 54%, respectively [19]. PTH increases the population of osteoblasts and decreases osteoblast apoptosis [10]. PTH administration elevates bone formation over that of resorption to increase bone mass. Additional therapies that target various aspects of osteoblast differentiation, activity, and lifespan are under investigation. For example, strontium ranelate simultaneously inhibits resorption and enhances formation [20]. Strontium ranelate stimulates osteoblast differentiation and

osteoblastic secretion of osteoprotegerin, a protein that inhibits osteoclast differentiation. This therapy is approved in Europe, but is not yet available in the United States.

Another emerging anabolic, but non-pharmacologic, therapy is biophysical stimuli. Biophysical stimuli can induce bone formation and increases mass. Additional benefits of exercise include better balance, agility, and muscle mass, which also reduce fracture risk. This type of therapy is effective in both children and adults. Implemented as a prevention strategy in children and young adults, exercise can maximize peak bone mass and skeletal size, thereby reducing fracture risk in adulthood. In adults, mechanical stimuli could be used alone or in combination with a drug therapy to avoid or attenuate pathological bone loss.

1.5 Bone Functional Adaptation

The origin for mechanical stimuli's potential is based on the ability of the skeleton to sense and adapt to its mechanical environment, a process call bone functional adaptation. Mechanical signals, either positive or negative, are converted to cellular signals in a process called mechanotransduction. As mentioned previously, the skeleton's primary function is to provide structural support for the body, using minimal bone mass without catastrophic failure or damage. The form of the skeleton, then, reflects the optimization between structural competency and metabolic cost (plus a safety factor), which allows us to perform our daily physical activities. Recognition of the connection between skeletal form and mechanical stimuli is generally credited to Julius Wolff in 1892 [21] and is referred to as "Wolff's Law".

Bone functional adaptation is hypothesized to operate under feedback loop control (Fig. 1.4a) [22]. As stated earlier, the skeleton is continuously undergoing remodeling. At steady state, bone formation and resorption are equivalent, with no net

change in bone mass. Under this condition, the skeleton is sufficiently equipped to withstand an individual's 'regular' mechanical stimuli. If bone perceives increased mechanical stimuli, such as a new exercise routine, remodeling with net bone formation occurs until the bone tissue can sufficiently withstand the increased mechanical environment. Conversely, decreased mechanical stimuli trigger resorption, such as in the case of microgravity [23] or bedrest [24], when the skeleton perceives its current environment is experiencing too little stimulus. Tissue is then resorbed until mechanical stimuli increases to the appropriate level.

Osteocytes are hypothesized to be the mechanosensors, the cells that perceive and interpret prevailing mechanical signals in bone [25, 26]. Osteocytes are the most numerous cells in bone and form an interconnected syncitium with other osteocytes, osteoblasts, and bone lining cells via processes within the canaliculi. Osteoblasts can also communicate with cells in bone marrow. The actual stimulus (or stimuli) derived from mechanical signals is currently unknown. Bone matrix deformation (engendering cell deformation) or micro-cracking, pressure gradients within the canaliculi, shear stresses induced by fluid flow over the osteocytes, stress-generated potentials, a combination of these, and/or perhaps unknown signals are potential derivatives of mechanical loading that triggers bone adaptation. In addition, the pathways of mechanotransduction are also unknown, but likely include stretch- and voltage-activated membrane channels, integrins, gap junctions between osteocytes, the cell cytoskeleton, and other factors that trigger a cascade of events that ultimately result in remodeling.

Estrogen interacts with mechanical loading to drive adaptation, but its role is unclear. Estrogen deficiency may reduce the level of mechanical stimuli that the skeleton perceives as 'regular', thereby driving net bone loss [27] (Fig. 1.4b and c). Alternatively, estrogen deficiency may impair the ability of bone cells to appropriately

respond to mechanical loading [27, 28]. Estrogen and mechanical loading are hypothesized to share a common pathway, both possibly mediated through estrogen receptors [27, 29, 30], which are found on the surface of all bone cells [5].

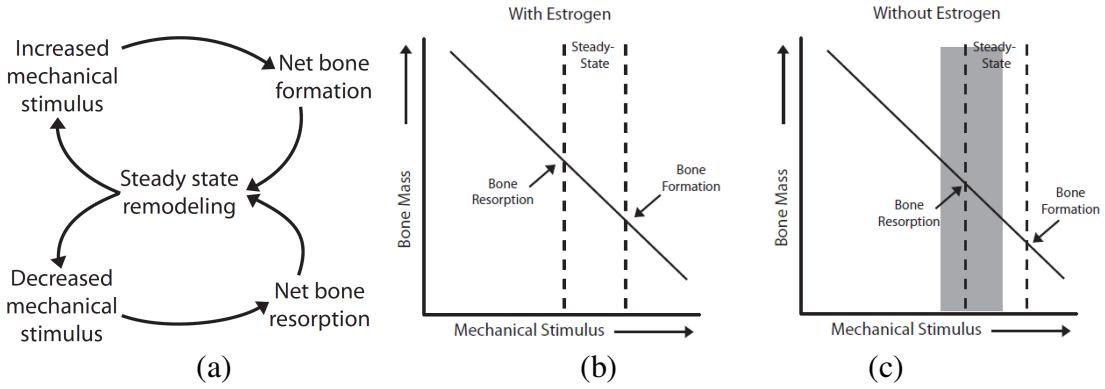

Figure 1.4 Schematic of the feedback theory governing bone functional adaptation and the effects of estrogen status. (a) At steady state, formation and resorption are balanced, with no net gain or loss in bone. When the skeleton perceives increased mechanical stimulus, net bone formation occurs. Conversely, when the skeleton perceives decreased mechanical stimulus induces, net resorption occurs. (b) Steady-state mechanical stimulus as perceived by the skeleton. (c) Following estrogen withdrawal, the mechanical stimulus required to maintain steady state remodeling increases (shaded box represents 'With Estrogen' steady-state), so that more stimulus is required to induce bone formation.

1.6 Exercise in Humans

In humans, exercise is generally an anabolic mechanical stimulus. The adaptive response of the skeleton is most robust during childhood and early adulthood, when skeletal growth is still occurring. High impact sports and exercises (i.e. jumping), even at moderate intensity and frequency, readily induce adaptation [31-34]. Because children and young adults are still acquiring bone mass, engaging them in athletic activities prior to or during puberty will maximize peak bone mass and may provide a buffer against bone loss in adulthood. Indeed, girls who began playing racquet sports or participating in step aerobics prior to or during puberty achieved greater gains in bone mass and density than those who started after [31-33, 35, 36].

While bone mass and density initially remained elevated in athletes after sport participation ended [37-40], these effects may erode long-term as long as some type of exercise is not maintained [41]. An added benefit is that exercise also induces architectural changes in the skeleton. These changes are especially important because they remain long after cessation of exercise and confer additional reductions to fracture risk in adulthood [42-44].

In addition, sexual dimorphism to functional adaptation emerges peri- and post-pubertally. Males continue to expand cortices periosteally while females reduce expansion in favor of medullary contraction [35, 45-47]. These differing adaptive mechanisms result in males having overall larger skeletons with greater structural strength (through larger moments of inertia). Therefore, initiating exercise prior to puberty is especially important for females.

Exercise in adult, pre-menopausal women has been effective at inducing moderate adaptation and increasing bone density, if training is progressively resistive and involves movements with high accelerations [48-55]. The densitometric benefits may erode initially after cessation of exercise [56], but increased muscle strength may confer long-term skeletal benefits [57]. Similarly, exercise likely imparts further reductions to fracture risk through better balance, increased muscle tone, or changes in architecture, all of which are not captured clinically using dual x-ray absorptiometry (DXA).

Interventions in post-menopausal women result in far more variable outcomes. Interventions using progressively resistive and high-intensity exercises over the course of 1 year or more, have marginally increased bone mass [58-61] or have prevented bone loss [62-65]. Combined, these studies support the use of mechanical loading to reduce risk for fracture by increasing bone mass and altering bone architecture. Understanding which particular mechanical signals best stimulate osteogenesis in an

elderly, osteopenic population is critical for enhancing current therapeutic approaches. Furthermore, understanding how aging and estrogen withdrawal modulate bone functional adaptation is essential to understanding the failure of the skeleton's ability to respond appropriately to mechanical signals in an aging population.

Experiments to study the effects of exercise in humans are limited for many reasons. Cross-sectional studies can only demonstrate a correlation between exercise and bone mass or density, and can not infer causation. In addition, when comparing athletes to non-athletes, selection bias may exist. Individuals may be successful at sports because they have larger, more robust skeletons and muscle mass. Longitudinal studies can be used to eliminate selection bias, but must be randomized. Non-randomized longitudinal studies allow participants to choose which group they belong to in an effort to maintain high participation, which may introduce selection bias. Randomized studies run the risk of insufficient power (low numbers of subjects) to detect meaningful significant changes with exercise and may confound interpretation of results. Finally, the mechanical environment of the skeleton during exercise is complex and difficult to characterize in humans. Using controlled in vivo animal models addresses many limitations of exercise. Animal models provide adequate sample sizes, strain gauges can be applied to their skeletons to measure in vivo strains during mechanical stimulation, and their skeletons can be harvested for various analyses.

1.7 In Vivo Models of Bone Adaptation and Osteoporosis

Several early seminal studies using controlled in vivo loading in animal models confirmed that bone adaptation can be induced by mechanical loading [66-71]. By applying controlled, well-defined loads to the skeleton, salient mechanical parameters can be characterized and related to the adaptive response. Specifically, the loads must

be applied dynamically rather than statically [66-68], and increasing the magnitude [69, 70] and rate of loading [71] enhances osteogenesis. These early models used invasive surgical techniques, which may have confounded interpretation of results. Since then, many non-invasive models have been developed for use in rodents (Fig. 1.5); first for rats, then adapted for mice. Rodent models are beneficial for their small size and, due to large sample numbers, the ability to detect statistically significant effects. Mice provide the added benefit of genetic manipulation. The majority of these more recent models are limited to characterization of the adaptive response in the mid-diaphysis of the long bones, even though cancellous bone is the more clinically relevant tissue. Therefore, targeting mechanical stimuli to these critical sites is most valuable for preventing fracture.

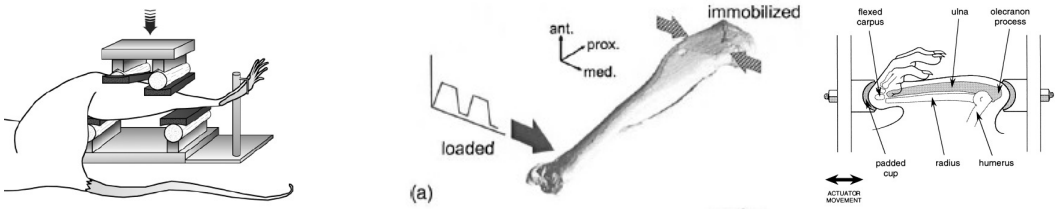

(a) (b) (c)

Figure 1.5 Controlled in vivo loading models developed for rodents. These models are used to investigate diaphyseal bone. (a) four-point bending of the tibia. From [72]. (b) Cantilever bending of the tibia. From [73]. (c) Compression of the ulna. From [74].

Few controlled loading models have been developed to investigate the adaptive response in cancellous bone. Isolation of cancellous tissue for applied loading is difficult because of the surrounding cortical shell. In addition, application of strain gauges to cancellous tissue is impossible. Two studies removed the cortical shell for direct application of mechanical loads [75, 76]. In the first, significant remodeling occurred after a hydraulic device, implanted in the distal femoral metaphysis, delivered controlled loads directly to exposed cancellous bone in dogs. The trabeculae were reoriented to align with the loading platens and, as demonstrated in cortical bone,

greater adaptation occurred when the loads were delivered at a faster rate. Using a similar approach, an implantable device applied loads directly to exposed cancellous tissue in the femoral condyles of rabbits and resulted in increased cancellous bone mass and bone formation. These models required removal of the surrounding cortical shell to expose cancellous tissue, which models the bone-implant interface but does not represent a normal physiologic condition. In addition, these models would be difficult to reproduce in rodents, which is the animal most often used in this body of work, because of their small size. A new approach to increasing bone mass is by applying low-magnitude, high-frequency vibration loads to the body through a vibrating plate. With this method, the vibrations are applied at frequencies much greater, resulting in skeletal mechanical strains much lower than are experienced during normal activities [77, 78]. Similar to results of exercise in adult and post-menopausal women [79-81], the effects of applying high-frequency vibrations to adult and estrogen-deficient rodents have been variable [82-84]. The focus of this thesis, however, is to examine the efficacy of physiological mechanical signals.

Vertebral pinning was used to apply compression to the entire 8^{th} caudal vertebrae through metal pins inserted in the 6^{th} and 7^{th} vertebrae. Vertebral compression induced cancellous bone formation in adult and growing rats once a sufficiently large stimulus was applied, and formation was enhanced with prolonged loading [85-87]. Formation increased by activating quiescent bone lining cells into osteoblastic cells, rather than proliferating osteoblasts. Osteoblastic cell density peaked at 48 hours after a single bout of loading [88], and osteoblast surface peaked at 9 days [86]. Vertebral pinning was recently adapted for use in mice. In growing mice, cancellous bone mass increased through trabecular thickening in a dose-dependent fashion and cortical shell expansion [89]. Vertebral pinning, though, applies extremely high loads (up to 150 N) and has resulted in woven bone formation on the cortical

shell [86]. The pinning process is also extremely invasive and may confound interpretation because indices of bone formation and resorption increase in pinned, non-loaded experimental groups [86, 87].

In vivo tibial compression was adapted from the ulnar compression model for investigation of cancellous bone adaptation because the proximal tibia has a greater volume of cancellous bone. Tibial compression, like ulnar compression, is a non-invasive, physiologic loading modality and applies loads across the entire limb, allowing investigation of both cortical and cancellous compartments (Fig. 1.6). Tibial compression increased cancellous and cortical bone mass in growing [90-93] and adult mice [94, 95], and prevented bone loss following orchidectomy [96], and therefore can be used to study other modulation factors of cancellous adaptation. In this body of work, the role of sex, age, and estrogen deficiency on cancellous adaptation is explored using tibial compression in C57Bl/6 mice.

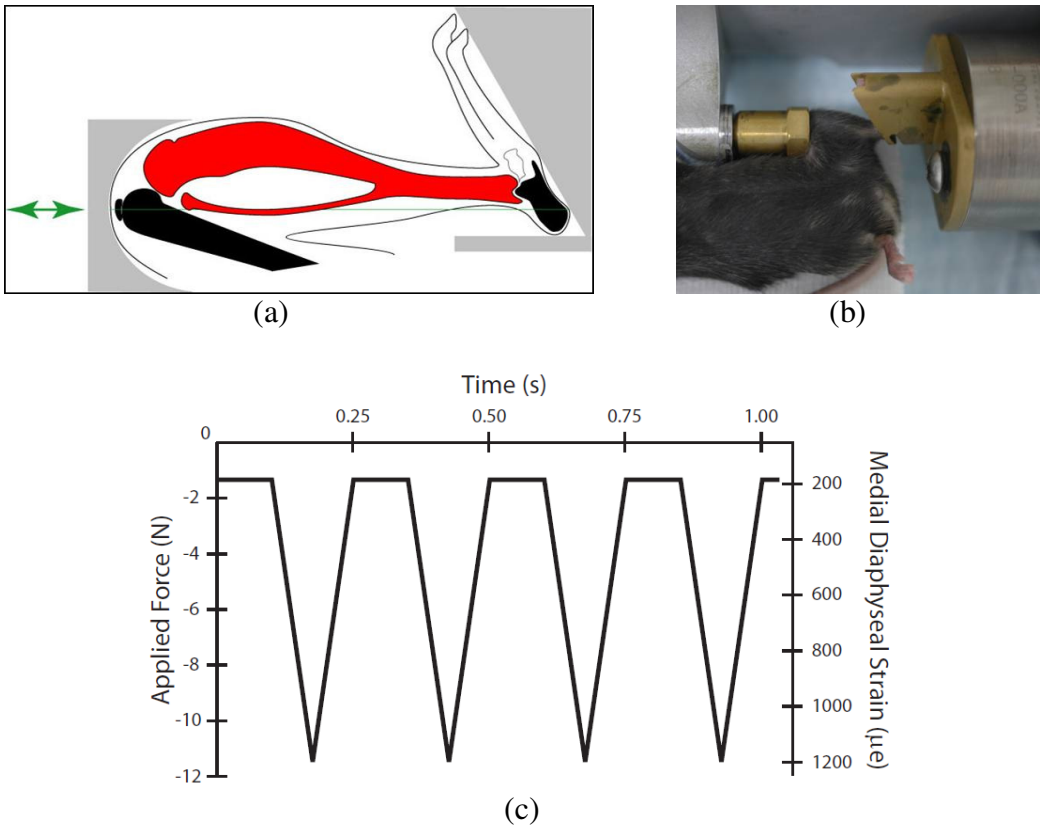

Figure 1.6 In vivo tibial compression. (a) Schematic of the tibia situated in the loading device. Arrows indicate direction of load application. (b) Photograph of the left limb of a mouse undergoing tibial compression. (c) Representative loading waveform schematic for 4 cycles (1 second) of the daily mechanical loading protocol. Peak applied force (N) is on the left side of the graph and the corresponding strain (με) at the medial mid-shaft is on the right side of the graph (see ***1.9 Methods***).

Effects of Sex

Because the effects of mechanical loading are greatest during growth, maximizing peak bone mass during this time will be effective at attenuating bone loss in adulthood [45, 97-99]. During and after puberty, dimorphism in the response to exercise emerges between males and females, but few studies have explicitly examined this effect [47, 100]. Determining the role of sex in skeletal adaptation is important to develop prevention strategies for children and young adults.

Whether sex affects the adaptive response in rodents is unclear. Treadmill running increased cross-sectional area and mineral content in the femoral neck of adult and growing male rats, but not in female rats [101]. However, BMD was greater in adult females than in males, suggesting differences in growth patterns. More mineral condensation in females may provide additional calcium stores for pregnancy. Using in vivo ulnar compression in growing rats, the magnitude of the loading-induced increase in bone area was 6 times greater in males than in females. But, when these increases were normalized relative to the effects of growth, males and females responded similarly [102]. No study has investigated the effect of sex on the adaptive response in cancellous bone. In this thesis, the focus of Chapter 2 will be to characterize the effects of sex on the response of cancellous bone to tibial compression in growing male and female mice.

Effects of Aging

The skeleton's responsiveness to mechanical loading reduces with age [73, 93, 103-110]. Results from various exercise treatments in rodents have been variable, with aged animals either responding more robustly [111, 112] or showing no difference with age [113-115]. Without knowing the mechanical environment of the skeleton during these exercises, explaining these discrepancies is difficult, and their usefulness is limited. Controlled in vivo loading studies demonstrated that the adaptive response in diaphyseal cortical bone is reduced with aging. The osteogenic threshold was reduced in aged rats (19mo) relative to adult rats (9mo) undergoing four-point bending [105, 106]. Only 60% of aged rats, compared to 100% of adult rats, exhibited woven bone formation at the periosteum. At similar peak applied loads and bending strains, the relative bone formation surface and bone formation rate of aged rats were 5- and 16-fold less than in adult rats. The calculated endocortical strain threshold for

osteogenesis was ~1000 με for adults and ~1700 for aged rats. Similarly, aging reduced responsiveness to cantilever bending in mice. No formation occurred in aged mice (21mo), but did in young adult mice (16wks) [73, 107] under similar loading conditions (peak strains ~1200 με). However, this loading protocol was transformed into an osteogenic one by inserting rests in between each loading cycle [107]. Indeed, at all ages, the skeleton desensitizes to repeated exposure to mechanical loading, even if the peak load magnitude is increased [116, 117]. In addition, breaking up 360 cycles into shorter, more frequent sessions (90 cycles, 4x per day) is more osteogenic than delivering them all at once [118]. Inserting rests into tibial compression loading has not enhanced bone formation in adult mice [93, 108, 119, 120], but the reason for this result is unclear. In Chapter 3, the peak strain magnitude and peak applied load, based on a tibial compression protocol determined to be osteogenic in growing mice, are each applied to groups of adult mice to determine the parameter that elicits greater adaptation. Determining an osteogenic protocol is necessary for exploring other factors that affect bone adaptation in adults, such as estrogen deficiency.

Effects of Estrogen Deficiency

A commonly used in vivo model for osteoporosis is the ovariectomized (OVX) rodent. Though menopause does not occur naturally in rodents, by surgically removing both ovaries, the primary source of estrogen production is disabled. Thus, OVX mimics the conditions of menopause in humans. OVX rats have been the predominant rodent model for human osteoporosis because they follow similar patterns of bone loss as adult and elderly women. Rats underwent a rapid phase of cancellous bone loss following OVX, which was detectable as early as 2 weeks post-surgery in the proximal tibia and in the distal femur [121, 122]. Bone loss in lumbar vertebrae was detectable 3 months post-surgery [123]. This accelerated phase lasted approximately 5

months, followed by a more gradual, continual phase of bone loss [121, 122, 124]. OVX lead to increased bone turnover and net bone loss, which occurred through the removal of trabeculae while the remaining trabeculae often became thicker [122, 125, 126]. OVX-induced bone loss was prevented with administration of estradiol, which suppressed both osteoclast and osteoblast activity [127], and administration of bisphosphonates, which suppressed osteoclasts [128]. However, when OVX-induced bone loss was allowed to occur, estradiol and bisphosphonates attenuated, but did not fully recover, cancellous bone [86].

Mice, especially genetically modified mice, have emerged as a powerful tool for investigating the genetic underpinnings of osteoporosis in addition to elucidating the specific role estrogen plays in bone adaptation. The effects of OVX on mice have not yet been fully characterized, but differ among genetic strains and skeletal locations [129-132]. For example, C3H mice were resistant to vertebral bone loss following OVX, but lost the greatest amount of bone from the proximal tibia relative to other strains [131]. This body of work uses the C57Bl/6 (B6) mouse because, while this strain has relatively lower bone mass [133-135], its response to mechanical loading is greatest [136, 137].

A few studies investigated the effects of OVX in the B6 skeleton, all in 12-17 week old (young) mice. Cancellous bone loss occurred readily at the distal femur of the B6 mouse following OVX, where BV/TV was reduced 50% within a month through increased trabecular separation. OVX also increased osteoclast and osteoblast surfaces, an indication of increased turnover [130, 138, 139]. Similar patterns of bone loss occurred in the vertebrae [131, 138]. The effects of OVX in the proximal tibia of mice were more variable. The proximal tibiae of young adult B6 mice were resistant to OVX-induced bone loss up to 1 month post-surgery [131, 140], but in growing mice, bone loss was detected within the same time period and continued through 11 wks due

to reduced trabecular separation and elevated turnover [141]. Because turnover is a substrate-driven process, B6 mice may be slower to manifest bone loss following estrogen withdrawal because BV/TV in the proximal tibia is relatively low (~10%). The magnitude of OVX-induced bone loss was correlated with baseline bone mass and may explain the slower response of the B6 strain [131, 132]. In other words, mice with more cancellous bone to begin with, such as C3H, lose more following estrogen withdrawal. In the same way, retired athletes, who have higher bone mass and density, lost more bone with aging than age-matched controls [37, 38]. Whether cancellous bone loss would occur in adult or aged B6 mice after more than 1 month post-surgery is unknown. Cortical bone in young B6 mice was also affected by estrogen withdrawal. Cortical bone area decreased through endosteal resorption and thinning of the cortices [131]. Indices of resorption were detected as early as 2 wks post-surgery, remained elevated as long as 4 wks, and returned to Sham levels after 8 wks [129, 142]. No studies have investigated the effects of OVX on adult or aged mice, so whether they exhibit different patterns of bone loss from young mice is unknown. Also, whether OVX B6 mice have a rapid phase of cancellous bone loss followed by a slower, age-related phase has yet to be determined.

Effects of Estrogen Deficiency on Bone Functional Adaptation

Combining OVX and mechanical loading is valuable for understanding the interaction between estrogen and mechanical signals and for elucidating the role estrogen deficiency plays in bone adaptation. Isolating the respective effects of aging and estrogen deficiency on bone adaptation is difficult in adults. For example, in women, menopause usually occurs during mid-life when bone mass has already been in decline due to aging (Fig. 1.2). Applying mechanical stimuli to an OVX, growing animal eliminates the aging effect, while applying stimuli to an intact osteopenic

animal eliminates the estrogen deficiency effect. OVX in an adult or aged mouse can also be used to model the conditions of peri- or post-menopausal women. When stimuli are applied to adult or aged mice after OVX-induced bone loss has occurred, the therapeutic potential of mechanical signals can be assessed. When stimuli are applied coincident with OVX, the preventative potential of mechanical stimuli can be assessed. In addition, these models can be used in combination with various drug therapies for further assessment.

Nearly all rodent studies combining OVX with mechanical loading have been exclusively in rats, and most employ various exercise modalities rather than controlled loading. In addition, very few characterize the resulting cancellous architecture. In general, mechanical loading suppressed indices of bone resorption while maintaining increased bone formation [143-145]. Running and jumping increased bone mass in aged and adult rats after OVX-induced bone loss had occurred [143, 144, 146], but all lost bone was not fully recovered [146]. In contrast, bone formation was greater in OVX than in Sham rats undergoing four-point bending, suggesting that some mechanical loading regimes may exploit increased bone turnover following OVX [147]. Few models have used mechanical loading to prevent OVX-induced bone loss. Tower climbing in aged rats prevented bone loss following estrogen withdrawal by suppressing both increased bone formation and resorption [146]. Running prevented a reduction in femoral fracture load, which was observed in OVX rats, but had no effect in Sham mice [101]. In growing rats, running attenuated increased bone formation and bone loss, but did not fully prevent it [145]. No studies have investigated if controlled loading could be used to prevent OVX-induced bone loss. Only one study investigated the combined effects of hormone deficiency and controlled loading on cancellous bone adaptation, but used male mice. Tibial compression prevented bone loss following orchidectomy in male mice [96], suggesting that tibial compression could be used

similarly in OVX mice. In Chapter 4, OVX adult mice serve as our model for osteoporosis. Applying tibial compression to these mice allows us to characterize the efficacy of mechanical loading for increasing cancellous bone mass in the adult estrogen-deficient skeleton.

1.8 Objectives

Mechanical loading shows promise for increasing cancellous bone mass in growing children and adults. Determining the salient mechanical parameters that stimulate cancellous bone formation is critical to harnessing the therapeutic potential of mechanical loading for enhancing peak bone mass and preventing osteoporosis. If mechanical loading is to be implemented during the growth period in humans, determining whether the adaptive response of cancellous bone is sex-specific is important for developing interventions in children (Objective 1). In addition, the efficacy of mechanical stimuli to increase cancellous bone mass in the adult skeleton (Objective 2), must also be demonstrated without the presence of estrogen (Objective 3). Our model for characterizing the adaptive response of cancellous bone is in vivo tibial compression applied in mice. Changes in cancellous bone mass, architecture, and dynamic formation are assessed using micro-computed tomography (microCT) for each experiment.

Objective 1

Because female mice are smaller than male mice [148-152], similar applied load magnitudes are hypothesized to induce larger strains, and therefore induce greater adaptation in growing female mice [153]. To determine if sex-specific responses to mechanical loading exists in cancellous bone, similar peak loads were applied to growing male and female mice using tibial compression for 2 weeks. First, the

relationship between applied load and resulting diaphyseal cortical strains was determined using strain gauging techniques. Cancellous bone mass, architecture, and dynamic formation in the proximal metaphysis were compared between loaded and control limbs via micro-computed tomography and histomorphometry. Finite element models of the proximal metaphysis were generated to characterize the cancellous tissue strains induced by tibial compression and the changes in metaphyseal stiffness following loading-induced adaptation.

Objective 2

The response of diaphyseal bone to mechanical loading diminishes with aging in a variety of animal models [104, 106, 107], but whether the responsiveness of cancellous bone diminishes as well is unclear. Determining the efficacy of mechanical loading to increase cancellous bone mass in the aged skeleton is essential for demonstrating the therapeutic potential of mechanical stimuli in an osteopenic adult population. The response of cancellous bone in adults is hypothesized to be reduced with aging, but can still be augmented with mechanical loading. To account for this reduced responsiveness, two mechanical parameters from Objective 1, peak diaphyseal strain and peak applied load, were separately applied to 2 groups of adult female mice for 2 weeks to determine which loading protocol was more osteogenic. In addition, the adaptive responses the cortical and cancellous compartments of the tibia and the cancellous adaptive responses of adult and growing mice were compared. Cancellous bone mass, architecture, and dynamic formation in the proximal metaphysis were compared between loaded and control limbs via micro-computed tomography and histomorphometry. Finite element models of the proximal metaphysis were generated to characterize the cancellous tissue strains induced by tibial

compression and the changes in metaphyseal stiffness following loading-induced adaptation.

Objective 3

Assessing the efficacy of using mechanical loading to increase cancellous mass in the target population of elderly, osteoporotic, post-menopausal women is critical. Estrogen deficiency may alter the ability of bone to respond to mechanical signals [27, 28]. Therefore, understanding how aging and estrogen deficiency modulate bone functional adaptation is essential to overcoming the skeleton's failure to respond appropriately to mechanical signals. Tibial loading was hypothesized to prevent cancellous bone loss due to estrogen deficiency in adult female mice. Ovariectomized female mice underwent tibial compression for 1, 2, and 6 weeks to determine the time-related changes in cancellous mass and architecture due to loading and OVX. Cancellous bone mass, architecture, and dynamic formation in the proximal metaphysis were compared between loaded and control limbs via micro-computed tomography and histomorphometry.

1.9 Methods

For each study, common methods were used to assess the adaptive changes in bone mass and architecture. To select the mechanical parameters of the loading waveform, specifically the peak applied load and resulting mid-diaphyseal deformation, diaphyseal stiffness was determined by in vivo strain gauging. Dynamic indices of bone formation and resorption during in vivo loading were assessed using fluorochrome-labeled histomorphometry. Loading-induced changes in bone mass and architecture were,determined using micro-computed tomography (microCT) scans.

The microCT scans were used to generate finite element models, from which metaphyseal stiffness and cancellous tissue strains during loading were calculated.

In Vivo Strain Gauging

Prior to tibial compression experiments, in vivo strain gauging was used to determine the relationship between peak applied load and the resulting strain at the medial mid-shaft, called diaphyseal stiffness (N/με). From diaphyseal stiffness, the peak applied load was chosen to engender +1200 με, which is a typical strain value across many vertebrates during normal locomotion [154, 155]. While the mouse was anesthetized, a single uniaxial strain gauge was attached to the medial mid-shaft of the tibia. Next, as the mouse underwent tibial compression, strain data from the gauge and force data from the load cell (Fig 1.7) were recorded simultaneously. From these data, the relationship between applied peak force and mid-shaft strains was determined. To assess the effects of tibial compression on diaphyseal stiffness, this relationship was determined in a subset of mice following completion of loading experiments.

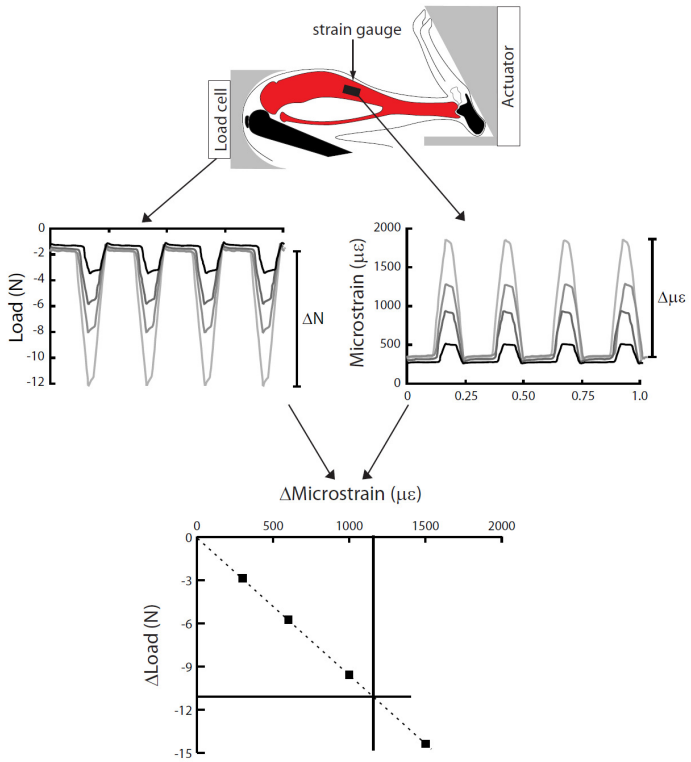

Figure 1.7 Schematic of the in vivo strain gauging procedure. Top to bottom: A single strain gauge is attached to the medial mid-shaft of the tibial. During tibial compression (see loading waveform in Fig. 1.6c), strain and load measurements are recorded simultaneously. From these measurements (data points), the relationship between peak applied load and resulting mid-diaphyseal strain, diaphyseal stiffness (N/με) (dashed line), is determined. Diaphyseal stiffness is used to determine the peak compressive load required to engender +1200 με.

Histomorphometry

Dynamic indices of in vivo bone formation and resorption were assessed using fluorochrome-labeled histomorphometry. The flourochrome labels attach to free calcium and are immediately incorporated into the bone matrix as bone formation is occurring. Two labels are injected at separate time points during an experiment and reflect the combined effects of osteoblast output and number at the time of injection.

Following euthanasia, tibiae were dissected free of soft tissue, fixed in 10% neutral buffered formalin for 48 hrs, then stored in 70% ethanol. Undecalcified tibiae were embedded in methyl methacrylate, then sectioned into 7 μm thick slides for

histomorphometric analysis using fluorescence microscopy. The length of the labels within a section is the mineralizing or labeled surface (LS/BS, %). The distance between the two labels divided by the time interval between the injection time points is the mineral apposition rate (MAR, μm/day), the rate at which bone is being formed. These two measures multiplied together is the bone formation rate (BFR, μm/yr), which combines the total surface being mineralized and how much bone is being laid down at that surface. Bone resorption is assessed by measuring the eroded surface (ES/BS, %), an indication of osteoclast activity [156, 157].

Micro-computed Tomography (microCT)

Following tibial compression, all pairs of tibiae were scanned using quantitative micro-computed tomography (microCT) to assess loading-induced changes in bone mass and architecture. MicroCT is a high-resolution, 3-dimensional (3D) CT scanner (Fig. 1.8). As the tibia rotates within the scanner at pre-determined angular intervals, a series of 2-dimensional images are taken. A full 3D image is constructed from the 2D images. The x-ray attenuation of each voxel is linearly correlated with mineral density based on the attenuation values of several phantom of standard calibration material [92]. From this correlation, grayscale values are converted to quantitative density measures. Within each image of a single tibia, a purely cancellous volume of interest (VOI) within the proximal metaphysis and a purely cortical VOI at the mid-diaphysis is isolated for analysis.

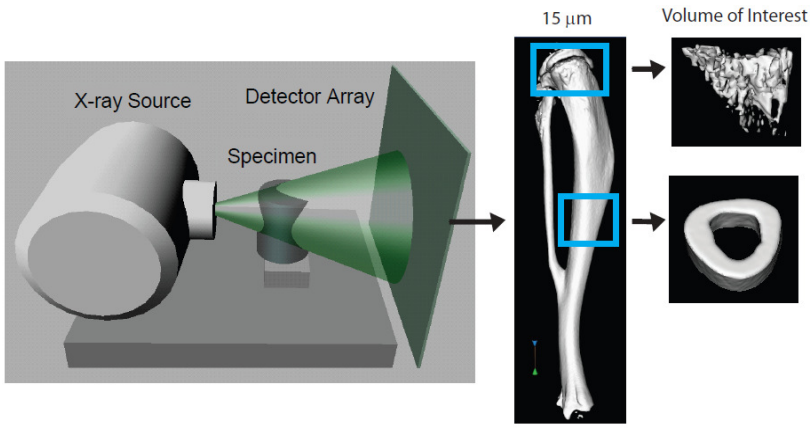

Figure 1.8 Schematic of micro-computed tomography (microCT). Left to right: A specimen is placed in the scanner between the x-ray source and the detector [REF?]. The specimen rotates within the scanner. At a specified angular interval, a single 2-dimensionsal image (2D) is taken. All the 2D images are converted into a single 3-dimensional (3D) image, comprised of 3D voxels of 15 µm resolution. Within the 3D image, volumes of interest (VOIs) are isolated. In the proximal metaphysis, a purely cancellous VOI is defined. At the tibial mid-shaft, a purely cortical VOI is defined.

For each VOI, a binary global threshold was used to segment mineralized tissue from water and soft tissue. The threshold was determined based on the bimodal histogram of the VOI, which is the relative frequency of x-ray attenuation values for all voxels within the VOI (Fig. 1.9). The cancellous threshold was 0.27 g/cc (1100 HU [92]). The cortical threshold was selected as 1/3 cortical bone peak.

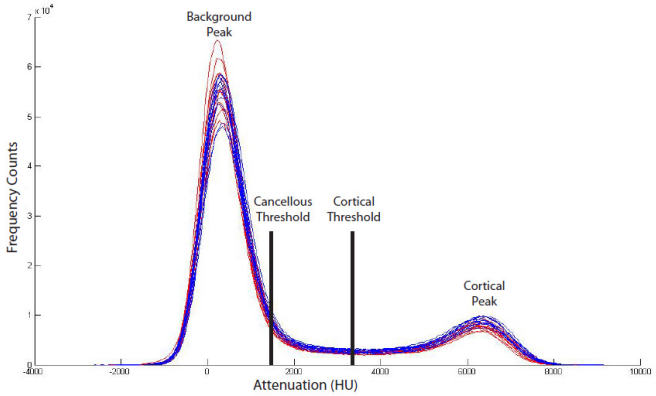

Figure 1.9 Representative histogram of a microCT VOI. The global threshold for analysis of cancellous bone was 0.27 g/cc. The global threshold for analysis of cortical was 1/3 cortical peak.

Loading-induced changes were assessed by comparing loaded limbs to control limbs. Cancellous mass was assessed by bone volume fraction (BV/TV) and tissue mineral density (tBMD, mg/cc), and cancellous architecture was assessed by trabecular thickness and trabecular separation (Tb.Th, Tb.Sp, μm). Cortical mass was assessed by cortical and medullary areas (A_C, A_M, respectively, mm^2), and cortical geometry was assessed by maximum and minimum moments of inertia (I_{MAX}, I_{MIN}, respectively, mm^4). Tibial morphology was assessed by whole bone radii of curvature in the anterioposterior and mediolateral directions (C_{AP}, C_{ML}, respectively, mm).

Finite Element (FE) Analysis

Finite element (FE) models of a subset of control limbs were created to assess the tissue strains in the proximal metaphysis during in vivo loading and to characterize loading-induced changes in the stiffness of the proximal metaphysis. FE VOIs were defined within the proximal metaphysis, centered within the microCT VOIs (Fig. 1.10). MicroCT scans were coarsened by combining 2x2x2 voxels to yield a single voxel with side length 0.03 mm, and coarsened voxels were converted into 8-noded linear brick elements. Elements were assigned isotropic material properties with a uniform modulus of 20 GPa and a Poisson's ratio of 0.3 [158]. Nodes at the distal surface of the model were restricted to in-plane motion and prevented from rigid-body motion. A uniformly-applied displacement was applied to the distal surface of the models.

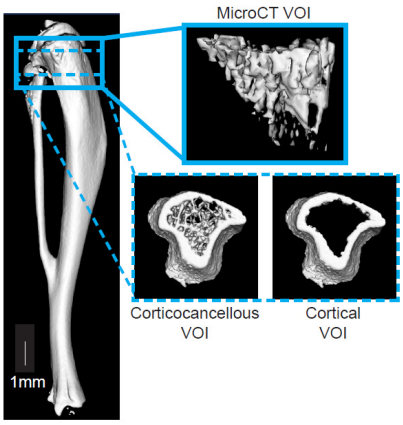

Figure 1.10 Representative cancellous VOIs used for microCT, and representative VOIs used to generate corticocancellous and cortical finite element models.

To characterize cancellous tissue strains during tibial loading, the applied displacement corresponded to the reaction force at the distal surface of the model that was equivalent to the peak load magnitude applied during tibial compression. Elements were identified in the corticocancellous models of control limbs that coincided with the cancellous microCT VOIs. Longitudinal strains were calculated at the element centroids.

To characterize the loading-induced changes in the apparent stiffness of the proximal metaphysis, the reaction force (N) was calculated for a uniform strain of -0.1% applied to the proximal surface of corticocancellous and cortical models. The proportion of the load transmitted through the cancellous tissue was determined from the ratio of the cortical to corticocancellous reaction forces, an indicator of load sharing between the metaphyseal cortex and cancellous tissue.

REFERENCES

1. Burge, R., Dawson-Hughes, B., Solomon, D. H., Wong, J. B., King, A., and Tosteson, A. Incidence and economic burden of osteoporosis-related fractures in the United States, 2005-2025. J Bone Miner Res 22*:*465-75; 2007.
2. Census Bureau, U. S. National Population Projections. U.S. Population Projections; 2009.
3. Vesterby, A., Mosekilde, L., Gundersen, H. J. G., Melsen, F., Mosekilde, L., Holme, K., and Sørensen, S. Biologically meaningful determinants of the in vitro strength of lumber vertebrae. Bone 12*:*219-224; 1991.
4. Mosekilde, L. Sex differences in age-related loss of vertebral trabecular bone mass and structure -- biomechanical consequences. Bone 10*:*425-432; 1989.
5. Riggs, B. L., Khosla, S., and Melton, L. J., 3rd Sex steroids and the construction and conservation of the adult skeleton. Endocr Rev 23*:*279-302; 2002.
6. NOF America's Bone Health: The State of Osteoporosis and Low Bone Mass in Our Nation. National Osteoporosis Foundation; 2002.
7. Riggs, B. L., Khosla, S., and Melton, L. J., 3rd A unitary model for involutional osteoporosis: estrogen deficiency causes both type I and type II osteoporosis in postmenopausal women and contributes to bone loss in aging men. J Bone Miner Res 13*:*763-73; 1998.
8. Manolagas, S. C. Birth and death of bone cells: basic regulatory mechanisms and implications for the pathogenesis and treatment of osteoporosis. Endocr Rev 21*:*115-37; 2000.
9. Schaffler, M. B. Role of bone turnover in microdamage. Osteoporos Int 14 Suppl 5*:*S73-7; discussion S77-80; 2003.

10. Canalis, E., Giustina, A., and Bilezikian, J. P. Mechanisms of anabolic therapies for osteoporosis. N Engl J Med 357*:*905-16; 2007.

11. Riggs, B. L., and Melton, L. J., 3rd Involutional osteoporosis. N Engl J Med 314*:*1676-86; 1986.

12. Parfitt, A. M. Age-related structural changes in trabecular and cortical bone: cellular mechanisms and biomechanical consequences. Calcif Tissue Int 36 Suppl 1*:*S123-8; 1984.

13. Parfitt, A. M., Mathews, C. H., Villanueva, A. R., Kleerekoper, M., Frame, B., and Rao, D. S. Relationships between surface, volume, and thickness of iliac trabecular bone in aging and in osteoporosis. Implications for the microanatomic and cellular mechanisms of bone loss. J Clin Invest 72*:*1396-409; 1983.

14. Riggs, B. L., and Melton, L. J., 3rd Evidence for two distinct syndromes of involutional osteoporosis. Am J Med 75*:*899-901; 1983.

15. Lindsay, R., Hart, D. M., Aitken, J. M., MacDonald, E. B., Anderson, J. B., and Clarke, A. C. Long-term prevention of postmenopausal osteoporosis by oestrogen. Evidence for an increased bone mass after delayed onset of oestrogen treatment. Lancet 1*:*1038-41; 1976.

16. Windahl, S. H., Andersson, G., and Gustafsson, J. A. Elucidation of estrogen receptor function in bone with the use of mouse models. Trends Endocrinol Metab 13*:*195-200; 2002.

17. Martino, S., Cauley, J. A., Barrett-Connor, E., Powles, T. J., Mershon, J., Disch, D., Secrest, R. J., and Cummings, S. R. Continuing outcomes relevant to Evista: breast cancer incidence in postmenopausal osteoporotic women in a randomized trial of raloxifene. J Natl Cancer Inst 96*:*1751-61; 2004.

18. Canalis, E. Update in new anabolic therapies for osteoporosis. J Clin Endocrinol Metab 95*:*1496-504; 2010.

19. Neer, R. M., Arnaud, C. D., Zanchetta, J. R., Prince, R., Gaich, G. A., Reginster, J. Y., Hodsman, A. B., Eriksen, E. F., Ish-Shalom, S., Genant, H. K., Wang, O., and Mitlak, B. H. Effect of parathyroid hormone (1-34) on fractures and bone mineral density in postmenopausal women with osteoporosis. N Engl J Med 344*:*1434-41; 2001.

20. Blahos, J. Treatment and prevention of osteoporosis. Wien Med Wochenschr 157*:*589-92; 2007.

21. Wolff, J. The law of bone remodeling. Berlin: Springer-Verlag; 1892.

22. Lanyon, L. E. Mechanical function and bone remodeling. In: Sumner-Smith G, editor: Bone in clinical orthopaedics.*:*273-304; 1982.

23. Vico, L., Collet, P., Guignandon, A., Lafage-Proust, M. H., Thomas, T., Rehaillia, M., and Alexandre, C. Effects of long-term microgravity exposure on cancellous and cortical weight-bearing bones of cosmonauts. Lancet 355*:*1607-11; 2000.

24. Donaldson, C. L., Hulley, S. B., Vogel, J. M., Hattner, R. S., Bayers, J. H., and McMillan, D. E. Effect of prolonged bed rest on bone mineral. Metab. 19*:*1071-1084; 1970.

25. Aarden, E. M., Burger, E. H., and Nijweide, P. J. Function of osteocytes in bone. J Cell Biochem 55*:*287-99; 1994.

26. Pearson, O. M., and Lieberman, D. E. The aging of Wolff's "law": ontogeny and responses to mechanical loading in cortical bone. Am J Phys Anthropol Suppl 39*:*63-99; 2004.

27. Turner, R. T. Mechanical signaling in the development of postmenopausal osteoporosis. Lupus 8*:*388-92; 1999.

28. Ehrlich, P. J., and Lanyon, L. E. Mechanical strain and bone cell function: a review. Osteoporos Int 13*:*688-700; 2002.

29. Lanyon, L. E. Using functional loading to influence bone mass and architecture: objectives, mechanisms, and relationship with estrogen of the mechanically adaptive process in bone. Bone 18*:*37S-43S; 1996.

30. Westerlind, K. C., Wronski, T. J., Ritman, E. L., Luo, Z. P., An, K. N., Bell, N. H., and Turner, R. T. Estrogen regulates the rate of bone turnover but bone balance in ovariectomized rats is modulated by prevailing mechanical strain. Proc Natl Acad Sci U S A 94*:*4199-204; 1997.

31. Kontulainen, S., Sievanen, H., Kannus, P., Pasanen, M., and Vuori, I. Effect of long-term impact-loading on mass, size, and estimated strength of humerus and radius of female racquet-sports players: a peripheral quantitative computed tomography study between young and old starters and controls. J Bone Miner Res 18*:*352-9; 2003.

32. Haapasalo, H., Kannus, P., Sievanen, H., Heinonen, A., Oja, P., and Vuori, I. Long-term unilateral loading and bone mineral density and content in female squash players. Calcif Tissue Int 54*:*249-55; 1994.

33. Kannus, P., Haapasalo, H., Sankelo, M., Sievanen, H., Pasanen, M., Heinonen, A., Oja, P., and Vuori, I. Effect of starting age of physical activity on bone mass in the dominant arm of tennis and squash players. Ann Intern Med 123*:*27-31; 1995.

34. Fuchs, R. K., Bauer, J. J., and Snow, C. M. Jumping improves hip and lumbar spine bone mass in prepubescent children: a randomized controlled trial. J Bone Miner Res 16*:*148-56; 2001.

35. Bass, S. L., Saxon, L., Daly, R. M., Turner, C. H., Robling, A. G., Seeman, E., and Stuckey, S. The effect of mechanical loading on the size and shape of bone

in pre-, peri-, and postpubertal girls: a study in tennis players. J Bone Miner Res 17:2274-80; 2002.

36. Heinonen, A., Sievanen, H., Kannus, P., Oja, P., Pasanen, M., and Vuori, I. High-impact exercise and bones of growing girls: a 9-month controlled trial. Osteoporos Int 11:1010-7; 2000.

37. Nordstrom, A., Karlsson, C., Nyquist, F., Olsson, T., Nordstrom, P., and Karlsson, M. Bone loss and fracture risk after reduced physical activity. J Bone Miner Res 20:202-7; 2005.

38. Kudlac, J., Nichols, D. L., Sanborn, C. F., and DiMarco, N. M. Impact of detraining on bone loss in former collegiate female gymnasts. Calcif Tissue Int 75:482-7; 2004.

39. Valdimarsson, O., Alborg, H. G., Duppe, H., Nyquist, F., and Karlsson, M. Reduced training is associated with increased loss of BMD. J Bone Miner Res 20:906-12; 2005.

40. Bass, S., Pearce, G., Bradney, M., Hendrich, E., Delmas, P. D., Harding, A., and Seeman, E. Exercise before puberty may confer residual benefits in bone density in adulthood: studies in active prepubertal and retired female gymnasts. J Bone Miner Res 13:500-7; 1998.

41. Karlsson, M. K., Linden, C., Karlsson, C., Johnell, O., Obrant, K., and Seeman, E. Exercise during growth and bone mineral density and fractures in old age. Lancet 355:469-70; 2000.

42. Fuchs, R. K., and Snow, C. M. Gains in hip bone mass from high-impact training are maintained: a randomized controlled trial in children. J Pediatr 141:357-62; 2002.

43. Warden, S. J., Fuchs, R. K., Castillo, A. B., Nelson, I. R., and Turner, C. H. Exercise when young provides lifelong benefits to bone structure and strength. J Bone Miner Res 22*:*251-9; 2007.

44. Warden, S. J., Fuchs, R. K., Castillo, A. B., and Turner, C. H. Mechanical loading during growth has long-term benefits to skeletal health. Amer Soc Bone Miner Res, pp. 1170. Nashville, TN; 2005.

45. Daly, R. M. The effect of exercise on bone mass and structural geometry during growth. Med Sport Sci 51*:*33-49; 2007.

46. Ward, K. A., Roberts, S. A., Adams, J. E., and Mughal, M. Z. Bone geometry and density in the skeleton of pre-pubertal gymnasts and school children. Bone 36*:*1012-8; 2005.

47. Valdimarsson, O., Sigurdsson, G., Steingrimsdottir, L., and Karlsson, M. K. Physical activity in the post-pubertal period is associated with maintenance of pre-pubertal high bone density-- a 5-year follow-up. Scand J Med Sci Sports 15*:*280-6; 2005.

48. Winters-Stone, K. M., and Snow, C. M. Site-specific response of bone to exercise in premenopausal women. Bone 39*:*1203-9; 2006.

49. Vainionpaa, A., Korpelainen, R., Leppaluoto, J., and Jamsa, T. Effects of high-impact exercise on bone mineral density: a randomized controlled trial in premenopausal women. Osteoporos Int 16*:*191-7; 2005.

50. Heinonen, A., Kannus, P., Sievanen, H., Oja, P., Pasanen, M., Rinne, M., Uusi-Rasi, K., and Vuori, I. Randomised controlled trial of effect of high-impact exercise on selected risk factors for osteoporotic fractures. Lancet 348*:*1343-7; 1996.

51. Friedlander, A. L., Genant, H. K., Sadowsky, S., Byl, N. N., and Gluer, C. C. A two-year program of aerobics and weight training enhances bone mineral density of young women. J Bone Miner Res 10*:*574-85; 1995.

52. Bassey, E. J., and Ramsdale, S. J. Increase in femoral bone density in young women following high-impact exercise. Osteoporos Int 4*:*72-5; 1994.

53. Vainionpaa, A., Korpelainen, R., Sievanen, H., Vihriala, E., Leppaluoto, J., and Jamsa, T. Effect of impact exercise and its intensity on bone geometry at weight-bearing tibia and femur. Bone 40*:*604-11; 2007.

54. Vainionpaa, A., Korpelainen, R., Vihriala, E., Rinta-Paavola, A., Leppaluoto, J., and Jamsa, T. Intensity of exercise is associated with bone density change in premenopausal women. Osteoporos Int 17*:*455-63; 2006.

55. Ahola, R., Korpelainen, R., Vainionpaa, A., Leppaluoto, J., and Jamsa, T. Time-course of exercise and its association with 12-month bone changes. BMC Musculoskelet Disord 10*:*138; 2009.

56. Winters, K. M., and Snow, C. M. Detraining reverses positive effects of exercise on the musculoskeletal system in premenopausal women. J Bone Miner Res 15*:*2495-503; 2000.

57. Sinaki, M., Itoi, E., Wahner, H. W., Wollan, P., Gelzcer, R., Mullan, B. P., Collins, D. A., and Hodgson, S. F. Stronger back muscles reduce the incidence of vertebral fractures: a prospective 10 year follow-up of postmenopausal women. Bone 30*:*836-41; 2002.

58. Kerr, D., Ackland, T., Maslen, B., Morton, A., and Prince, R. Resistance training over 2 years increases bone mass in calcium-replete postmenopausal women. J Bone Miner Res 16*:*175-81; 2001.

59. Kohrt, W. M., Ehsani, A. A., and Birge, S. J., Jr. Effects of exercise involving predominantly either joint-reaction or ground-reaction forces on bone mineral density in older women. J Bone Miner Res 12*:*1253-61; 1997.

60. Kerr, D., Morton, A., Dick, I., and Prince, R. Exercise effects on bone mass in postmenopausal women are site-specific and load-dependent. J Bone Miner Res 11*:*218-25; 1996.

61. Kohrt, W. M., Snead, D. B., Slatopolsky, E., and Birge SJ, J. r. Additive effects of weight-bearing exercise and estrogen on bone mineral density in older women. J Bone Miner Res 10*:*1303-1311; 1995.

62. Engelke, K., Kemmler, W., Lauber, D., Beeskow, C., Pintag, R., and Kalender, W. A. Exercise maintains bone density at spine and hip EFOPS: a 3-year longitudinal study in early postmenopausal women. Osteoporos Int 17*:*133-42; 2006.

63. von Stengel, S., Kemmler, W., Kalender, W. A., Engelke, K., and Lauber, D. Differential effects of strength versus power training on bone mineral density in postmenopausal women: a 2-year longitudinal study. Br J Sports Med 41*:*649-55; discussion 655; 2007.

64. Snow, C. M., Shaw, J. M., Winters, K. M., and Witzke, K. A. Long-term exercise using weighted vests prevents hip bone loss in postmenopausal women. J Gerontol A Biol Sci Med Sci 55*:*M489-91; 2000.

65. Pruitt, L. A., Taaffe, D. R., and Marcus, R. Effects of a one-year high-intensity versus low-intensity resistance training program on bone mineral density in older women. J Bone Miner Res 10*:*1788-95; 1995.

66. Hert, J., Liskova, M., and Landa, J. Reaction of bone to mechanical stimuli. 1. Continuous and intermittent loading of tibia in rabbit. Folia Morphol (Praha) 19*:*290-300; 1971.

67. Liskova, M., and Hert, J. Reaction of bone to mechanical stimuli. 2. Periosteal and endosteal reaction of tibial diaphysis in rabbit to intermittent loading. Folia Morphol (Praha) 19*:*301-17; 1971.

68. Lanyon, L. E., and Rubin, C. T. Static vs dynamic loads as an influence on bone remodelling. J Biomech 17*:*897-905; 1984.

69. Goodship, A. E., Lanyon, L. E., and McFie, H. Functional adaptation of bone to increased stress. An experimental study. J Bone Joint Surg Am 61*:*539-46; 1979.

70. Churches, A. E., and Howlett, C. R. Functional adaptation of bone in response to sinusoidally varying controlled compressive loading of the ovine metacarpus. Clin Orthop Relat Res*:*265-80; 1982.

71. O'Connor, J. A., Lanyon, L. E., and MacFie, H. The influence of strain rate on adaptive bone remodelling. J Biomech 15*:*767-81; 1982.

72. Robling, A. G., Burr, D. B., and Turner, C. H. Partitioning a daily mechanical stimulus into discrete loading bouts improves the osteogenic response to loading. J Bone Miner Res 15*:*1596-602; 2000.

73. LaMothe, J. M., Hamilton, N. H., and Zernicke, R. F. Strain rate influences periosteal adaptation in mature bone. Med Eng Phys 27*:*277-84; 2005.

74. Mosley, J. R., March, B. M., Lynch, J., and Lanyon, L. E. Strain magnitude related changes in whole bone architecture in growing rats. Bone 20*:*191-8; 1997.

75. Goldstein, S. A., Matthews, L. S., Kuhn, J. L., and Hollister, S. J. Trabecular bone remodeling: an experimental model. J Biomech 24 Suppl 1*:*135-50; 1991.

76. van der Meulen, M. C., Morgan, T. G., Yang, X., Baldini, T. H., Myers, E. R., Wright, T. M., and Bostrom, M. P. Cancellous bone adaptation to in vivo loading in a rabbit model. Bone 38*:*871-7; 2006.

77. Judex, S., Lei, X., Han, D., and Rubin, C. Low-magnitude mechanical signals that stimulate bone formation in the ovariectomized rat are dependent on the applied frequency but not on the strain magnitude. J Biomech 40*:*1333-9; 2007.

78. Rubin, C., Turner, A. S., Muller, R., Mittra, E., McLeod, K., Lin, W., and Qin, Y. X. Quantity and quality of trabecular bone in the femur are enhanced by a strongly anabolic, noninvasive mechanical intervention. J Bone Miner Res 17*:*349-57; 2002.

79. Verschueren, S. M., Roelants, M., Delecluse, C., Swinnen, S., Vanderschueren, D., and Boonen, S. Effect of 6-month whole body vibration training on hip density, muscle strength, and postural control in postmenopausal women: a randomized controlled pilot study. J Bone Miner Res 19*:*352-9; 2004.

80. Kiiski, J., Heinonen, A., Jarvinen, T. L., Kannus, P., and Sievanen, H. Transmission of vertical whole body vibration to the human body. J Bone Miner Res 23*:*1318-25; 2008.

81. Rubin, C., Recker, R., Cullen, D., Ryaby, J., McCabe, J., and McLeod, K. Prevention of postmenopausal bone loss by a low-magnitude, high-frequency mechanical stimuli: a clinical trial assessing compliance, efficacy, and safety. J Bone Miner Res 19*:*343-51; 2004.

82. Brouwers, J. E., van Rietbergen, B., Ito, K., and Huiskes, R. Effects of vibration treatment on tibial bone of ovariectomized rats analyzed by in vivo micro-CT. J Orthop Res 28*:*62-9; 2010.

83. Sehmisch, S., Galal, R., Kolios, L., Tezval, M., Dullin, C., Zimmer, S., Stuermer, K. M., and Stuermer, E. K. Effects of low-magnitude, high-frequency mechanical stimulation in the rat osteopenia model. Osteoporos Int 20*:*1999-2008; 2009.

84. Christiansen, B. A., Kotiya, A. A., and Silva, M. J. Constrained tibial vibration does not produce an anabolic bone response in adult mice. Bone 45*:*750-9; 2009.

85. Kim, B. T., Mosekilde, L., Duan, Y., Zhang, X. Z., Tornvig, L., Thomsen, J. S., and Seeman, E. The structural and hormonal basis of sex differences in peak appendicular bone strength in rats. J Bone Miner Res 18*:*150-5; 2003.

86. Abe, T., Chow, J. W., Lean, J. M., and Chambers, T. J. Estrogen does not restore bone lost after ovariectomy in the rat. J Bone Miner Res 8*:*831-8; 1993.

87. Jagger, C. J., Chambers, T. J., and Chow, J. W. Stimulation of bone formation by dynamic mechanical loading of rat caudal vertebrae is not suppressed by 3-amino-1-hydroxypropylidene-1-bisphosphonate (AHPrBP). Bone 16*:*309-13; 1995.

88. Chow, J. W., Wilson, A. J., Chambers, T. J., and Fox, S. W. Mechanical loading stimulates bone formation by reactivation of bone lining cells in 13-week-old rats. J Bone Miner Res 13*:*1760-7; 1998.

89. Webster, D., Wasserman, E., Ehrbar, M., Weber, F., Bab, I., and Muller, R. Mechanical loading of mouse caudal vertebrae increases trabecular and cortical bone mass-dependence on dose and genotype. Biomech Model Mechanobiol; 2010.

90. Sugiyama, T., Saxon, L. K., Zaman, G., Moustafa, A., Sunters, A., Price, J. S., and Lanyon, L. E. Mechanical loading enhances the anabolic effects of intermittent parathyroid hormone (1-34) on trabecular and cortical bone in mice. Bone 43*:*238-48; 2008.

91. Marenzana, M., De Souza, R. L., and Chenu, C. Blockade of beta-adrenergic signaling does not influence the bone mechano-adaptive response in mice. Bone 41*:*206-15; 2007.

92. Fritton, J. C., Myers, E. R., Wright, T. M., and van der Meulen, M. C. Loading induces site-specific increases in mineral content assessed by microcomputed tomography of the mouse tibia. Bone 36*:*1030-8; 2005.

93. De Souza, R. L., Matsuura, M., Eckstein, F., Rawlinson, S. C., Lanyon, L. E., and Pitsillides, A. A. Non-invasive axial loading of mouse tibiae increases cortical bone formation and modifies trabecular organization: a new model to study cortical and cancellous compartments in a single loaded element. Bone 37*:*810-8; 2005.

94. Sugiyama, T., Price, J. S., and Lanyon, L. E. Functional adaptation to mechanical loading in both cortical and cancellous bone is controlled locally and is confined to the loaded bones. Bone 46*:*314-21; 2010.

95. Moustafa, A., Sugiyama, T., Saxon, L. K., Zaman, G., Sunters, A., Armstrong, V. J., Javaheri, B., Lanyon, L. E., and Price, J. S. The mouse fibula as a suitable bone for the study of functional adaptation to mechanical loading. Bone 44*:*930-5; 2009.

96. Fritton, J. C., Myers, E. R., Wright, T. M., and van der Meulen, M. C. Bone mass is preserved and cancellous architecture altered due to cyclic loading of the mouse tibia after orchidectomy. J Bone Miner Res 23*:*663-71; 2008.

97. Borer, K. T. Physical activity in the prevention and amelioration of osteoporosis in women : interaction of mechanical, hormonal and dietary factors. Sports Med 35*:*779-830; 2005.

98. Karlsson, M. K. Does exercise during growth prevent fractures in later life? Med Sport Sci 51*:*121-36; 2007.

99. Tabensky, A., Duan, Y., Edmonds, J., and Seeman, E. The contribution of reduced peak accrual of bone and age-related bone loss to osteoporosis at the

spine and hip: insights from the daughters of women with vertebral or hip fractures. J Bone Miner Res 16*:*1101-7; 2001.

100. Ryan, A. S., Ivey, F. M., Hurlbut, D. E., Martel, G. F., Lemmer, J. T., Sorkin, J. D., Metter, E. J., Fleg, J. L., and Hurley, B. F. Regional bone mineral density after resistive training in young and older men and women. Scand J Med Sci Sports 14*:*16-23; 2004.

101. Jarvinen, T. L., Kannus, P., Pajamaki, I., Vuohelainen, T., Tuukkanen, J., Jarvinen, M., and Sievanen, H. Estrogen deposits extra mineral into bones of female rats in puberty, but simultaneously seems to suppress the responsiveness of female skeleton to mechanical loading. Bone 32*:*642-51; 2003.

102. Mosley, J. R., and Lanyon, L. E. Growth rate rather than gender determines the size of the adaptive response of the growing skeleton to mechanical strain. Bone 30*:*314-9; 2002.

103. Bassey, E. J., Rothwell, M. C., Littlewood, J. J., and Pye, D. W. Pre- and postmenopausal women have different bone mineral density responses to the same high-impact exercise. J Bone Miner Res 13*:*1805-13; 1998.

104. Rubin, C. T., Bain, S. D., and McLeod, K. J. Suppression of the osteogenic response in the aging skeleton. Calcif Tissue Int 50*:*306-13; 1992.

105. Turner, C. H., Forwood, M. R., Rho, J. Y., and Yoshikawa, T. Mechanical loading thresholds for lamellar and woven bone formation. J Bone Miner Res 9*:*87-97; 1994.

106. Turner, C. H., Takano, Y., and Owan, I. Aging changes mechanical loading thresholds for bone formation in rats. J Bone Miner Res 10*:*1544-9; 1995.

107. Srinivasan, S., Agans, S. C., King, K. A., Moy, N. Y., Poliachik, S. L., and Gross, T. S. Enabling bone formation in the aged skeleton via rest-inserted mechanical loading. Bone 33*:*946-55; 2003.

108. Brodt, M. D., and Silva, M. J. Aged mice have enhanced endocortical response and normal periosteal response compared to young-adult mice following 1 week of axial tibial compression. J Bone Miner Res; 2010.

109. Hoshi, A., Watanabe, H., Chiba, M., and Inaba, Y. Effects of exercise at different ages on bone density and mechanical properties of femoral bone of aged mice. Tohoku J Exp Med 185*:*15-24; 1998.

110. Silbermann, M., Bar-Shira-Maymon, B., Coleman, R., Reznick, A., Weisman, Y., Steinhagen-Thiessen, E., von der Mark, H., and von der Mark, K. Long-term physical exercise retards trabecular bone loss in lumbar vertebrae of aging female mice. Calcif Tissue Int 46*:*80-93; 1990.

111. Leppanen, O. V., Sievanen, H., Jokihaara, J., Pajamaki, I., Kannus, P., and Jarvinen, T. L. Pathogenesis of age-related osteoporosis: impaired mechano-responsiveness of bone is not the culprit. PLoS ONE 3*:*e2540; 2008.

112. Buhl, K. M., Jacobs, C. R., Turner, R. T., Evans, G. L., Farrell, P. A., and Donahue, H. J. Aged bone displays an increased responsiveness to low-intensity resistance exercise. J Appl Physiol 90*:*1359-64; 2001.

113. Jarvinen, T. L., Pajamaki, I., Sievanen, H., Vuohelainen, T., Tuukkanen, J., Jarvinen, M., and Kannus, P. Femoral neck response to exercise and subsequent deconditioning in young and adult rats. J Bone Miner Res 18*:*1292-9; 2003.

114. Raab, D., Smith, E., Crenshaw, T., and Thomas, D. Bone mechanical properties after exercise training in young and old rats. J Appl Physiol 68*:*130-134; 1990.

115. Umemura, Y., Ishiko, T., Tsujimoto, H., Miura, H., Mokushi, N., and Suzuki, H. Effects of jump training on bone hypertrophy in young and old rats. Int J Sports Med 16*:*364-7; 1995.

116. Schriefer, J. L., Warden, S. J., Saxon, L. K., Robling, A. G., and Turner, C. H. Cellular accommodation and the response of bone to mechanical loading. J Biomech 38*:*1838-45; 2005.

117. Srinivasan, S., Weimer, D. A., Agans, S. C., Bain, S. D., and Gross, T. S. Low-magnitude mechanical loading becomes osteogenic when rest is inserted between each load cycle. J Bone Miner Res 17*:*1613-20; 2002.

118. Robling, A. G., Hinant, F. M., Burr, D. B., and Turner, C. H. Shorter, more frequent mechanical loading sessions enhance bone mass. Med Sci Sports Exerc 34*:*196-202; 2002.

119. Main, R. P., Lynch, M. E., and Van der Meulen, M. C. H. In vivo tibial stiffness is maintained by whole bone morphology and cross-sectional geometry in growing female mice. Journal of Biomechanics; 2010.

120. Lynch, M. E., Main, R. P., Xu, Q., Walsh, D. J., Schaffler, M. B., Wright, T. M., and van der Meulen, M. C. H. Cancellous bone adaptation to tibial compression is not sex-dependent in growing mice. Journal of Applied Physiology; 2010.

121. Wronski, T. J., Cintron, M., and Dann, L. M. Temporal relationship between bone loss and increased bone turnover in overiectomized rats. Calcif. Tissue Int. 43*:*179-183; 1988.

122. Waarsing, J. H., Day, J. S., Verhaar, J. A., Ederveen, A. G., and Weinans, H. Bone loss dynamics result in trabecular alignment in aging and ovariectomized rats. J Orthop Res 24*:*926-35; 2006.

123. Mosekilde, L., Danielsen, C. C., and Knudsen, U. B. The effect of aging and ovariectomy on the vertebral bone mass and biomechanical properties of mature rats. Bone 14*:*1-6; 1993.

124. Wronski, T. J., Dann, L. M., Scott, K. S., and Cintron, M. Long-term effects of ovariectomy and aging on the rat skeleton. Calcif. Tissue Int. 45*:*360-366; 1989.

125. Baldock, P. A., Need, A. G., Moore, R. J., Durbridge, T. C., and Morris, H. A. Discordance between bone turnover and bone loss: effects of aging and ovariectomy in the rat. J Bone Miner Res 14*:*1442-8; 1999.

126. Ito, M., Nishida, A., Nakamura, T., Uetani, M., and Hayashi, K. Differences of three-dimensional trabecular microstructure in osteopenic rat models caused by ovariectomy and neurectomy. Bone 30*:*594-8; 2002.

127. Wronski, T. J., Cintron, M., Doherty, A. L., and Dann, L. M. Estrogen treatment prevents osteopenia and depresses bone turnover in ovariectomized rats. Endocrin. 123*:*681-686; 1988.

128. Chow, J., Tobias, J. H., Colston, K. W., and Chambers, T. J. Estrogen maintains trabecular bone volume in rats not only by suppression of bone resorption but also by stimulation of bone formation. J Clin Invest 89*:*74-8; 1992.

129. Li, C. Y., Schaffler, M. B., Wolde-Semait, H. T., Hernandez, C. J., and Jepsen, K. J. Genetic background influences cortical bone response to ovariectomy. J Bone Miner Res 20*:*2150-8; 2005.

130. Iwaniec, U. T., Yuan, D., Power, R. A., and Wronski, T. J. Strain-dependent variations in the response of cancellous bone to ovariectomy in mice. J Bone Miner Res 21*:*1068-74; 2006.

131. Bouxsein, M. L., Myers, K. S., Shultz, K. L., Donahue, L. R., Rosen, C. J., and Beamer, W. G. Ovariectomy-induced bone loss varies among inbred strains of mice. J Bone Miner Res 20:1085-92; 2005.

132. Klinck, J., and Boyd, S. K. The Magnitude and Rate of Bone Loss in Ovariectomized Mice Differs Among Inbred Strains as Determined by Longitudinal In vivo Micro-Computed Tomography. Calcif Tissue Int 83:70-9; 2008.

133. Sheng, M. H., Baylink, D. J., Beamer, W. G., Donahue, L. R., Rosen, C. J., Lau, K. H., and Wergedal, J. E. Histomorphometric studies show that bone formation and bone mineral apposition rates are greater in C3H/HeJ (high-density) than C57BL/6J (low-density) mice during growth. Bone 25:421-9; 1999.

134. Sheng, M. H., Baylink, D. J., Beamer, W. G., Donahue, L. R., Lau, K. H., and Wergedal, J. E. Regulation of bone volume is different in the metaphyses of the femur and vertebra of C3H/HeJ and C57BL/6J mice. Bone 30:486-91; 2002.

135. Beamer, W. G., Donahue, L. R., Rosen, C. J., and Baylink, D. J. Genetic variability in adult bone density among inbred strains of mice. Bone 18:397-403; 1996.

136. Robling, A. G., and Turner, C. H. Mechanotransduction in bone: genetic effects on mechanosensitivity in mice. Bone 31:562-9; 2002.

137. Akhter, M. P., Cullen, D. M., Pedersen, E. A., Kimmel, D. B., and Recker, R. R. Bone response to in vivo mechanical loading in two breeds of mice. Calcif Tissue Int 63:442-9; 1998.

138. Wright, L. E., Christian, P. J., Rivera, Z., Van Alstine, W. G., Funk, J. L., Bouxsein, M. L., and Hoyer, P. B. Comparison of Skeletal Effects of

Ovariectomy Versus Chemically-Induced Ovarian Failure in Mice. J Bone Miner Res; 2008.

139. Cano, A., Dapia, S., Noguera, I., Pineda, B., Hermenegildo, C., del Val, R., Caeiro, J. R., and Garcia-Perez, M. A. Comparative effects of 17beta-estradiol, raloxifene and genistein on bone 3D microarchitecture and volumetric bone mineral density in the ovariectomized mice. Osteoporos Int 19*:*793-800; 2008.

140. Modder, U. I., Riggs, B. L., Spelsberg, T. C., Fraser, D. G., Atkinson, E. J., Arnold, R., and Khosla, S. Dose-response of estrogen on bone versus the uterus in ovariectomized mice. Eur J Endocrinol 151*:*503-10; 2004.

141. Zhou, H., Iida-Klein, A., Lu, S. S., Ducayen-Knowles, M., Levine, L. R., Dempster, D. W., and Lindsay, R. Anabolic action of parathyroid hormone on cortical and cancellous bone differs between axial and appendicular skeletal sites in mice. Bone 32*:*513-20; 2003.

142. Emerton, K. B., Hu, B., Woo, A. A., Sinofsky, A., Hernandez, C., Majeska, R. J., Jepsen, K. J., and Schaffler, M. B. Osteocyte apoptosis and control of bone resorption following ovariectomy in mice. Bone 46*:*577-83.

143. Yeh, J. K., Aloia, J. F., Chen, M. M., Tierney, J. M., and Sprintz, S. Influence of exercise on cancellous bone of the aged female rat. J Bone Miner Res 8*:*1117-25; 1993.

144. Iwamoto, J., Takeda, T., and Ichimura, S. Effect of exercise on tibial and lumbar vertebral bone mass in mature osteopenic rats: bone histomorphometry study. J Orthop Sci 3*:*257-63; 1998.

145. Peng, Z. Q., Vaananen, H. K., and Tuukkanen, J. Ovariectomy-induced bone loss can be affected by different intensities of treadmill running exercise in rats. Calcif Tissue Int 60*:*441-8; 1997.

146. Notomi, T., Okimoto, N., Okazaki, Y., Nakamura, T., and Suzuki, M. Tower climbing exercise started 3 months after ovariectomy recovers bone strength of the femur and lumbar vertebrae in aged osteopenic rats. J Bone Miner Res 18*:*140-9; 2003.

147. Hagino, H., Raab, D. M., Kimmel, D. B., Akhter, M. P., and Recker, R. R. Effect of ovariectomy on bone response to in vivo external loading. J Bone Miner Res 8*:*347-57; 1993.

148. Somerville, J. M., Aspden, R. M., Armour, K. E., Armour, K. J., and Reid, D. M. Growth of C57BL/6 mice and the material and mechanical properties of cortical bone from the tibia. Calcif Tissue Int 74*:*469-75; 2004.

149. Price, C., Herman, B. C., Lufkin, T., Goldman, H. M., and Jepsen, K. J. Genetic variation in bone growth patterns defines adult mouse bone fragility. J Bone Miner Res 20*:*1983-91; 2005.

150. Glatt, V., Canalis, E., Stadmeyer, L., and Bouxsein, M. L. Age-related changes in trabecular architecture differ in female and male C57BL/6J mice. J Bone Miner Res 22*:*1197-207; 2007.

151. Ferguson, V. L., Ayers, R. A., Bateman, T. A., and Simske, S. J. Bone development and age-related bone loss in male C57BL/6J mice. Bone 33*:*387-98; 2003.

152. Brodt, M. D., Ellis, C. B., and Silva, M. J. Growing C57Bl/6 mice increase whole bone mechanical properties by increasing geometric and material properties. J Bone Miner Res 14*:*2159-66; 1999.

153. Turner, C. H. Three rules for bone adaptation to mechanical stimuli. Bone 23*:*399-407; 1998.

154. Biewener, A. A. Safety factors in bone strength. Calcif Tissue Int 53 Suppl 1*:*S68-74; 1993.

155. Rubin, C. T., and Lanyon, L. E. Dynamic strain similarity in vertebrates; an alternative to allometric limb bone scaling. J Theor Biol 107*:*321-7; 1984.

156. Parfitt, A. M., Drenzer, M. K., Glorieux, F. H., Kanis, J. A., Malluche, H., Meunier, P. J., Ott, S. M., and Recker, R. R. Bone histomorphometry: standardization of nomenclature, symbols, and units. J. Bone Miner. Res. 2*:*595-610; 1987.

157. Ott, S. M. Histomorphometric measurements of bone turnover, mineralization, and volume. Clin J Am Soc Nephrol 3 Suppl 3*:*S151-6; 2008.

158. van der Meulen, M. C., Yang, X., Morgan, T. G., and Bostrom, M. P. The effects of loading on cancellous bone in the rabbit. Clin Orthop Relat Res 467*:*2000-6; 2009.

CHAPTER 2[1]

CANCELLOUS BONE ADAPTATION TO TIBIAL COMPRESSION IS NOT SEX-DEPENDENT IN GROWING MICE

2.1 Introduction

The skeleton has the intrinsic ability to sense and respond to its mechanical environment, and this adaptive ability is most pronounced at young ages [1, 2]. Strategies designed to increase bone mass and alter architecture prior to the attainment of peak mass may be the most effective at reducing fracture risk when bone loss occurs [3-6]. Exercise studies in young adults suggest sexual dimorphism exists in the response to mechanical loading, but few comparisons have been made between female and male cohorts [7-10]. Differentiating sex-specific responses will enable mechanical loading strategies to be developed to maximize bone growth in both sexes.

Whether sex-specific factors affect the skeletal response to loading is unclear [7, 9-13]. Male tennis players have larger upper extremities, in both dominant and non-dominant arms, than females [9, 10]. Similarly, after resistive training, males had greater spinal and femoral mineral density [7]. However, extremely small sample sizes and short experimental duration limited the power of these studies and confounded interpretation. Additionally, the skeletons of male rodents, but not of females, were responsive to treadmill running [12, 13]. However, the mechanical environment induced in the skeleton during these activities was unknown. When similar *in vivo* loads were applied in rats, the cortical tissue of both sexes responded similarly to ulnar

[1] Lynch, M. E., Main, R. P., Xu, Q., Walsh, D. J., Schaffler, M. B., Wright, T. M., and van der Meulen, M. C. H. Cancellous bone adaptation to tibial compression is not sex-dependent in growing mice. *Journal of Applied Physiology*; 2010. Article in press, doi:10.1152/japplphysiol.00210.2010. Used with permission from The Am Physiol Soc.

compression [11]. To date, no study has examined the effect of sex on the anabolic response to controlled *in vivo* loading in the cancellous compartment of mice.

The mechanical environment in the skeleton is difficult to characterize during exercise studies, thus the characteristics of mechanical loading critical to anabolic bone adaptation have been examined by applying controlled *in vivo* loads in animal models. Functional adaptation has primarily been studied in the diaphyses of mammalian long bones [14-18]; however, most clinical skeletal fractures occur at sites with large volumes of cancellous bone, such as the hip, the spine, and the distal radius. Noninvasive compression has been used to apply physiological loads to the mouse tibia allowing the adaptive response of both cancellous and cortical sites to be investigated. *In vivo* tibial compression increased bone formation and mineral content in the metaphyses of healthy growing mice [19-22], prevented bone loss due to hormone-deficiency in growing male mice [23], and enhanced the effect of parathyroid hormone treatment in adult female mice [20]. Based on these studies, applied mechanical loads can be used to increase peak bone mass in the cancellous compartment in young subjects.

In this study, we applied *in vivo* tibial compression to growing, young adult male and female mice to determine if cancellous adaptation is sex-dependent during skeletal growth. We applied peak loads that engendered similar physiological diaphyseal and metaphyseal strains in both sexes [24-27]. Bone mass, architecture, and dynamic formation in the proximal metaphysis in response to dynamic mechanical loading were compared between males and females via micro-computed tomography and histomorphometry. The mechanical environment in the proximal metaphysis during loading was characterized using finite element analysis.

2.2 Materials and Methods

Animals

Nine week old male and female C57Bl/6 mice (Jackson Labs) were acclimatized in our facility for one week. Mice were housed by sex in groups of 4 to 5 with *ad libitum* access to food and water. Body masses were recorded daily and used to monitor the health of the mice over the course of the experiment. At the start of the experiment, male and female mice weighed 22.3±1.3 g and 16.9±0.8 g, respectively. All experimental procedures were approved by Cornell University's Institutional Animal Care and Use Committee.

In vivo Load-Strain Calibration

The relationship between applied compression and bone tissue deformation for the left tibia was established for 10 week old mice *in vivo* (n=5/sex). This relationship was used to determine the applied load that engendered +1200 με at the medial midshaft of the tibia [19, 22]. This strain magnitude corresponded to peak strain values in the rat ulna during unrestricted running [26] and typical peak strain values in a number of vertebrates during normal locomotion [18, 28, 29]. Single element strain gauges (EA-06-015LA-120, Micromeasurements) were prepared [26-28] and attached to the medial surface of the tibial midshaft aligned with the bone's long axis. While mice were anesthetized, a range of dynamic compressive loads (peak loads ranging from -2 to -25 N) were applied, and strain measurements recorded simultaneously (National Instruments, Labview v8.2). No tibial failures occurred within this load range. The slopes of the strain-load regressions were determined to be -0.0130 N/με (95% CI [-0.006, -0.020]) for female mice and -0.0084 N/με (95% CI [-0.003, -0.014]) for male mice and were not significantly different from each other by t-test. Therefore,

we chose the lower of the two regression slopes (male), which required approximately -11 N to induce +1200 με.

Mechanical Loading

The mice (n=14/sex) underwent dynamic compression of the left tibia 5 days per week for 10 days over 2 weeks using a custom-made tibial loading device [19, 23] (Figure 2.1). 1200 loading cycles were applied at 4 Hz [19, 23] with -11.5±0.3 N peak load (corresponding to ~+1300 με) and a constant -2.3±0.3 N during the dwell period [19]. The loading device was modified from our previous design [19, 23] to implement feedback control of the applied loads (National Instruments, Labview v8.2) using an in-line force transducer (ELFS-T3E-20L, Measurement Specialties). The right tibia served as the contralateral control. During all loading sessions, the mice were under isoflurane anesthesia (2% Isoflurane, 1.0 L/min, Webster). Normal cage activity was allowed between loading sessions.

Intraperitoneal injections of calcein (20 mg/kg, Sigma Aldrich) and demeclocycline (20 mg/kg, Sigma Aldrich) were administered 4 and 14 days prior to euthanasia, respectively. Mice were euthanized by CO_2 inhalation 2 weeks after loading commenced. Tibiae were dissected free of soft tissue and fixed in 10% neutral buffered formalin for 48 hrs, then stored in 70% ethanol.

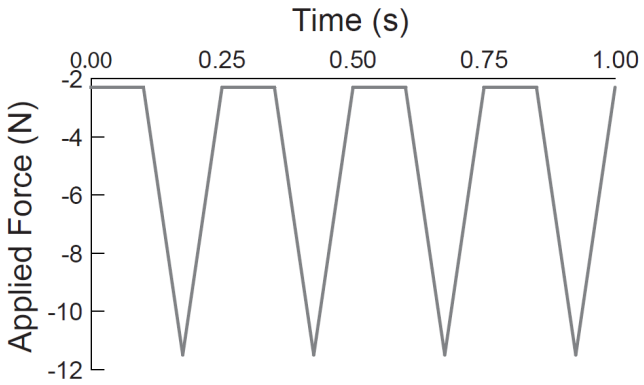

Figure 2.1 Schematic for 4 cycles (1 second) of the daily mechanical loading protocol. Peak compressive loads of -11.5N corresponds to +1200με at the medial midshaft of the tibia.

Micro-computed Tomography (MicroCT)

All pairs of tibiae were scanned using quantitative micro-computed tomography (MS-8 MicroCT, GE Healthcare Systems) [19]. Isotropic voxel resolution was 15 μm. A global threshold of 1100 HU (0.27 g/cc) was used to segment mineralized tissue from water and soft tissue. For each tibia, a single volume of interest (VOI) was defined in the proximal metaphysis excluding the cortical shell. The VOI began approximately 0.5 mm distal to the growth plate to exclude the primary spongiosa and extended 10% of the total tibial length (Figure 2.2a). Measurable outcomes for the cancellous VOI included bone volume fraction (BV/TV), tissue mineral density (tBMD, mg/cc), and trabecular thickness (Tb.Th, μm) and separation (Tb.Sp, μm).

Finite Element (FE) Analysis

Because strains cannot be measured directly in cancellous bone, specimen-specific FE models were used to calculate strains in the cancellous tissue during loading and to determine the stiffness of the metaphysis. FE VOIs were defined in a subset of representative tibiae (n=5/per sex) and used to generate corticocancellous

and cortical models. The FE VOIs extended 5% of total tibial length and were centered within the microCT VOIs (Figure 2.2b). Corticocancellous VOIs included both the cancellous tissue and the cortical shell; cortical VOIs included only the cortical shell. MicroCT image data were converted to FE models using custom software (MATLAB v7.5, The Mathworks, Inc.). MicroCT scans were coarsened (following a convergence study) by combining 2x2x2 voxels to yield a single voxel with side length 0.03 mm, and coarsened voxels were converted into 8-noded linear brick elements (~54K elements per model). Elements were assigned isotropic material properties with a uniform modulus of 20 GPa and a Poisson's ratio of 0.3 (Abaqus v6.7, Dassault Systèmes Simulia Corp) [30]. Nodes at the distal surface of the model were restricted to in-plane motion and prevented from rigid-body motion. Strains were determined at the element centroids.

To characterize the tissue strain environment during the loading experiment, a uniform displacement was applied to the proximal surface of the models that resulted in an 11.5 N compressive reaction force at the distal surface. Elements were identified in the control corticocancellous models that coincided with the cancellous VOIs used for the microCT analysis (see MicroCT above). In these elements, the longitudinal strains (e_{33}) were determined. We assumed that strains in the control limbs under simulated loading conditions were representative of the strains induced at the onset of the experiment. In females, a uniform -0.09% apparent strain applied at the proximal surface resulted in -11.5 N reaction force at the distal surface. The cancellous tissue strains ranged from -2437$\pm$155 με to +455$\pm$221 με (average Min to Max). In males, a uniform -0.07% apparent strain resulted in -11.5 N reaction force at the distal surface, and the cancellous tissue strains ranged from -2134$\pm$430 με to +286$\pm$94 με. The maximum and minimum strain values did not differ statistically between the sexes by linear mixed-model. Metaphyseal cancellous tissue experienced primarily compressive

longitudinal strains during *in vivo* applied loading. The mean tissue strains were 19% lower (p=0.003) in males (-341±31 με) versus females (-421±31 με).

To characterize the effects of adaptation on the apparent stiffness of the proximal metaphysis, the reaction force (N) was calculated for a uniform strain of -0.1% applied to the proximal surface of all models. The proportion of the load transmitted through the cancellous tissue was determined from the ratio of the cortical to corticocancellous reaction forces, an indicator of load sharing between the metaphyseal cortex and cancellous tissue.

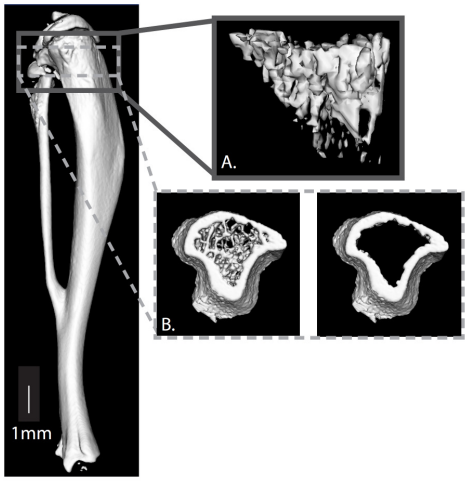

Figure 2.2 (a) Representative cancellous volume of interest (VOI) used for microCT analysis. Each cancellous VOI was defined in the proximal end of the tibia and excluded the cortical shell. The proximal end of the VOI began below the primary spongiosa and extended distally 10% of total tibial length. (b) Representative VOIs used for FE analysis. Each VOI was 5% of total tibial length and was centered within the VOI used for microCT analysis (dashed box). Corticocancellous VOIs (left) included both cancellous and cortical bone, and cortical VOIs (right) included only the cortical shell.

Histomorphometry

Histomorphometric analyses were performed on the proximal tibiae for a subset of mice (n=5/sex) using methods detailed elsewhere [31]. Briefly, after fixation the bones were stained en bloc with Villanueva Mineralized Bone Stain (Arizona

Histology & Histomorphometry Services) for 5 days, dehydrated with ethylene glycol monoethyl ether, cleared in methyl salicylate, and then embedded in methyl methacrylate. Undecalcified 7 µm thick frontal sections were cut using a rotary microtome (Leica 2265, Nussloch) equipped with a tungsten carbide knife. Sections were cover-slipped and used for fluorescence microscopy analysis of bone resorption and formation. Sections were analyzed using an OsteoMeasure system (Osteometrics Inc.) connected to a microscope (Zeiss Axioskop, Carl Zeiss). All measurements were made by a single observer who was blinded to the specimen identity.

Measurements within the cancellous compartment and the endosteal and periosteal cortical surfaces of the proximal metaphysis were performed on a 1 mm wide x 2.5 mm long region beginning 0.5 mm below the growth plate. Bone resorption was assessed from eroded surface [ES/BS = eroded surface/bone surface measured as eroded perimeter (EPm)bone perimeter (BPm), %]; bone formation was assessed from the mineralizing (fluorochrome labeled) surface (LS/BS = labeled surface/BS measured as dLS +0.5 sLS from single and double LS, %), mineral apposition rate (MAR, µm/day) and surface based bone formation rate (BFR = mineralizing surface x MAR/B.Pm, µm/yr).

Statistical Analysis

The effects of sex and loading on the adaptive response to tibial loading and change in body mass were determined with a linear mixed-model with repeated-measures (JMP v7.0, SAS Institute Inc.). The within-subject factor was limb, loaded (L) or control (C), and the between-subject factor was sex. Statistical significance was set at $\alpha \leq 0.05$. All results presented are significant unless otherwise stated. If no significant interaction was present, then only main effects are reported. Percentage differences were calculated for the effects of loading ([Loaded –

Control]*100/Control) and sex ([males – females]*100/females). All values are represented as the mean ± SD.

2.3 Results

Effect of Loading

Two weeks of *in vivo* tibial compression significantly increased cancellous bone mass in both sexes (Figure 2.3). Cancellous BV/TV increased 73% in the loaded tibiae relative to control tibiae (Figure 2.4). Increases in bone mass corresponded to changes in cancellous architecture and tissue properties (Figure 2.4). Mean Tb.Th increased (+75%) while Tb.Sp decreased (-19%). Increased tBMD (+18%) contributed to greater bone mass in the loaded tibiae following 2 weeks of compression. Loading did not affect tibial length.

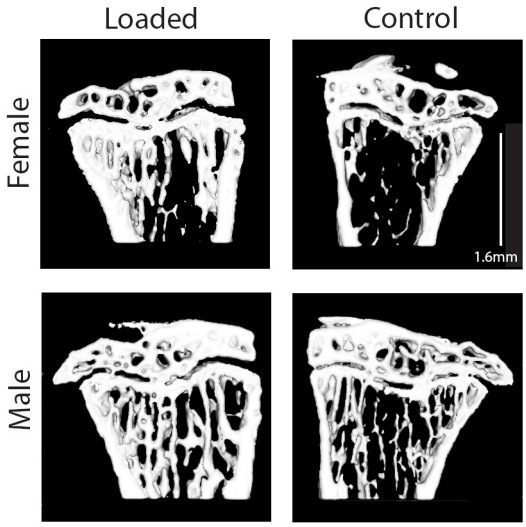

Figure 2.3 Sagittal sections through the proximal metaphysis taken from representative microCT scans. Representative loaded (left) and control (right) tibiae are shown from both females (top) and males (bottom).

Increased cellular activity contributed to increases in cancellous bone mass (Table 2.1). Bone formation was enhanced with loading in the cancellous envelope. In purely cancellous surfaces, LS/BS increased 22%, which corresponded to higher MAR (+97%) and BFR (+137%), in loaded limbs relative to control limbs. Bone resorption was also enhanced with loading in cancellous bone. At the periosteal and endosteal cortical surfaces in the proximal metaphysis, only ES/BS was altered with loading. ES/BS decreased 45% at the periosteal surface of loaded limbs. Large changes were seen at the endosteal surface, where ES/BS increased 395% after 2 weeks of tibial compression.

Adaptation in cancellous tissue mass and architecture resulted in stiffer proximal metaphyses in the loaded limbs. For the 0.01% deformation applied in the FE analysis, the reaction force in the loaded limbs was greater than in the control limbs (L: 27.0$\pm$1.8 N vs. C: 14.4$\pm$2.7 N). In loaded limbs, a greater proportion of load was carried by cancellous rather than cortical tissue, as reflected by 10% decreased cortical to corticocancellous load ratio (L: 0.55±0.06 vs. C: 0.61±0.07).

Effect of Sex on the Response to Loading

For all measurements, the differences between loaded versus control limbs were similar between male and female mice. Male mice had more cancellous tissue (+53% BV/TV) due to greater Tb.Th (+9.1%) and tBMD (+2.9%), and smaller Tb.Sp (-36%) when compared to females (Figure 2.4). As a result, metaphyseal tissue was stiffer in males, as reflected by 14% greater corticocancellous compressive reaction force (males: 22±6.6 N vs. females: 19±7.1 N) and a 16% lower cortical to corticocancellous load ratio (males: 0.53±0.05 vs. females: 0.63±0.05). Cellular activity did not differ by sex.

Over the 2 week experimental period, males and females continued to grow as indicated by increased body mass. Body mass increased similarly in males and females (+2.7%); to 22.9±1.2 g in males and to 17.4±0.9 g in females. Males were 32% heavier and had 4% longer tibiae than females (males: 17.1±0.2 mm vs. females 16.4±0.2 mm).

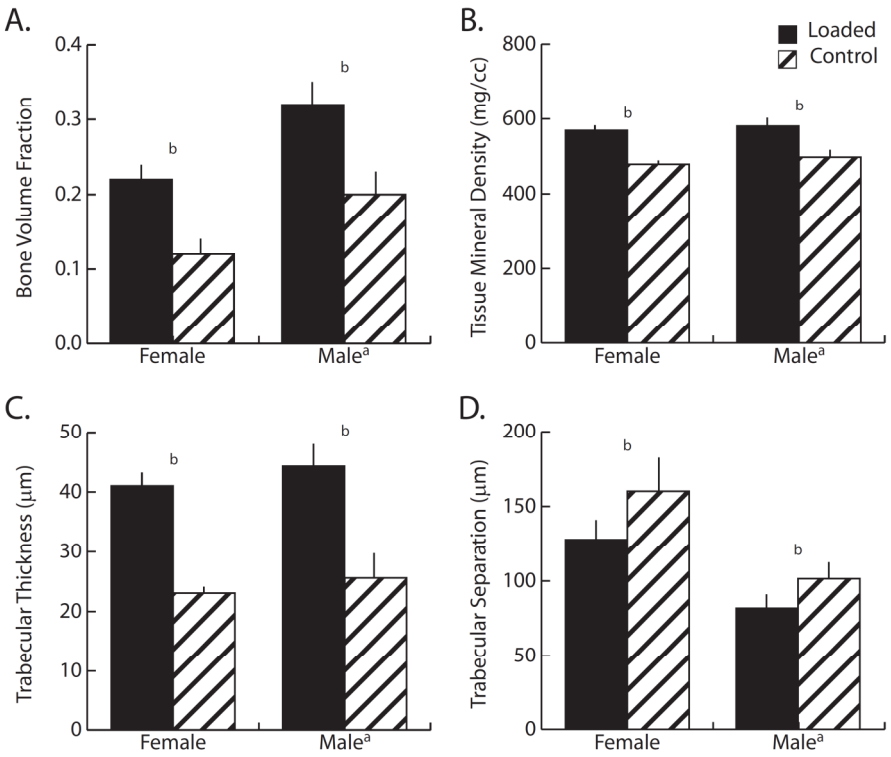

Figure 2.4 Indices of cancellous adaptation determined by microCT analysis of VOIs from the proximal metaphysis of loaded and control tibiae from female and male mice after 2 weeks of loading. Loading induced significant changes in all parameters, but changes did not differ by sex (non-significant interaction term). Males had significantly greater BV/TV, Tb.Th, and tBMD and lower Tb.Sp. (A) Bone volume fraction increased +95% in females and +65% in males. BV/TV was 53% larger in males than in females. (B) Tissue mineral density (mg/cc) increased +19% in females and + 17% in males. tBMD was 2.9% higher in males than in females. (C) Trabecular thickness (µm) increased +77% in females and +78% in males. Tb.Th was 9.1% larger in males than females. (D) Trabecular separation (µm) decreased -19% in both males and females. Tb.Sp was 36% lower in males than females. Data are represented as mean + SD.
[a]Sex effect, [b]Loading effect, $p<0.05$ by linear mixed-model with repeated measures

Table 2.1 Dynamic histomorphometry for the proximal metaphysis of male and female mice after 2 weeks of *in vivo* tibial compression. Data are represented as mean ± SD.

Variable	Sex	Loaded (Left)	Control (Right)
Cancellous Surface			
ES/BS	Female	15±7.1	13±3.0
	Male	16±5.0	18±5.0
LS/BS	Female	23±2.7[b]	20±4.2
	Male	20±4.5[b]	16±3.8
MAR (μm/day)	Female	1.9±0.48[b]	0.66±0.86
	Male	1.7±0.40[b]	1.1±0.72
BFR (%/yr)	Female	160±49[b]	55±79
	Male	123±23[b]	61±42
Proximal Metaphyseal Periosteal Surface			
ES/BS	Female	0.49±0.30[b]	0.64±0.30
	Male	0.33±0.17[b]	0.82±0.20
LS/BS	Female	0.04±0.06	0.00±0.00
	Male	0.04±0.11	0.06±0.14
MAR (μm/day)	Female	0.53±0.82	0.00±0.00
	Male	0.55±1.4	0.27±0.66
BFR (%/yr)	Female	0.22±0.37	0.00±0.00
	Male	0.54±1.3	0.33±0.81
Proximal Metaphyseal Endosteal Surface			
ES/BS	Female	0.17±0.19[b]	0.03±0.04
	Male	0.15±0.09[b]	0.04±0.05
LS/BS	Female	0.77±0.10	0.81±0.10
	Male	0.82±0.10	0.70±0.15
MAR (μm/day)	Female	2.5±0.63	2.4±0.40
	Male	2.0±0.45	2.7±0.71
BFR (%/yr)	Female	7.2±2.3	7.1±1.32
	Male	6.1±1.4	7.1±2.70

Data are represented as means +/- SD. ES/BS, eroded surface; LS/BS, mineralizing surface; MAR, mineral apposition rate; BRF, bone formation rate.
[b]Loading, $p<0.05$ by linear mixed-model with repeated-measures.

2.4 Discussion

Tibial compression increased cancellous bone mass and altered architecture similarly in growing adult male and female mice. The increases in cancellous bone mass seen in experimentally loaded tibiae were produced by dramatic increases (2-3 fold) in bone formation rates compared to control limbs. As a result, the stiffness of

cancellous tissue increased with adaptation, and more load was transmitted through cancellous than cortical tissue in loaded than in control limbs.

The effects of sex on cortical adaptation to increasing mechanical loading have been variable. In growing and mature rodents, females showed no response to treadmill running while males increased geometric measures in the diaphyses [12, 13]. Mechanical parameters such as applied load and strain magnitude are seldom measured in exercise studies, thus the results cannot be related directly to the mechanical environment experienced by the skeleton. A strength of our model is that well-defined, controlled physiological loads are delivered to the tibia. In an analogous model delivering compression to the rat ulna, the relative cortical response was similar in males and females despite greater absolute deposition rates in males [11], a finding similar to our morphometric results in cancellous bone. Furthermore, the peak applied loads in the rat were chosen to produce matching peak strains at the midshaft in each sex, a methodology identical to ours. Our focus, however, was on the response of cancellous bone to loading within a physiological range of strains measured in cortical bone [18, 26, 27]. Mechanical strains can be measured *in vivo* only on bone surfaces, which limited our measurements to cortical sites. We chose the mid-diaphysis because functional strain levels at this site are conserved across a range of animals and are well-documented. These opposing results with sex across studies may reflect fundamental differences in adaptation between controlled *in vivo* loading and exercise. Because the adaptive changes to loading in male and female limbs were nearly identical in the present study, detecting a significant interactive effect of sex and loading would require a prohibitive number of animals (e.g. >600 animals with 90% confidence for BV/TV measurements, based on post hoc power analysis).

Based on body size alone, greater strains at the medial diaphysis would be expected in female mice than in male mice for similar applied loads. Female mice are

smaller than age-matched male mice as indicated by body mass [32, 33], femoral and tibial cross-sectional area [32, 34-36], and tibial length and moment of inertia [32]. Female mice also have lower vertebral and distal femoral bone volume fraction and trabecular thickness than age-matched males [33]. However, the strain-load relationship from *in vivo* strain-gauging established that similar loads were required to engender target strain levels in males and females. Cortical material property differences may compensate for the geometric effects. Conflicting data exist on sex-specific material properties or composition of mouse bone tissue [12, 32]. We did not observe any differences associated with sex in tissue mineral density, suggesting other factors not examined in this study may contribute to whole bone mechanical behavior.

Because the strain environment within the proximal tibia during loading cannot be determined *in vivo*, specimen-specific FE models of proximal metaphyses were used to simulate tibial compression and quantify cancellous strains and changes in stiffness. FE models based on microCT image data have become a common technique for estimating the mechanical environment of cancellous bone [30, 37], and this approach has been shown to replicate experimental data [38]. *In vivo* loading was simulated by applying a uniform displacement to the proximal metaphysis producing a compressive reaction force of 11.5 N. The applied displacement required to achieve the -11.5 N reaction force in the corticocancellous models differed between males and females, reflecting that male control tibiae had greater cancellous mass and thicker trabeculae in the proximal metaphysis. However, the resulting peak cancellous strain values did not differ by sex, as they did for our cortical strain measurements, verifying that we were inducing similar strain environments in the proximal metaphysis in males and females. These results were influenced by using partial models, applying homogenous moduli to both new and existing bone, and using an applied displacement boundary condition.

Few *in vivo* models are available to study the response of cancellous bone to mechanical loading. Previous models have induced an adaptive response in cancellous compartments [39-41], but required invasive surgery, which can confound interpretations of the response to loading due to associated healing processes. Also, non-physiological loading regimes were often employed [42, 43]. Our model addresses several of these limitations. Compression of the tibia is non-invasive, and adaptation is present when the applied loads are physiologic in magnitude and direction. Our approach has the potential to address the effects of numerous variables, such as age and genetic factors, on the mechanisms modulating cancellous bone adaptation. Tibial compression may alter the soft tissues in the knee joint, but the present study focused on bony adaptation.

Our results in female mice are more pronounced than other tibial loading studies that applied similar load levels. A different load-strain dose response was observed in this study relative to previous studies in our laboratory. Previously, growing (10 wk) male C57Bl/6 mice increased BV/TV by only 13% after 2 weeks of loading at -3 N with no significant changes in trabecular thickness or separation [19]. The osteogenic response of male mice in the current study was greater (Figure 2.4), likely due to the higher peak load magnitude used here (-11.5 N). The greater load was chosen based on *in vivo* strain calibration, which resulted in a different strain-load relationship than was established previously. Because the tibia is a highly curved bone, small variations in gauge position can produce significant changes in strain readings. In the present study, bone strains were measured over a smaller area due to smaller strain gauges, which are more accurate, and may explain our lower strain readings. Discrepancies with other studies [20-22] are likely attributable to different loading parameters, including the number of applied cycles, frequency, and duration of pauses. In these other tibial compression studies, a 10-second rest was inserted

between each loading cycle [20-22] and far fewer total loading cycles were applied per session than in our study (40 versus 1,200). In addition, in these prior studies the animals were loaded only 3 times per week compared with 5 times per week in our study. Combined, the total time the skeleton was experiencing loads was much less compared to our protocol (120 cycles/week versus 6,000 cycles/week) and likely contributed to our enhanced osteogenic response.

Gains in cancellous mass due to loading were achieved through increased cellular activity. In the cancellous envelope, both MAR and BFR increased after 2 weeks in the loaded limbs relative to control limbs. In a similar study with male mice, MAR increased at a similar rate, but BFR decreased after 6 weeks of tibial compression [23]. The longer time period in that study may have allowed cells to reach a steady state response while bone formation may have still been in a transient phase in our study [44]. In addition, osteoclastic activity was enhanced at the endosteal surface of the proximal metaphysis, further suggesting that adaptation is ongoing in our study. Increased osteoclastic activity at the endosteum and reduced activity at the periosteum may reflect an effort to increase the overall size of the cancellous envelope at the expense of the cortex, thereby increasing load transfer through cancellous bone. A similar cortical-cancellous relationship is evident when vertebrae from C57Bl/6 mice were compared to other genetic strains [45]. Taken together with our FE-based stiffness, increased mechanical loading of corticocancellous sites amplifies load transfer through the cancellous envelope.

In summary, through non-invasive and well-defined mechanical loading, substantial increases in bone mass were observed in the cancellous bone of growing male and female mice. Whether or not these gains would be maintained after cessation of loading, and for how long, remains to be determined. Peak applied loads corresponded to similar peak strains at the tibial midshaft and in the cancellous tissue

of the proximal metaphysis. Our tibial loading regime elicited enhanced adaptation in the cancellous compartment compared to previous *in vivo* loading studies, likely due to differences in loading parameters. In the future, additional variables such as estrogen status and age need to be investigated to understand their role in bone functional adaptation. To address bone loss and osteoporosis, the ability of mechanical loading to increase bone mass or attenuate bone loss in osteopenic subjects will need to be demonstrated.

REFERENCES

1. Kontulainen, S., Sievanen, H., Kannus, P., Pasanen, M., and Vuori, I. Effect of long-term impact-loading on mass, size, and estimated strength of humerus and radius of female racquet-sports players: a peripheral quantitative computed tomography study between young and old starters and controls. J Bone Miner Res 18*:*352-9; 2003.
2. Kannus, P., Haapasalo, H., Sankelo, M., Sievanen, H., Pasanen, M., Heinonen, A., Oja, P., and Vuori, I. Effect of starting age of physical activity on bone mass in the dominant arm of tennis and squash players. Ann Intern Med 123*:*27-31; 1995.
3. Karlsson, M. K. Does exercise during growth prevent fractures in later life? Med Sport Sci 51*:*121-36; 2007.
4. Borer, K. T. Physical activity in the prevention and amelioration of osteoporosis in women : interaction of mechanical, hormonal and dietary factors. Sports Med 35*:*779-830; 2005.
5. Daly, R. M. The effect of exercise on bone mass and structural geometry during growth. Med Sport Sci 51*:*33-49; 2007.
6. Tabensky, A., Duan, Y., Edmonds, J., and Seeman, E. The contribution of reduced peak accrual of bone and age-related bone loss to osteoporosis at the spine and hip: insights from the daughters of women with vertebral or hip fractures. J Bone Miner Res 16*:*1101-7; 2001.
7. Ryan, A. S., Ivey, F. M., Hurlbut, D. E., Martel, G. F., Lemmer, J. T., Sorkin, J. D., Metter, E. J., Fleg, J. L., and Hurley, B. F. Regional bone mineral density after resistive training in young and older men and women. Scand J Med Sci Sports 14*:*16-23; 2004.

8. Ballard, T. L., Specker, B. L., Binkley, T. L., and Vukovich, M. D. Effect of protein supplementation during a 6-month strength and conditioning program on areal and volumetric bone parameters. Bone 38*:*898-904; 2006.

9. Ducher, G., Courteix, D., Meme, S., Magni, C., Viala, J. F., and Benhamou, C. L. Bone geometry in response to long-term tennis playing and its relationship with muscle volume: a quantitative magnetic resonance imaging study in tennis players. Bone 37*:*457-66; 2005.

10. Jones, H. H., Priest, J. D., Hayes, W. C., Tichenor, C. C., and Nagel, D. A. Humeral hypertrophy in response to exercise. J Bone Joint Surg Am 59*:*204-8; 1977.

11. Mosley, J. R., and Lanyon, L. E. Growth rate rather than gender determines the size of the adaptive response of the growing skeleton to mechanical strain. Bone 30*:*314-9; 2002.

12. Jarvinen, T. L., Kannus, P., Pajamaki, I., Vuohelainen, T., Tuukkanen, J., Jarvinen, M., and Sievanen, H. Estrogen deposits extra mineral into bones of female rats in puberty, but simultaneously seems to suppress the responsiveness of female skeleton to mechanical loading. Bone 32*:*642-51; 2003.

13. Wallace, J. M., Rajachar, R. M., Allen, M. R., Bloomfield, S. A., Robey, P. G., Young, M. F., and Kohn, D. H. Exercise-induced changes in the cortical bone of growing mice are bone- and gender-specific. Bone 40*:*1120-7; 2007.

14. Rubin, C. T., and Lanyon, L. E. Kappa Delta Award paper. Osteoregulatory nature of mechanical stimuli: function as a determinant for adaptive remodeling in bone. J Orthop Res 5*:*300-10; 1987.

15. Hert, J., Liskova, M., and Landa, J. Reaction of bone to mechanical stimuli. 1. Continuous and intermittent loading of tibia in rabbit. Folia Morphol (Praha) 19:290-300; 1971.

16. Torrance, A. G., Mosley, J. R., Suswillo, R. F., and Lanyon, L. E. Noninvasive loading of the rat ulna in vivo induces a strain-related modeling response uncomplicated by trauma or periostal pressure. Calcif Tissue Int 54:241-7; 1994.

17. Turner, C. H., Akhter, M. P., Raab, D. M., Kimmel, D. B., and Recker, R. R. A noninvasive, in vivo model for studying strain adaptive bone modeling. Bone 12:73-79; 1991.

18. Lee, K. C., Maxwell, A., and Lanyon, L. E. Validation of a technique for studying functional adaptation of the mouse ulna in response to mechanical loading. Bone 31:407-12; 2002.

19. Fritton, J. C., Myers, E. R., Wright, T. M., and van der Meulen, M. C. Loading induces site-specific increases in mineral content assessed by microcomputed tomography of the mouse tibia. Bone 36:1030-8; 2005.

20. Sugiyama, T., Saxon, L. K., Zaman, G., Moustafa, A., Sunters, A., Price, J. S., and Lanyon, L. E. Mechanical loading enhances the anabolic effects of intermittent parathyroid hormone (1-34) on trabecular and cortical bone in mice. Bone 43:238-48; 2008.

21. Marenzana, M., De Souza, R. L., and Chenu, C. Blockade of beta-adrenergic signaling does not influence the bone mechano-adaptive response in mice. Bone 41:206-15; 2007.

22. De Souza, R. L., Matsuura, M., Eckstein, F., Rawlinson, S. C., Lanyon, L. E., and Pitsillides, A. A. Non-invasive axial loading of mouse tibiae increases cortical bone formation and modifies trabecular organization: a new model to

study cortical and cancellous compartments in a single loaded element. Bone 37:810-8; 2005.

23. Fritton, J. C., Myers, E. R., Wright, T. M., and van der Meulen, M. C. Bone mass is preserved and cancellous architecture altered due to cyclic loading of the mouse tibia after orchidectomy. J Bone Miner Res 23:663-71; 2008.

24. Rubin, C. T., and Lanyon, L. E. Limb mechanics as a function of speed and gait: a study of functional strains in the radius and tibia of horse and dog. J Exp Biol 101:187-211; 1982.

25. Lanyon, L. E., Hampson, W. G., Goodship, A. E., and Shah, J. S. Bone deformation recorded in vivo from strain gauges attached to the human tibial shaft. Acta Orthop Scand 46:256-268; 1975.

26. Mosley, J. R., March, B. M., Lynch, J., and Lanyon, L. E. Strain magnitude related changes in whole bone architecture in growing rats. Bone 20:191-8; 1997.

27. Hillam, R. A., and Skerry, T. M. Inhibition of bone resorption and stimulation of formation by mechanical loading of the modeling rat ulna in vivo. J Bone Miner Res 10:683-689; 1995.

28. Biewener, A. A. Safety factors in bone strength. Calcif Tissue Int 53 Suppl 1:S68-74; 1993.

29. Rubin, C. T., and Lanyon, L. E. Dynamic strain similarity in vertebrates; an alternative to allometric limb bone scaling. J Theor Biol 107:321-7; 1984.

30. van der Meulen, M. C., Yang, X., Morgan, T. G., and Bostrom, M. P. The effects of loading on cancellous bone in the rabbit. Clin Orthop Relat Res 467:2000-6; 2009.

31. Li, C. Y., Jepsen, K. J., Majeska, R. J., Zhang, J., Ni, R., Gelb, B. D., and Schaffler, M. B. Mice lacking cathepsin K maintain bone remodeling but

develop bone fragility despite high bone mass. J Bone Miner Res 21:865-75; 2006.

32. Somerville, J. M., Aspden, R. M., Armour, K. E., Armour, K. J., and Reid, D. M. Growth of C57BL/6 mice and the material and mechanical properties of cortical bone from the tibia. Calcif Tissue Int 74:469-75; 2004.

33. Glatt, V., Canalis, E., Stadmeyer, L., and Bouxsein, M. L. Age-related changes in trabecular architecture differ in female and male C57BL/6J mice. J Bone Miner Res 22:1197-207; 2007.

34. Brodt, M. D., Ellis, C. B., and Silva, M. J. Growing C57Bl/6 mice increase whole bone mechanical properties by increasing geometric and material properties. J Bone Miner Res 14:2159-66; 1999.

35. Ferguson, V. L., Ayers, R. A., Bateman, T. A., and Simske, S. J. Bone development and age-related bone loss in male C57BL/6J mice. Bone 33:387-98; 2003.

36. Price, C., Herman, B. C., Lufkin, T., Goldman, H. M., and Jepsen, K. J. Genetic variation in bone growth patterns defines adult mouse bone fragility. J Bone Miner Res 20:1983-91; 2005.

37. Kabel, J., van Rietbergen, B., Dalstra, M., Odgaard, A., and Huiskes, R. The role of an effective isotropic tissue modulus in the elastic properties of cancellous bone. J Biomech 32:673-80; 1999.

38. Bourne, B. C., and van der Meulen, M. C. Finite element models predict cancellous apparent modulus when tissue modulus is scaled from specimen CT-attenuation. J Biomech 37:613-21; 2004.

39. Goldstein, S. A., Matthews, L. S., Kuhn, J. L., and Hollister, S. J. Trabecular bone remodeling: an experimental model. J Biomech 24 Suppl 1:135-50; 1991.

40. van der Meulen, M. C., Morgan, T. G., Yang, X., Baldini, T. H., Myers, E. R., Wright, T. M., and Bostrom, M. P. Cancellous bone adaptation to in vivo loading in a rabbit model. Bone 38*:*871-7; 2006.

41. Guldberg, R. E., Caldwell, N. J., Guo, X. E., Goulet, R. W., Hollister, S. J., and Goldstein, S. A. Mechanical stimulation of tissue repair in the hydraulic bone chamber. J Bone Miner Res 12*:*1295-302; 1997.

42. Chow, J. W., Jagger, C. J., and Chambers, T. J. Characterization of osteogenic response to mechanical stimulation in cancellous bone of rat caudal vertebrae. Am J Physiol 265*:*E340-7; 1993.

43. Kim, C. H., Takai, E., Zhou, H., von Stechow, D., Muller, R., Dempster, D. W., and Guo, X. E. Trabecular bone response to mechanical and parathyroid hormone stimulation: the role of mechanical microenvironment. J Bone Miner Res 18*:*2116-25; 2003.

44. Lanyon, L. E. Using functional loading to influence bone mass and architecture: objectives, mechanisms, and relationship with estrogen of the mechanically adaptive process in bone. Bone 18*:*37S-43S; 1996.

45. Tommasini, S. M., Wearne, S. L., Hof, P. R., and Jepsen, K. J. Percolation theory relates corticocancellous architecture to mechanical function in vertebrae of inbred mouse strains. Bone 42*:*743-50; 2008.

CHAPTER 3

THE ADAPTIVE RESPONSE TO TIBIAL COMPRESSION IN ADULT FEMALE MICE VARIES WITH APPLIED LOAD MAGNITUDE

3.1 Introduction

The skeleton's ability to adapt to its mechanical environment diminishes with age, hampering efforts to prevent or recover bone loss due to aging and osteoporosis, particularly at cancellous sites [1]. In premenopausal women, high-impact and high-velocity exercises increase bone mass at critical cancellous sites [2-5]. The results are more variable in postmenopausal women, but exercise can prevent bone loss [6-10] and even induce marginal gains in bone mass [11-13], indicating that mechanical stimuli may be a potential therapy for treating osteoporotic bone loss and preventing associated fractures.

Several in vivo loading studies have demonstrated that adult rodents are able to respond positively to increased mechanical stimuli at mid-diaphyseal sites, but less data are available for cancellous bone, which is more susceptible to osteoporotic fracture. Adult rodents increased cortical bone mass in limbs subjected to controlled, in vivo loading by tibial four-point [14, 15] and cantilever bending [16, 17], and ulnar compression [18, 19]. As observed in humans, the adaptive response of cortical bone to loading was reduced with aging [15, 16]. Similar increases in bone mass at predominately cancellous sites have not yet been demonstrated with in vivo loading in rodents. In vivo tibial compression increased cortical bone mass, but did not alter cancellous bone mass in the proximal tibia of adult and aged mice [20, 21]. However, different loading protocols have not been compared to determine if the adaptive response can be enhanced by altering the characteristics of the applied loading. A more robust osteogenic response was observed in growing mice in our laboratory than

others have reported [20, 22, 23], suggesting that a more osteogenic approach may be possible in adult female mice.

The objective of this study was to demonstrate that cancellous bone, like cortical bone, can be augmented in osteopenic [24] adult animals using in vivo mechanical loading. To account for the possibility of diminished responsiveness to tibial compression in the adult skeleton, we investigated two different loading protocols that were based on a protocol used in growing female mice [23]. Previously, we applied -11.5 N to the hindlimbs of 10 week old female mice, corresponding to +1200 με at the mid-diaphysis. In the present study, we applied the same peak compressive loads to one group of adult female mice (Load-Matched) and the same peak mid-diaphyseal strains to a second group of adult female mice (Strain-Matched) to determine which protocol was more osteogenic in osteopenic adult mice. The adaptive response in both groups was compared to that measured in growing mice to determine the effects of aging on skeletal adaptation.

3.2 Materials and Methods

Animals

Forty-one female C57Bl/6 mice (Jackson Labs) were received and acclimatized in our animal facility for one week. Mice were housed 3-5 per cage with ad libitum access to food and water. Body masses were recorded daily and used to monitor the health of the mice over the course the experiment. At 26 weeks of age, mice were divided into a basal strain calibration group (n=5) and two tibial loading groups: Load-Matched (LM, n=18) and Strain-Matched (SM, n=18). The loading groups were assigned based on a previous study by our group using 10 week old female mice that received peak compressive loads of -11.5 N corresponding to +1200 με at the tibial medial mid-diaphysis [23]. The Load-Matched (LM) group received

matching peak loads (-11.5 N) while the Strain-Matched (SM) group received loads corresponding to matching peak mid-diaphyseal strains (+1200 με). At the start of the experiment, mice weighed 23.1±1.9 g. All experimental procedures were approved by Cornell University's Institutional Animal Care and Use Committee.

In vivo Load-Strain Calibration

To determine the peak applied load that engendered +1200 με at the medial midshaft of the tibia for the SM group and the diaphyseal strains engendered by a -11.5 N load for the LM group, the in vivo strain-load relationship was established for the tibiae of 26 week old basal mice using methods previously described [25]. In brief, single element strain gauges (EA-06-015LA-120, Micromeasurements) were prepared and attached to the medial surface of the tibial midshaft aligned with the tibial long axis. While mice were anesthetized, a range of dynamic compressive loads (peak loads ranging from -4 to -12 N) were applied, and strain measurements recorded simultaneously (Labview v8.2, National Instruments). Diaphyseal stiffness (N/με) was calculated as the change in load (ΔN) over the change in strain (Δμε) during the loading portion of the waveform and averaged across four consecutive load cycles [25].. Diaphyseal stiffness in the left and right tibiae was similar (left: --0.00504 N/με (95% CI: [-0.00619, -0.00389]); right: -0.00680 N/με (95% CI: [-0.00784, -0.00577]), $p>0.05$, paired t-test). Using the stiffness of the left tibia, a 6.0 N peak compressive load was required to engender +1200 με at the medial mid-diaphysis in the 26 week old mice while an 11.5 N peak compressive load engendered +2100 με (Table 3.1). Diaphyseal stiffness was also measured following 2 weeks of loading, in a subset of loaded animals (SM, n=6; LM, n=5). Three animals in the SM group and one animal in the LM were excluded from post-adaptation stiffness calculations because

placement of the gauges was too far from the midshaft (>5% of bone's length) [25], leaving 3 SM mice and 4 LM mice.

Table 3.1 Peak applied compressive loads and resulting peak mid-diaphyseal strains on the medial tibia and peak proximal metaphyseal cancellous tissue strains.

Experimental Group	Applied Load (N)	Mid-diaphyseal Strains (με)[b]	Cancellous Tissue Strains (με)[c]
Growing[a]	-11.5±0.3	+1200	-2437±155
Load-Matched	-11.3±0.5	+2200	-2130±273
Strain-Matched	-5.9±0.5	+1200	-1178±109

[a]10wk female mice undergoing 2wks in vivo loading [23]; [b]Determined by in vivo strain gauging at the medial mid-diaphysis; [c]Determined by finite element modeling of the proximal metaphysis in control limbs. Data represented as mean ± SD where appropriate.

In vivo Mechanical Loading

The loading protocol for both loading groups consisted of 1200 cycles administered to the left limb at 4 Hz for 5 days/week over 2 weeks (Days 1-5, 8-12). The LM group received an average peak compressive load of 11.3±0.5 N, corresponding to +2100 με, at the tibial mid-shaft. The SM group received a mean peak compressive load of 5.9±0.5 N, corresponding to +1200 με. The average load during the rest phase between loading cycles for both groups was -1.5±0.6 N (Fig. 3.1). The right tibia served as the contralateral control limb. During all loading sessions, mice were maintained under general anesthesia (2% Isoflurane, 1.0 L/min, Webster). Normal cage activity was allowed between loading sessions. Mice were euthanized on Day 15 by CO_2 inhalation. Tibiae were dissected free of soft tissue and fixed in 10% neutral buffered formalin for 48 hrs, then stored in 70% ethanol.

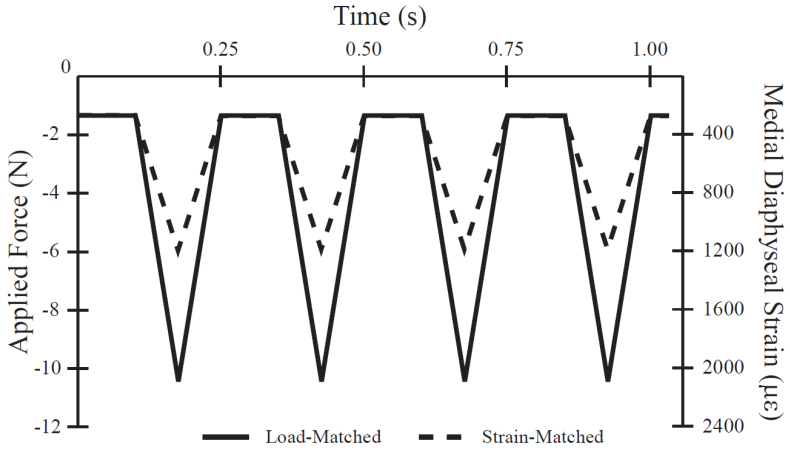

Figure 3.1 Schematic for 4 cycles (1 second) of the daily mechanical loading protocol. The average peak load delivered to the Load-Matched group (solid line) was -11.3±0.5 N, corresponding to ~+2100 με on the medial mid-diaphysis. The average peak load delivered to the Strain-Matched group (dashed line) was -5.9±0.5 N, corresponding to +1200 με. Both groups received average minimum compressive loads of 1.5±0.6 N.

Micro-computed Tomography (microCT)

All pairs of tibiae were scanned using micro-computed tomography (MS-8 MicroCT, GE Healthcare Systems) [22]. Isotropic voxel resolution was 15 μm. Cancellous and cortical volumes of interest (VOIs) were defined in each tibia. The purely cancellous VOI began approximately 0.5 mm distal to the growth plate, excluding the primary spongiosa and cortical shell, and extended 10% of the total tibial length. A global threshold of 0.27 g/cc (1100 HU) was used to segment cancellous mineralized tissue from water and soft tissue. Cancellous outcomes included bone volume fraction (BV/TV), tissue mineral density (TMD, mg/cc), and trabecular thickness and separation (Tb.Th and Tb.Sp, mm). The cortical VOI was centered at the mid-diaphysis and spanned 2.5% of the total tibial length. A global threshold of 0.64 g/cc (2684 HU) was used to segment cortical mineralized tissue from water and soft tissue. Cortical outcomes included tissue mineral density (TMD, mg/cc), cortical and medullary area (A_C, A_M, mm^2) and principal moments of inertia (I_{MIN}, I_{MAX}, mm^4). Total tibial length (L_T, mm) and whole bone radii of curvature in

the anterioposterior and mediolateral (C_{AP}, C_{ML}, respectively, mm) directions were also measured[25].

Finite Element (FE) Analysis

Specimen-specific FE models were used to calculate strains in the cancellous tissue during loading and to determine the stiffness of the metaphysis in control and loaded tibiae. FE VOIs were defined in a subset of representative tibiae (n=5/per group) and used to generate corticocancellous and cortical models. The FE VOIs extended 5% of total tibial length and were centered length-wise within the cancellous microCT VOIs [23]. Corticocancellous VOIs included both the cancellous tissue and the cortical shell; cortical VOIs included only the cortical shell. MicroCT image data were converted to FE models using custom software (MATLAB v7.5, The Mathworks, Inc.). MicroCT scans were coarsened by combining 2x2x2 voxels (following a convergence study) to yield a single voxel with side length 0.03 mm. The coarsened voxels were converted into 8-noded linear brick elements (~49K elements per corticocancellous model) and were assigned isotropic material properties with a uniform modulus of 20 GPa and a Poisson's ratio of 0.3 (Abaqus v6.7, Dassault Systèmes Simulia Corp) [26]. Nodes at the distal surface were restricted to in-plane motion and prevented from rigid-body motion. Strains were determined at the element centroids.

Because bone mass is fairly constant in adult mice [24], we assumed that tissue strains in the control limbs with loading were representative of the strains induced at the onset of the experiment. The strain environment during the loading experiment was characterized by applying a uniform displacement to the proximal surface of the corticocancellous models of the control (right) tibiae. Elements were identified within the models that coincided with the cancellous VOIs used for the microCT analysis (see

MicroCT above). In these elements, the longitudinal strains (e_{33}) were determined. For LM animals, a uniform 0.08% apparent strain applied at the proximal surface resulted in -11.3 N at the distal surface. The cancellous tissue strains ranged from -2130±273 με to +338±118 με (average Min to Max, -506±71 με mean) (Table 1). For SM animals, a uniform 0.05% apparent strain applied at the proximal surface resulted in -5.9 N at the distal surface. Similar to the measured in vivo diaphyseal strains, cancellous tissue strains engendered in the SM animals were approximately half those in the LM animals, ranging from -1178±109 με to +165±42 με (average Min to Max, -233±29 με mean) (Table 1).

To characterize the effects of adaptation on the apparent stiffness of the proximal metaphysis in both groups, the reaction force (N) was calculated for a uniform strain of 0.07% applied to the proximal surface of corticocancellous and cortical models. The proportion of the load transmitted through the cancellous tissue was determined from the ratio of the cortical to corticocancellous reaction forces, an indicator of load sharing between the metaphyseal cortex and cancellous tissue [23].

Statistical Analysis

The effects of the two loading protocols on the adaptive response in the cancellous and cortical compartments, on tibial length, and on body mass were determined using a linear mixed-model with repeated-measures (JMP v8.0, SAS Institute Inc.). The between-subject factor was loading protocol (LM versus SM) and the within-subject factor was loading [loaded (L) versus control (R) tibia] for the microCT and FE measurements or time (Day 1 versus Day 15) for body mass. All results presented are significant unless otherwise stated. If no significant interaction was present, only main effects are reported. Percentage difference for the main effect of loading combined data for the LM and SM groups and was calculated as [(LM +

SM Loaded limbs) – (LM + SM Control limbs)]*100/(LM + SM Control limbs). If the interaction term was significant, a post-hoc means comparisons analysis was conducted with a Bonferroni correction. Statistical significance was set at $p<0.05$. All values are represented as the mean $\pm$ SD.

3.3 Results

Only the LM group increased cancellous bone mass after 2 weeks of in vivo tibial compression (Fig. 3.2). BV/TV in the loaded limbs of the LM group was +49% greater than control limbs (Fig. 3.2A). Cancellous mass increased primarily through trabecular thickening. Tb.Th in the loaded limbs of the LM group was +64% greater than control limbs (Fig. 3.2C). Cancellous TMD also increased in the loaded limbs of the LM group by +12% (Fig. 3.2B). Tb.Sp in loaded limbs was 14% lower than in control limbs [(LM + SM loaded) vs. (LM + SM control)] (Fig. 3.2D). Control limbs between LM and SM groups did not differ for any cancellous measure.

Metaphyseal stiffness of the LM group was increased by in vivo loading. Compressive reaction forces nearly doubled in the corticocancellous FE models for the loaded tibiae relative to the control tibiae (L: 18.3$\pm$1.6 N vs. C: 9.5$\pm$0.7 N, LM and SM). However, the proportion of load carried by cancellous tissue relative to the cortical shell was not altered by loading in either loading group. The proportion of load borne by the cortical relative to corticocancellous bone was 0.75$\pm$0.03 (LM and SM) in both loaded and control limbs.

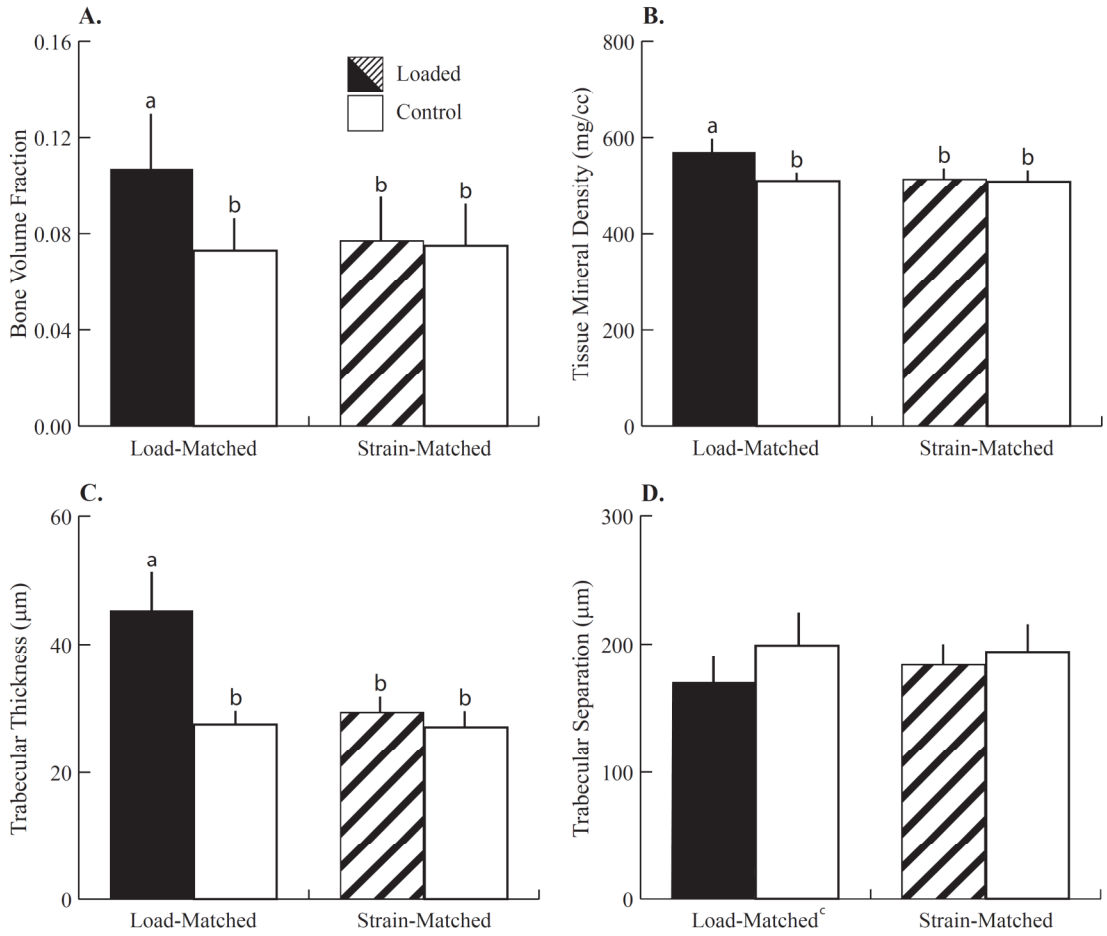

Figure 3.2 Cancellous parameters after 2 weeks of loading, analyzed by microCT from a purely cancellous VOI in the proximal metaphysis. Significant effects of loading were detected only in the Load-Matched group. (A) Bone volume fraction increased 49%, (B) Tissue mineral density (mg/cc) increased 12%, and (C) Trabecular thickness (mm) increased 62%, in loaded limbs of the LM group relative to control limbs. (D) Trabecular separation (mm) decreased 14% due to loading ([LM + SM loaded limbs] vs [LM + SM control limbs]). Data are represented as mean + SD. $^{a\text{-}b}$groups with different letters are significantly different $p<0.05$ by linear-mixed model with repeated measures followed by means comparisons with Bonferroni correction. $^{c}p<0.05$ main effect of loading.

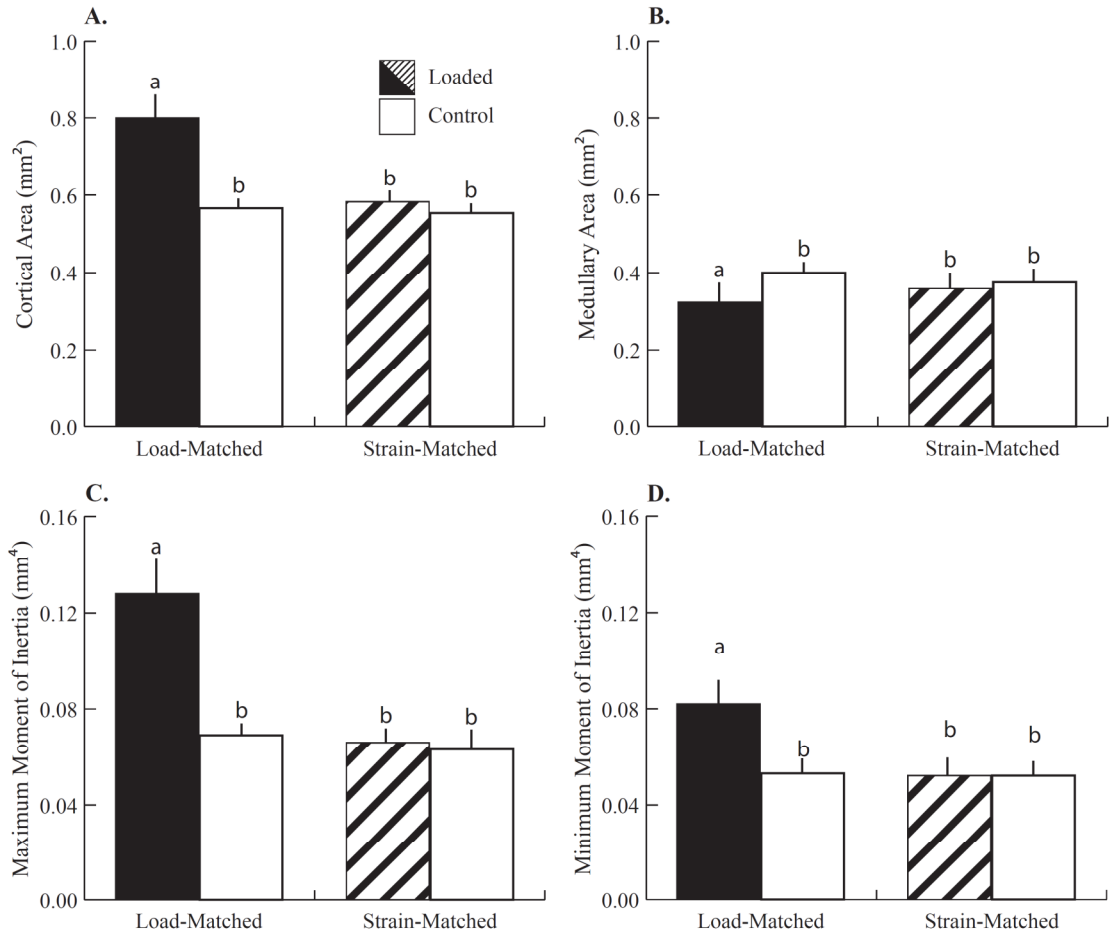

Figure 3.3 Cortical parameters after 2 weeks of loading, analyzed by microCT from a VOI centered at the mid-diaphysis. Significant effects of loading were detected only in the Load-Matched group. (A) Cortical area (mm^2) increased 41%, (B) Medually area (mm^2) decreased 19%, (C) Maximum moment of inertia (mm^4) increased 88%, and (D) Minimum moment of inertia (mm^4) increased 54% in loaded limbs relative to control limbs. Mean + SD.

[a-b]groups with different letters are significantly different $p<0.05$ by linear-mixed model with repeated measures followed by means comparisons with Bonferroni correction.

Similarly, when cortical adaptation at the mid-diaphysis was examined, only the cortices of the LM group responded to 2 weeks of tibial compression (Fig. 3). Cortical area increased 41% through a 19% reduction in A_M in the loaded limbs of the LM group relative control limbs (Fig. 3A-B). Medullary contraction with applied load ($0.071mm^2$) was responsible for one third of the total difference in cortical area between the loaded and control limbs ($0.216mm^2$). Thus, periosteal deposition was responsible for the majority of the increase in cortical bone mass with load. Consequently, the principal moments of inertia increased in the loaded limbs of the LM group relative to control limbs. I_{MAX} and I_{MIN} in the loaded tibiae were +88% and +54% greater than in control tibiae, respectively (Fig. 3C-D). Cortical TMD decreased 4% with loading in the LM group (L: 1124$\pm$21 mg/cc vs. C: 1166$\pm$18 mg/cc) and did not change in the SM group (L + C: 1172$\pm$13 mg/cc). C_{AP} decreased 4.4% with loading [(LM + SM loaded) vs. (LM + SM control)] and curvature was not different between LM and SM groups. C_{ML} was not affected by loading. Control limbs between LM and SM groups did not differ in any microCT-derived parameter. Post-adaptation diaphyseal stiffness was -0.0052 N/με (95% CI: [-0.0063, -0.0042], all groups pooled together) and was not altered by loading in either group. L_T was 16.7$\pm$0.42 mm and was not different following tibial compression.

After 2 weeks, body mass was not altered by loading (22.4$\pm$1.5 g, all mice). Two mice were lost during the loading experiment. One mouse in the SM group died due to complications with anesthesia and one mouse in the LM was euthanized due to a fracture during loading, leaving 12 LM mice and 11 SM mice remaining.

3.4 Discussion

In vivo tibial compression successfully elicited a robust adaptive response in adult, osteopenic female mice (LM group) in both cancellous and cortical

compartments. Cancellous bone mass increased primarily through trabecular thickening. Cortical bone mass increased through medullary contraction and periosteal expansion, resulting in greater principal moments of inertia. Bone mass and metaphyseal tissue stiffness increased with loading in adult mice when similar peak compressive forces, or similar metaphyseal strains and doubled diaphyseal strains, were applied relative to those used in growing mice. In contrast, diaphyseal tissue strain levels that were osteogenic in growing mice were not in adult mice (SM group), suggesting that aging reduces the skeleton's responsiveness to mechanical stimuli. Taken together, despite reduced mechanoresponsiveness with aging, cancellous and cortical mass and architecture were enhanced with tibial compression in adult mice.

While the cancellous compartment in adult LM animals increased bone mass, the response to mechanical loading was reduced relative to that in 10 week old animals, though the peak tissue strains were similar. Despite this reduction, in vivo tibial compression recovered age-related bone loss to levels equivalent to the control limbs of young mice [23] (Fig. 3.4). In addition to a reduction in cellular population and activity with aging [27-31], bone formation in the cancellous compartment in adults may also be substrate-limited by the smaller available surface area for bone deposition (Fig. 3.4). The absolute BV in control limbs of adult mice was lower than that in young animals (adult: 0.10 ± 0.02; young 0.16 ± 0.02). The control limbs in adults had thicker, more widely separated trabeculae, leading to an overall reduced bone mass, as others have also reported [23, 24]. Other studies using tibial compression, in addition to ours, have also reported reduced cancellous responses to loading in adult mice. Loading increased bone mass in young mice (8-12 wk old) while adult mice (20-30 wk old) lost bone mass with loading [20, 21]. However, our results demonstrate that mechanical loading can be used to recover cancellous bone loss due to aging with

potential applications to other causes of pathological bone loss, such as estrogen withdrawal.

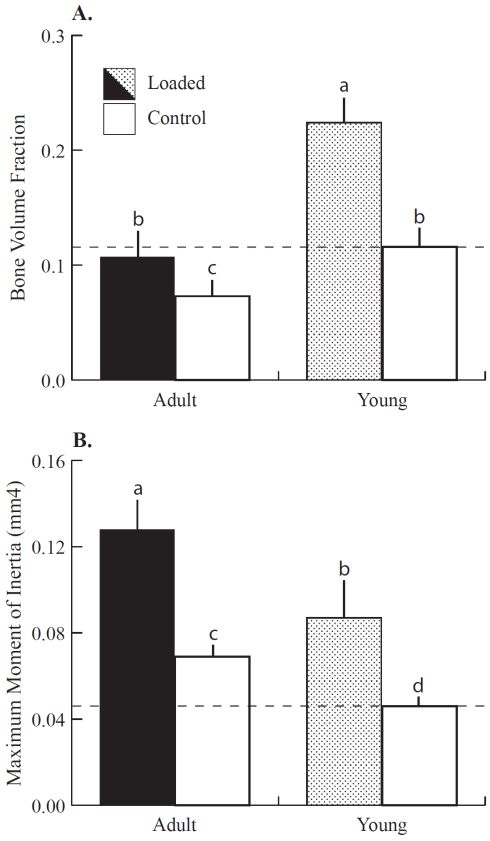

Figure 3.4 Comparison between the Load-Matched group ('Adult') and 10 week old female mice ('Young'), both loaded for 2 weeks. (A) Bone volume fraction was reduced 38% in adult mice (control limbs). Adult mice demonstrated a reduced response to loading relative to Young mice (+49% versus +95%, loaded versus control). Loading increased bone mass in Adult mice to control levels in Young mice (Adult loaded limbs versus Young control limbs). (B) Maximum moment of inertia increased 48% in Adult mice (control limbs) due to expanding cortices. Adult mice achieved greater gains with loading than Young mice (+90% versus +87%, loaded versus control). Dashed lines represent mean values from control limbs in Young female mice loaded for 2 weeks. Data for 10 week old mice are from {Lynch, 2010 #78}. Mean + SD.
[a-d]groups with different letters are significantly different $p<0.05$ by linear-mixed model with repeated measures followed by means comparisons with Bonferroni correction. Within-subject factor: loading; between-subject factor: age.

In contrast to cancellous tissue, the diaphyseal cortex in the LM group exhibited an enhanced response to mechanical loading relative to that measured in young (12 wk old) animals [20, 21]. With LM loading, medullary area decreased more in adults (-19.3%) than in young animals (-9.2%) indicating an enhanced endocortical response in adults. Conversely, periosteal expansion accounted for 85% of the increase in cortical area in 10wk old mice and 2/3 of the increased cortical area in 26wk old mice, indicating an enhanced periosteal response in the young relative to old mice. In addition, adult animals had greater cortical area; thus available substrate for bone formation was not a limiting factor [32, 33]. Modest bone formation at the periosteum of a larger cortex will have a greater impact on bending resistance (I_{MAX}, I_{MIN}) than in a smaller cortex. Indeed, maximum moment of inertia was greater in adults, as was the magnitude of the increase with loading, than in young animals. However, these load-induced differences were similar when normalized to control limbs (+88% vs +90% respectively, adult versus young) (Fig. 4).

Using tibial compression, mid-diaphyseal strains of +1200 με were osteogenic in young (12 wk old) mice, but were insufficient to elicit a cortical or cancellous response in adult mice. Cortical bone formation was increased when applying loads corresponding to tibial mid-diaphyseal strains of +1200 με, using cantilever bending in adult (21.5 mo old) mice [16] and four-point bending in adult (19 mo old) rats [15]. However, tibial compression represents a more physiological loading condition than four-point or cantilever bending, therefore the introduction of a novel strain distribution may account for the osteogenic response in other loading models [34]. The peak cancellous tissue strains in the proximal metaphysis of the SM group were half of those observed in growing mice and in the LM group (Table 1), and likely not great enough to elicit a response in an adult mouse [35]. Other factors could be contributing to the lack of response in addition to peak applied load and resulting tissue strains. For

example, the applied strain rate in the SM group is half of that applied to the LM group. Therefore, osteogenesis may have occurred if the strain rate was increased while other the parameters were maintained [36].

The reduced cortical response to in vivo loading with aging has previously been characterized by histomorphometry [15, 16, 37]. When peak induced strains were matched across ages, the skeletons of the older animals either did not respond to loading [37], or exhibited a reduced osteogenic response that did not resulted in increased cross-sectional area [15, 16]. When peak strains were doubled in adult (21.5 mo old) mice undergoing tibial cantilever bending, the boney response was not improved relative to those with matched strains [16]. In the cantilever bending model, the mice were senescent and likely less responsive than the young adults (26 wk old) examined here [38]. In our study, doubling the diaphyseal strains, which increased the strain rate, enhanced cortical adaptation, as would be expected [19, 36].

The applied load required to engender +1200 με at the medial mid-shaft in 26 week old mice was half that used in growing 10 week old mice [23], despite larger cortical cross-sectional geometries in adult mice. Greater tibial curvature in the adult mice than in young mice (C_{AP}: +28%, C_{ML}: +200%, adult vs. young) induced greater bending moments in the adult tibiae during axial loading overcoming age-related increases in cortical geometry to cause decreased stiffness in adult tibiae relative to young mice. Thus, inducing similar diaphyseal deformations in young and adult mice required lower peak applied loads in adults. In addition, cancellous tissue strains during tibial compression in the LM group were similar to those observed in growing mice despite adults having lower adult BV and BV/TV. This result may reflect a larger metaphyseal cortical shell in adult mice. Diaphyseal cortical cross-sectional area and shell thickness are larger in adults [32, 33] and the proximal cortical shell has been shown to expand with tibial compression [39, 40]. Based on FE results, the

metaphyseal cortical shell in adults transmits a greater proportion of applied load than the metaphyseal shell in young mice (cortical:corticocancellous load ratio 0.76 in adult vs 0.61 in young mice), possibly contributing to lower cancellous tissue strains in adult SM mice.

In vivo models are required to study functional adaptation and have contributed to our understanding of osteogenic stimuli. The ability to control the loading applied to the skeleton is a strength of our approach and was critical to our research objective. Loading of the mouse tibia allows this process to be studied simultaneously at cortical and cancellous sites within the same bone. Furthermore, the applied loading combines both compression and bending within the tibia as experienced in vivo. We applied loading to only the left limb while the right limb was the internal, non-loaded control; adaptation is assessed by comparing differences between the loaded and control limbs. This methodology controls for systemic factors beyond our control, such as differences in cage activity level, body mass, etc. among the mice. Despite controlling the applied stimulus, coupling between the loading parameters was unavoidable. The increased load in the LM group also increased the strain rate of load application, a parameter also known to influence adaptation [36]. However, matching the strain rates would have increased the pause between load cycles in the SM group, another variable that enhances the skeletal response [16]. Despite these potential ambiguities, our data demonstrate definitively different outcomes between the two loading protocols and confirm that bone mass can be restored to young control levels with appropriately chosen loading parameters. Whether this response could be improved upon further can only be established with experiments varying additional parameters.

In summary, in vivo tibial compression enhanced bone mass and architecture in adult osteopenic mice when the peak applied load was of similar magnitude to loads

applied in growing mice. Even though the cancellous adaptive response was reduced with age, loading increased metaphyseal stiffness and increased cancellous mass to levels seen in young mice. In contrast, the cortical adaptive response was improved relative to that in young mice, likely due to greater cortical bone surface upon which to form new bone. When the peak applied diaphyseal strains were similar to those applied in growing mice, osteogenesis did not occur in either compartment. This result suggests that, to be most effective, mechanical loading should be employed earlier in life, when loading-induced architectural changes readily occur and remain after cessation of loading [41-43]. The osteogenic protocol (LM) found here for adult mice can be used to investigate how other factors, such as reduced bioavailable estrogen, interact with age to modulate cancellous bone adaptation. Results from such studies will help direct the use of mechanical loading to induce architectural changes that will increase bone strength and reduce fracture risk..

REFERENCES

1. Bassey, E. J., Rothwell, M. C., Littlewood, J. J., and Pye, D. W. Pre- and postmenopausal women have different bone mineral density responses to the same high-impact exercise. J Bone Miner Res 13*:*1805-13; 1998.
2. Heinonen, A., Kannus, P., Sievanen, H., Oja, P., Pasanen, M., Rinne, M., Uusi-Rasi, K., and Vuori, I. Randomised controlled trial of effect of high-impact exercise on selected risk factors for osteoporotic fractures. Lancet 348*:*1343-7; 1996.
3. Kato, T., Terashima, T., Yamashita, T., Hatanaka, Y., Honda, A., and Umemura, Y. Effect of low-repetition jump training on bone mineral density in young women. J Appl Physiol 100*:*839-43; 2006.
4. Vainionpaa, A., Korpelainen, R., Leppaluoto, J., and Jamsa, T. Effects of high-impact exercise on bone mineral density: a randomized controlled trial in premenopausal women. Osteoporos Int 16*:*191-7; 2005.
5. Vainionpaa, A., Korpelainen, R., Vihriala, E., Rinta-Paavola, A., Leppaluoto, J., and Jamsa, T. Intensity of exercise is associated with bone density change in premenopausal women. Osteoporos Int 17*:*455-63; 2006.
6. von Stengel, S., Kemmler, W., Kalender, W. A., Engelke, K., and Lauber, D. Differential effects of strength versus power training on bone mineral density in postmenopausal women: a 2-year longitudinal study. Br J Sports Med 41*:*649-55; discussion 655; 2007.
7. Nurzenski, M. K., Briffa, N. K., Price, R. I., Khoo, B. C., Devine, A., Beck, T. J., and Prince, R. L. Geometric indices of bone strength are associated with

physical activity and dietary calcium intake in healthy older women. J Bone Miner Res 22:416-24; 2007.

8. Korpelainen, R., Keinanen-Kiukaanniemi, S., Heikkinen, J., Vaananen, K., and Korpelainen, J. Effect of impact exercise on bone mineral density in elderly women with low BMD: a population-based randomized controlled 30-month intervention. Osteoporos Int 17:109-18; 2006.

9. Stengel, S. V., Kemmler, W., Pintag, R., Beeskow, C., Weineck, J., Lauber, D., Kalender, W. A., and Engelke, K. Power training is more effective than strength training for maintaining bone mineral density in postmenopausal women. J Appl Physiol 99:181-8; 2005.

10. Snow, C. M., Shaw, J. M., Winters, K. M., and Witzke, K. A. Long-term exercise using weighted vests prevents hip bone loss in postmenopausal women. J Gerontol A Biol Sci Med Sci 55:M489-91; 2000.

11. Kohrt, W. M., Ehsani, A. A., and Birge, S. J., Jr. Effects of exercise involving predominantly either joint-reaction or ground-reaction forces on bone mineral density in older women. J Bone Miner Res 12:1253-61; 1997.

12. Kerr, D., Morton, A., Dick, I., and Prince, R. Exercise effects on bone mass in postmenopausal women are site-specific and load-dependent. J Bone Miner Res 11:218-25; 1996.

13. Kohrt, W. M., Snead, D. B., Slatopolsky, E., and Birge SJ, J. r. Additive effects of weight-bearing exercise and estrogen on bone mineral density in older women. J Bone Miner Res 10:1303-1311; 1995.

14. Raab-Cullen, D. M., Akhter, M. P., Kimmel, D. B., and Recker, R. R. Bone response to alternate-day mechanical loading of the rat tibia. J Bone Miner Res 9:203-11; 1994.

15. Turner, C. H., Takano, Y., and Owan, I. Aging changes mechanical loading thresholds for bone formation in rats. J Bone Miner Res 10*:*1544-9; 1995.
16. Srinivasan, S., Agans, S. C., King, K. A., Moy, N. Y., Poliachik, S. L., and Gross, T. S. Enabling bone formation in the aged skeleton via rest-inserted mechanical loading. Bone 33*:*946-55; 2003.
17. LaMothe, J. M., Hamilton, N. H., and Zernicke, R. F. Strain rate influences periosteal adaptation in mature bone. Med Eng Phys 27*:*277-84; 2005.
18. Saxon, L. K., Robling, A. G., Alam, I., and Turner, C. H. Mechanosensitivity of the rat skeleton decreases after a long period of loading, but is improved with time off. Bone 36*:*454-64; 2005.
19. Mosley, J. R., March, B. M., Lynch, J., and Lanyon, L. E. Strain magnitude related changes in whole bone architecture in growing rats. Bone 20*:*191-8; 1997.
20. De Souza, R. L., Matsuura, M., Eckstein, F., Rawlinson, S. C., Lanyon, L. E., and Pitsillides, A. A. Non-invasive axial loading of mouse tibiae increases cortical bone formation and modifies trabecular organization: a new model to study cortical and cancellous compartments in a single loaded element. Bone 37*:*810-8; 2005.
21. Brodt, M. D., and Silva, M. J. Aged mice have enhanced endocortical response and normal periosteal response compared to young-adult mice following 1 week of axial tibial compression. J Bone Miner Res; 2010.
22. Fritton, J. C., Myers, E. R., Wright, T. M., and van der Meulen, M. C. Loading induces site-specific increases in mineral content assessed by microcomputed tomography of the mouse tibia. Bone 36*:*1030-8; 2005.
23. Lynch, M. E., Main, R. P., Xu, Q., Walsh, D. J., Schaffler, M. B., Wright, T. M., and van der Meulen, M. C. H. Cancellous bone adaptation to tibial

compression is not sex-dependent in growing mice. Journal of Applied Physiology; 2010.

24. Glatt, V., Canalis, E., Stadmeyer, L., and Bouxsein, M. L. Age-related changes in trabecular architecture differ in female and male C57BL/6J mice. J Bone Miner Res 22*:*1197-207; 2007.

25. Main, R. P., Lynch, M. E., and Van der Meulen, M. C. H. In vivo tibial stiffness is maintained by whole bone morphology and cross-sectional geometry in growing female mice. Journal of Biomechanics; 2010.

26. van der Meulen, M. C., Yang, X., Morgan, T. G., and Bostrom, M. P. The effects of loading on cancellous bone in the rabbit. Clin Orthop Relat Res 467*:*2000-6; 2009.

27. Donahue, S. W., Jacobs, C. R., and Donahue, H. J. Flow-induced calcium oscillations in rat osteoblasts are age, loading frequency, and shear stress dependent. Am J Physiol Cell Physiol 281*:*C1635-41; 2001.

28. Fedarko, N. S., Vetter, U. K., Weinstein, S., and Robey, P. G. Age-related changes in hyaluronan, proteoglycan, collagen, and osteonectin synthesis by human bone cells. J Cell Physiol 151*:*215-27; 1992.

29. Tonna, E. A. Skeletal Cell Aging and Its Effects on the Osteogenetic Potential. Clin Orthop Relat Res 40*:*57-81; 1965.

30. Tonna, E. A. Electron microscopy of aging skeletal cells. III. The periosteum. Lab Invest 31*:*609-32; 1974.

31. Tonna, E. A. Electron microscopic study of bone surface changes during aging. The loss of cellular control and biofeedback. J Gerontol 33*:*163-77; 1978.

32. Brodt, M. D., Ellis, C. B., and Silva, M. J. Growing C57Bl/6 mice increase whole bone mechanical properties by increasing geometric and material properties. J Bone Miner Res 14*:*2159-66; 1999.

33. Price, C., Herman, B. C., Lufkin, T., Goldman, H. M., and Jepsen, K. J. Genetic variation in bone growth patterns defines adult mouse bone fragility. J Bone Miner Res 20*:*1983-91; 2005.

34. Rubin, C. T., and Lanyon, L. E. Kappa Delta Award paper. Osteoregulatory nature of mechanical stimuli: function as a determinant for adaptive remodeling in bone. J Orthop Res 5*:*300-10; 1987.

35. Turner, C. H., Forwood, M. R., Rho, J. Y., and Yoshikawa, T. Mechanical loading thresholds for lamellar and woven bone formation. J Bone Miner Res 9*:*87-97; 1994.

36. Turner, C. H., Owan, I., and Takano, Y. Mechanotransduction in bone: role of strain rate. Am J Physiol 269*:*E438-42; 1995.

37. Rubin, C. T., Bain, S. D., and McLeod, K. J. Suppression of the osteogenic response in the aging skeleton. Calcif Tissue Int 50*:*306-13; 1992.

38. Priemel, M., Schilling, A. F., Haberland, M., Pogoda, P., Rueger, J. M., and Amling, M. Osteopenic mice: animal models of the aging skeleton. J Musculoskelet Neuronal Interact 2*:*212-8; 2002.

39. Sugiyama, T., Price, J. S., and Lanyon, L. E. Functional adaptation to mechanical loading in both cortical and cancellous bone is controlled locally and is confined to the loaded bones. Bone; 2009.

40. Sugiyama, T., Saxon, L. K., Zaman, G., Moustafa, A., Sunters, A., Price, J. S., and Lanyon, L. E. Mechanical loading enhances the anabolic effects of intermittent parathyroid hormone (1-34) on trabecular and cortical bone in mice. Bone 43*:*238-48; 2008.

41. Daly, R. M. The effect of exercise on bone mass and structural geometry during growth. Med Sport Sci 51*:*33-49; 2007.

42. Fujie, H., Miyagaki, J., Terrier, A., Rakotomanana, L., Leyvraz, P. F., and Hayashi, K. Detraining effects on the mechanical properties and morphology of rat tibiae. Biomed Mater Eng 14:219-33; 2004.

43. Jarvinen, T. L., Pajamaki, I., Sievanen, H., Vuohelainen, T., Tuukkanen, J., Jarvinen, M., and Kannus, P. Femoral neck response to exercise and subsequent deconditioning in young and adult rats. J Bone Miner Res 18:1292-9; 2003.

CHAPTER 4

ESTROGEN DEFICIENCY AND TIBIAL COMPRESSION ALTER CANCELLOUS ARCHITECTURE IN MICE THROUGH DIFFERENT MECHANISMS

4.1 Introduction

Osteoporosis is a pathological skeletal condition characterized by decreased bone mass and increased risk for fracture. Two million men and women over the age of 50 experience skeletal fractures due to osteoporosis every year in the US [1]. Women are particularly susceptible to fracture and account for 70% all of fractures [1]. Associated annual costs of these fractures are currently $17 billion and projected to rise over $25 million by 2025 [1]. Therefore, implementing therapeutic and preventative strategies are critical to reducing associated costs.

Mechanical stimuli are a potential anabolic therapy for pathological bone loss. With exercise, bone mass is increased readily in children [2, 3] and pre-menopausal adults [4-6]. But, in post-menopausal women, results are more variable. The role of estrogen deficiency in reduced responsiveness to mechanical signals is unclear, but may be due to reduced bone substrate upon which to form new bone, decreased responsiveness of bone cells or increased level of mechanical stimulus required for skeletal homeostasis [7, 8]. Progressively resistive and high-intensity interventions that last one year or more, marginally increased bone mass [9-12] or prevented bone loss [13-16]. Combined, these studies support the use of mechanical loading to reduce risk for fracture by increasing bone mass and altering bone architecture. Determining which particular mechanical signals best stimulate osteogenesis in an osteopenic and estrogen deficient population is critical for enhancing current therapeutic approaches that are predominantly anti-catabolic rather than anabolic. Furthermore, understanding

how aging and estrogen deficiency modulate bone functional adaptation is essential to overcoming the skeleton's failure to respond appropriately to mechanical signals.

Ovariectomy (OVX) in rats and mice is often used to model osteoporosis. Similar to postmenopausal women, rats exhibit both a transient phase of rapid bone turnover concomitant with bone loss, which then slows to a more gradual rate that is equivalent to that in non-OVX rats [17, 18]. As in Type I osteoporosis [19, 20], OVX-induced cancellous bone loss occurs chiefly through increased trabecular separation or reduced trabecular number [21-25]. The OVX mouse is not yet fully characterized, but bone mass decreased through mechanisms similar to those in the rat at the distal femur, vertebrae, and proximal tibia [26-30]. The changes in trabecular thickness following OVX are unclear in both rats and mice, where remaining trabeculae thicken [21], thickness does not change [22, 23, 26] or is reduced [27, 30]. Increased indices of bone resorption are detected as early as 2 weeks post-surgery [17, 31], but cancellous bone loss is not measured until after 4 weeks [21, 28].

Exercise therapies in rats have been used to prevent or attenuate cancellous bone loss immediately following OVX [25, 32, 33] or recover bone loss after skeletal adaptation to OVX has been established [32, 34, 35] by suppressing osteoclastic activity. Of these studies, only one characterized the resulting cancellous architecture between OVX and Sham controls. Three months of tower climbing recovered some bone loss by thickening remaining trabeculae without a change in separation [32]. However, the mechanical environment of the skeleton is unknown during exercise; therefore salient mechanical parameters, such as peak load magnitude, cannot be directly related to adaptation. Controlled, in vivo tibial compression increased cancellous bone mass in growing mice predominantly through thickening of trabeculae without a change in separation [36, 37] and sometimes with a relatively smaller change in separation [38]. Loading-induced changes in cancellous bone are

more variable in adult female mice [39-41]. To date, only one study investigated the combined effects of hormone deficiency and controlled in vivo loading on the cancellous bone and the resulting architectural changes. Similar to OVX, orchidectomy (ORX) increased trabecular separation without affecting thickness. Tibial compression preserved cancellous bone mass in growing male mice following ORX, although the ORX mice had fewer remaining trabeculae that were thickened with loading [42]. These results suggest loading and hormone deficiency affect cancellous mass through differing mechanisms.

The objective of this study was to characterize the effects of estrogen withdrawal on the adaptive response to in vivo loading in adult female mice. Previously, cancellous bone mass increased in adult female mice following 2 weeks of loading [43]. In vivo tibial compression was hypothesized to prevent bone loss due to estrogen deficiency when initiated immediately following OVX. Mechanical loading continued for 1, 2 and 6 weeks to determine the initial cellular events as well as characterize the steady-state [42] effects on cancellous and cortical architecture in the mouse tibia.

4.2 Materials and Methods

Seventy-two female C57Bl/6 mice (Jackson Labs, Bar Harbor, ME) were received and acclimatized in our animal facility. Mice were housed 4-5 per cage with ad libitum access to food and water. Body masses were recorded daily and used to monitor the health of the mice over the course the experiment. At the start of the experiment, mice weighed 22.9±1.9 g. Cornell University's Institutional Animal Care and Use Committee approved all experimental procedures.

Experimental Procedure

At 26 weeks of age, mice were randomly selected for either ovariectomy (OVX) or sham surgery (Figure 4.1). Immediately following surgery, in vivo loading commenced. Mice were divided into 3 loading groups, including 24 mice each (n=12 for OVX and Sham): 1 week (1 Wk), 2 weeks (2 Wk), and 6 weeks (6 Wk) duration. The loading protocol for both loading groups consisted of 1200 cycles administered to the left limb at 4 Hz, 5 days/week [37, 38, 42, 43]. All groups received 9.0 N peak compressive load and 1.0 N minimum compressive dwell load. The right limb served as the contralateral control limb. During all loading sessions, mice were maintained under anesthesia (2% Isoflurane, 1.0 L/min, Webster). Normal cage activity was allowed between loading sessions.

Intraperitoneal injections of tetracycline (20 mg/kg, Sigma Aldrich) were administered on Day 1, 4, and Day 31 for the 1Wk, 2 Wk, and 6 Wk groups, respectively. Intraperitoneal injections of calcein (10 mg/kg, Sigma Aldrich) were administered on Day 5, 12, and 39 for each group respectively (Figure 4.1). At the end of the loading period, mice were euthanized by CO_2 inhalation. Tibiae were dissected free of soft tissue and fixed in 10% neutral buffered formalin for 48 hrs, then stored in 70% ethanol. Ovariectomy was confirmed by measuring uterine horn mass.

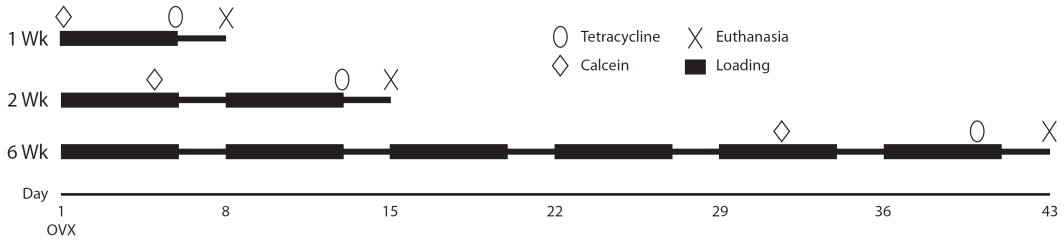

Figure 4.1 Experimental design and timetable.

Micro-computed Tomography (microCT)

Paired tibiae were scanned using micro-computed tomography at 15 µm isotropic resolution (µCT35, Scanco Medical AG). Cancellous and cortical volumes of interest (VOIs) were defined for each tibia. The purely cancellous VOI began approximately 0.5 mm distal to the growth plate, excluding the primary spongiosa and cortical shell, and extended approximately 10% of the total tibial length. Cancellous mineralized tissue was segmented from water and soft tissue using a global threshold of 0.27 g/cc (~190 HU). Cancellous outcomes included bone volume fraction (BV/TV), volumetric tissue mineral density (tBMD, mg/cc), and trabecular thickness and separation (Tb.Th and Tb.Sp, mm). The cortical VOI was centered at the mid-diaphysis and spanned 2.5% of the total tibial length. A global threshold of 0.34 g/cc (~2650 HU) was used to segment cortical mineralized tissue from water and soft tissue. Cortical outcomes included cortical area (Ct.Ar, mm^2) and principal moments of inertia (I_{MIN}, I_{MAX}, mm^4).

Statistical Analysis

The effects of experimental duration, estrogen status, and loading were determined using a full factorial linear-mixed model with repeated measures (JMP v8.0, SAS Institute Inc., Cary, NC). The between-subject factors were duration (1, 2, and 6 weeks) and estrogen status (Sham versus OVX) and the within-subject factor was loading [loaded (L) versus control (C) tibia]. All results presented are significant unless otherwise stated. If no significant interaction was present, then only main effects are reported. If a second degree interaction term was significant, then data was pooled as appropriate, followed by a post-hoc means comparisons analysis with a Bonferroni correction. Similarly, if the third degree interaction term was significant, a post-hoc means comparisons analysis with a Bonferroni correction was conducted

among all groups. Statistical significance was set at $p<0.05$. All values are represented as the mean $\pm$ SD.

4.3 Results

The changes in cancellous mass were biphasic in adult female mice, due to the competing effects of loading on trabecular thickness and effects of estrogen withdrawal on trabecular separation. Therefore, BV/TV was affected by loading, experimental duration, and estrogen status. Tb.Th increased with loading at all time points, and tBMD increased with loading after 2 and 6 weeks. Tb.Sp increased overall with loading (+4.9%: pooled L vs. pooled R) and was the only parameter affected by estrogen status. Age-related increases in Tb.Sp were accelerated in the OVX group starting at 2 weeks post-surgery. Tb.N decreased only with experimental duration, but exhibited a trend for interaction between duration and estrogen status ($p=0.07$). All cortical measures increased with loading and experimental duration, but not estrogen deficiency.

After 1 week of loading, only the OVX group increased BV/TV (+35%) in loaded limbs relative to control limbs (Figure 4.2). At this time, Tb.Th increased 20% (pooled L: Sham + OVX vs. pooled C: Sham + OVX) (Figure 4.3). No effect of loading was detected in tBMD (Figure 4.2) or in Tb.Sp and Tb.N (Figure 4.3). After 2 weeks of loading, BV/TV did not differ between loaded and control limbs or between Sham and OVX groups. Loading-induced increases in Tb.Th were similar after 1 and 2 weeks (2 Wk: +30%; pooled L vs. pooled C). tBMD increased 5.6% (pooled L vs. pooled C). Simultaneously, Tb.Sp increased 11% and Tb.N decreased 9.3% from 1 to 2 weeks, due to effects of aging (pooled 1 Wk vs pooled 2 Wk). After 6 weeks of loading, BV/TV increased similarly in the Sham and OVX groups (+95%, +159%, respectively) in loaded relative to control limbs. Loading-induced increases in Tb.Th

were greatest after 6 weeks. Tb.Th increased 65% and tBMD increased 8.1% (pooled L vs. pooled C). Age-related increases in Tb.Sp did not continue after 6 weeks in the Sham group, but did in the OVX group. Tb.Sp in the 6 Wk OVX group was 15% greater than the corresponding Sham group, and 11% greater than in the 2 Wk OVX group (L and C pooled at each time point). Tb.N decreased an additional 9.1% from 2 to 6 weeks.

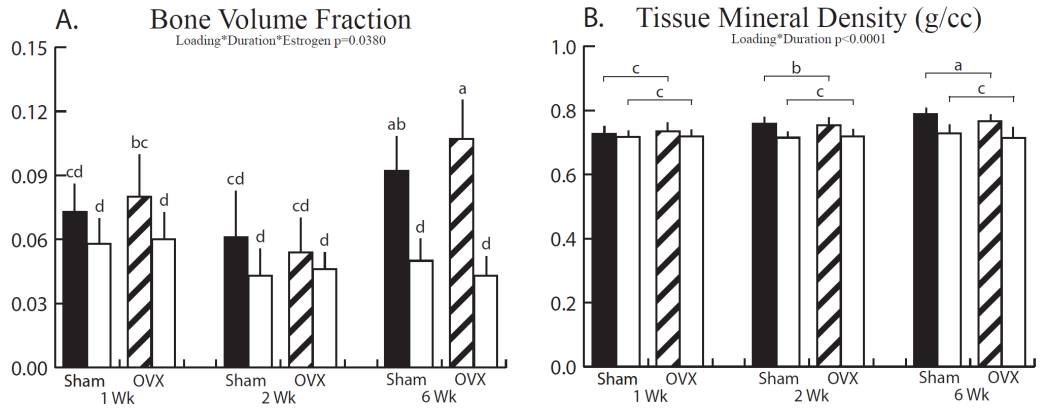

Figure 4.2 Cancellous mass parameters (mean±SD) analyzed by microCT from a purely cancellous VOI in the proximal metaphysis. A. BV/TV was affected by loading, duration, and estrogen status, therefore a means comparison analysis was conducted with Bonferroni correction among all groups. After 1 wk of loading, only the OVX group increased 35%. No change in BV/TV occurred after 2 wks of loading. After 6 wks of loading, OVX and Sham groups increased BV/TV similarly, +159% and +95%, respectively. B. tBMD was affected by loading and duration, therefore means comparisons were conducted on groups where OVX and Sham groups pooled together. tBMD increased 5.6% and 8.1% in loaded limbs relative to control limbs after 2 and 6 wks of loading.
$^{a\text{-}d}p<0.05$, groups with different letters are significantly different by means comparisons analysis with Bonferroni correction. Data is pooled where appropriate.

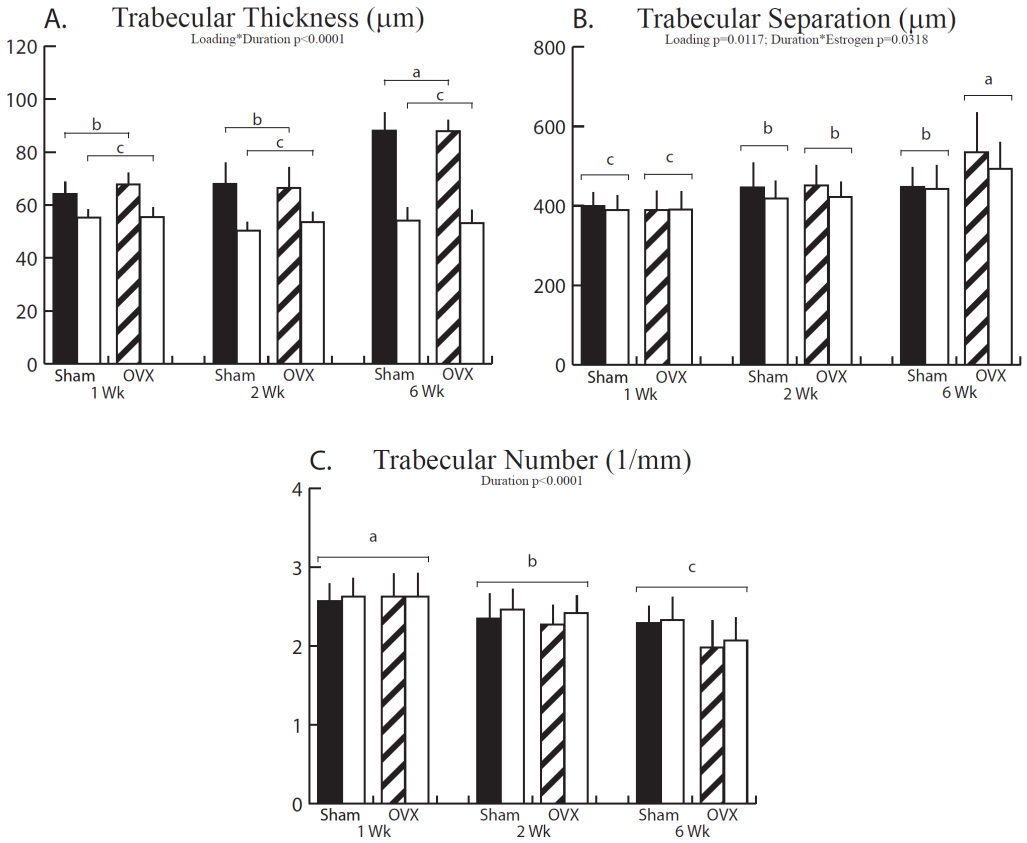

Figure 4.3 Cancellous architecture parameters (mean±SD) analyzed by microCT from a purely cancellous VOI in the proximal metaphysis. A. Tb.Th was affected by loading and duration. Tb.Th increasead 20%, 30%, and 65% in loaded limbs relative to control limbs after 1, 2, and 6 wks of loading. B. Tb.Sp was affected by loading (main effect) and duration and estrogen status. Tb.Sp was 4.9% greater in loaded limbs (pooled) compared to control limbs (pooled). Tb.Sp was similar between Sham and OVX up until 6 wks, where the OVX group had 15% greater Tb.Sp than the Sham group. C. Tb.N was affected by duration (main effect). Tb.N decreased 9.3% from 1 Wk to 2 Wk and decreased an additional 9.2% from 2 Wk to 6 Wk.
$^{a\text{-}d}p<0.05$, groups with different letters are significantly different by means comparisons analysis with Bonferroni correction. Data is pooled where appropriate.

In the cortical compartment, the effects of loading increased in a dose-dependent manner (Figure 4). Ct.Ar increased 7.3%, 16%, and 24% after 1, 2, and 6 weeks of loading, respectively (pooled L vs. pooled C). Increases in bone mass improved bending resistance after 2 weeks of loading. I_{MAX} increased 31% and 45% while I_{MAX} increased 19% and 28% after 2 and 6 weeks of loading, respectively (pooled L vs. pooled C). Control limbs did not differ among time points for any cortical measure. In addition, cortical parameters were not affected by estrogen deficiency.

Body mass decreased 6.9% only in the 1 Wk OVX group (Table 4.1). After 2 weeks body mass was fully recovered in the OVX groups. No other group lost a significant amount of body mass. Estrogen deficiency resulted in uterine horn atrophy as early as 1 week after OVX. Uterine horn mass was 57%, 47%, and 73% smaller in the OVX group than in the Sham group after 1, 2, and 6 weeks of OVX, respectively (Table 4.1). Loaded limbs were 0.6% longer than control limbs (pooled L: 18.7$\pm$0.6 mm vs. pooled C: 18.6$\pm$0.5 mm) (Table 4.2). Tibial length was similar between OVX and Sham animals up until 6 weeks, at which time the tibiae in the OVX group were 2.3% longer than those in the Sham group.

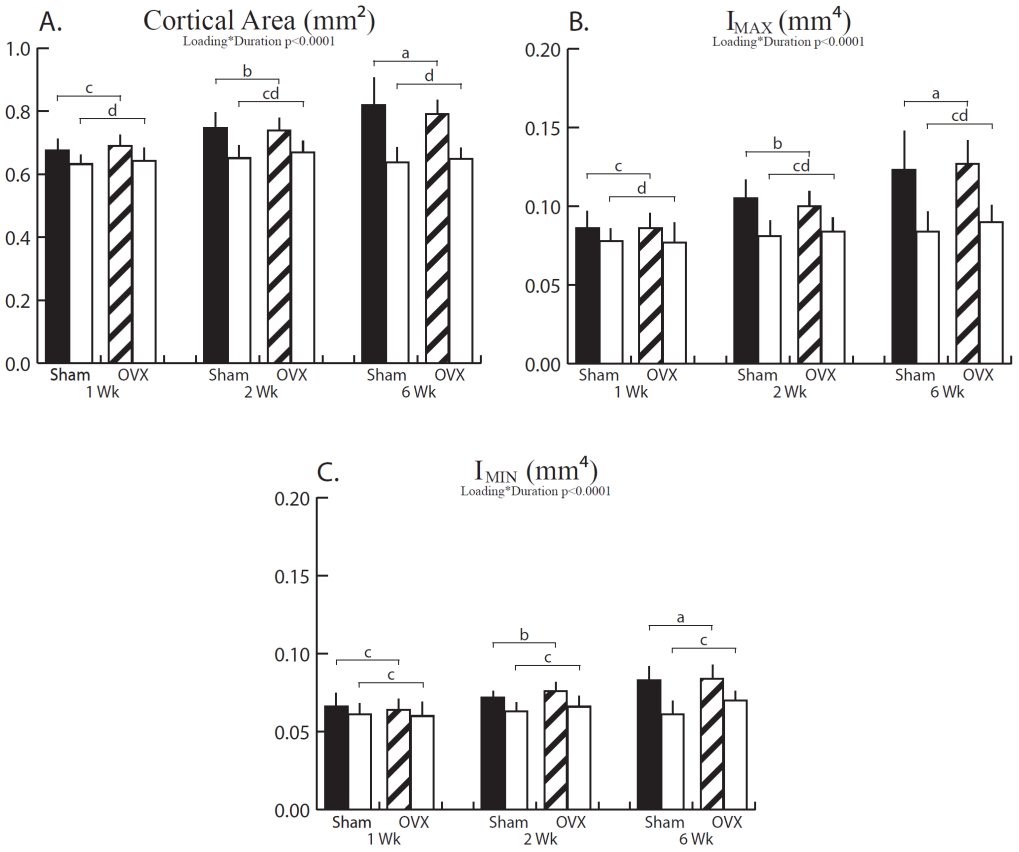

Figure 4.4 Cortical parameters (mean±SD) analyzed by microCT from a VOI centered at the mid-diaphysis. All parameters were affected only by loading and duration, therefore means comparisons analysis was conducted on groups where Sham and OVX were pooled. A. Ct.Ar increased 7.3%, 16%, and 25% in loaded limbs relative to control limbs after 1, 2, and 6 wks, respectively. B. I_{MAX} increased 12%, 31%, and 46% in loaded limbs relative to control limbs after 1, 2, and 6 wks, respectively. C. I_{MIN} increased 11% and 29% in loaded limbs relative to control limbs after 2 and 6 wks, respectively.
[a-d]$p<0.05$, groups with different letters are significantly different by means comparisons analysis with Bonferroni correction.

Four mice were lost prior to completing the experiment. One mouse died due to surgical complications (6 Wk Sham), one mouse was euthanized due to a fracture during loading (6 Wk Sham), and two mice died due to unknown reasons (2 Wk Sham and 6 Wk Sham). The losses resulted in n=12/group in the 1 Wk group, n=11 Sham and n=12 OVX in the 2 Wk group, and n=10 Sham and n=11 OVX in 6 Wk group.

Table 4.1 Body mass of mice over the course of loading experiment and uterine horn mass at end of experiment. Data are represented as mean±SD.

Duration	Estrogen	Body Mass (g)			Uterine Horn Mass[c] (mg)
		Day 1	Euth. Day	Δ	
1 Wk	Sham	21.3±1.4	20.9±1.4	0.3±0.8	85±22
	OVX	22.6±2.1	21.0±1.6[a]	1.6±1.0	37±6
2 Wk	Sham	22.6+1.6	21.5+1.2	1.1+0.9	69+16
	OVX	23.7±1.7	24.0±1.4[b]	-0.3±0.8	37±7
6 Wk	Sham	23.1±2.4	21.7±2.2	1.2±0.6	89±29
	OVX	24.0±1.4	24.1±1.2[b]	-0.1±0.8	24±9

[a]versus corresponding Day 1, $p<0.05$.
[b]versus corresponding 1 Wk group, $p<0.05$.
[c]Main effect of estrogen status, $p<0.05$. Uterine horn mass of the Sham group was significantly larger than of the OVX group at every time point.

Table 4.2 Tibial length of loaded and control limbs at completion of loading experiment. Data are represented as mean+SD.

Duration	Estrogen	Tibial Length (mm)		
		L[a]	C	Δ=L-C
1 Wk	Sham	18.3±0.3	18.2±0.2	0.09±0.1
	OVX	18.2±0.2	18.1±0.3	0.07±0.2
2 Wk	Sham	18.8±0.4	18.6±0.3	0.21±0.3
	OVX	18.9±0.4	18.8±0.3	0.10±0.3
6 Wk	Sham	19.0±0.6	18.8±0.5	0.19±0.3
	OVX[b,c]	19.4±0.3	19.3±0.3	0.08±0.3

[a]Main effect of loading, $p<0.05$. Loaded limbs (L) were significantly longer than control limbs (C).
[b]versus corresponding Sham group (loaded and control limbs pooled), $p<0.05$.
[c]versus corresponding 2 Wk group (loaded and control limbs pooled), $p<0.05$.

4.4 Discussion

In vivo tibial compression increased cancellous and cortical bone mass in osteopenic, estrogen-deficient adult female mice after 6 weeks of loading. Cancellous bone mass in loaded limbs exhibited a bimodal distribution with time due to the competing architectural effects of loading and estrogen deficiency. Estrogen deficiency did not affect cortical bone mass or its adaptive capacity.

Mechanical loading and ovariectomy altered cancellous bone architecture through different mechanisms. In a prior OVX study with decreased cancellous mass in the proximal tibia of mice, reductions occurred through decreased trabecular number concomitant with increased trabecular separation, whereas trabecular thickness was not altered [28]. These patterns of bone loss were also observed in the distal femur and lumbar vertebrae [26, 28, 29]. In rats, OVX-induced reductions in cancellous mass of the proximal tibia also occurred through increased separation and reduced number without changes in thickness [22, 23, 25]. In one case, remaining trabeculae became thicker than in Sham rats after an extended period of time (34 weeks) [21]. This pattern of cancellous bone loss through removal of individual trabeculae followed by thickening of remaining struts also occurs in post-menopausal women [19, 20]. In contrast to estrogen-deficiency, tibial loading increased cancellous mass primarily through trabecular thickening [42]. In estrogen-replete growing and adult mice, trabecular thickening was also the primary source of loading-induced increases in bone mass [36, 37, 43]. Whether thickening of fewer remaining trabeculae maintains or increases the strength of cancellous tissue following OVX is unclear. Cancellous mass and architecture, measured by microCT, are used as proxy for mechanical strength. Additional factors that contribute to strength, such as material properties or trabecular orientation, are not analyzed by microCT analysis. Finite

element analysis, either of the proximal metaphysis or the entire tibia, could be used to address this limitation parametrically [38, 43, 44].

Estrogen deficiency has been hypothesized to negatively impact the skeleton's ability to respond appropriately to its mechanical environment, though the exact mechanisms are unknown. Estrogen deficiency may raise the (normal) level of mechanical stimuli required to maintain bone, thereby producing net bone loss when activity levels are maintained or decreased [8]. Alternatively, estrogen deficiency may impair the ability of bone cells to appropriately respond to mechanical loading [7, 8]. Estrogen and mechanical loading may share a common pathway, both possibly mediated through the estrogen receptor [8, 25, 45], which is present in all bone cells [46]. In the current study, estrogen deficiency in adult female mice did not inhibit loading-induced adaptation in cancellous bone, though more time after OVX may be required to detect a detrimental effect on adaptation.

Few studies have characterized the changes in cancellous architecture and mass using combined estrogen deficiency and mechanical loading. Three months of tower jumping, initiated 3 months after surgery, only partially recovered OVX-induced bone loss in aged rats through trabecular thickening [32]. Reduced bone mass persisted in OVX rats relative to Sham rats due to elevated trabecular separation. Similarly, when tibial loading was applied to orchidectomized (ORX) growing male mice for 6 weeks starting three days after surgery, trabecular thickening and separation were greatest, and number lowest, in the loaded limbs of the ORX group [42]. Therefore, hormone deficiency removed individual trabeculae while the remaining struts thickened with loading. Combined with the present findings, the anabolic effects of mechanical loading do not appear to be hindered by estrogen deficiency in mice for up 6 weeks. But, if the effects of estrogen deficiency are allowed to be established prior to the anabolic stimulus, then mechanical loading will likely be less effective at

increasing bone mass, especially in an aged individual. Therefore, to maximize the anabolic effects of loading without circulating estrogen, mechanical loading should be initiated coincident with estrogen withdrawal. For example, a strongly anabolic stimulus would be most effective at counteracting bone loss due to estrogen deficiency in peri-menopausal women. A basal group was not included in this study, which would have provided a reference point for both loading- and OVX-associated changes. A strength of the study is that adult mice were used, which prevented the confounding effects of estrogen withdrawal on growth [47]. Additionally, cancellous bone mass is constant in adult female mice [43, 48], which was also observed here upon comparison of control limbs. Therefore, a basal group was not necessary.

Loading and estrogen deficiency altered cancellous mass at different rates in adult female mice, similar to results in growing female mice (Figure 4.5). In young adult mice who have reached peak bone mass, cancellous mass and architecture did not change in the tibial proximal metaphysis up to 4 weeks following OVX [27]. Furthermore, increased indices of resorption were not detected in the cortical compartment of the tibia until 2-4 weeks while reductions in cortical geometry did not appear until 16 weeks after OVX [31, 49]. In growing mice, OVX-induced reductions in mass appeared sometime between 4 and 5 weeks, although the timing has been variable [28, 50]. Growing mice also experience a bimodal change in BV/TV following OVX, where reductions occurred at 4 weeks, disappeared at 7 weeks, and reappeared again at 11 weeks post-surgery [28]. Based on those results, adult mice would not be expected to exhibit bone loss at least up until 6 weeks post-surgery. However, no study to date has characterized OVX-induced changes in cancellous mass or architecture, or in resorptive activity of the proximal tibia in adult mice. The amount of cancellous mass lost following OVX has been correlated with baseline BV/TV, where mouse strains with the lowest mass lost the least amount of bone

(C57Bl/6) and strains with the greatest mass (C3H) lost the most [27, 50]. Bone turnover is a substrate-limited process, and the sluggish response of the C57Bl/6 strain to OVX may be due in part to the small surface area upon which new bone tissue can be deposited. This effect would likely be exacerbated in the osteopenic adult mice used in the present study.

In contrast to the effects of estrogen deficiency, the effects of tibial compression on bone formation were evident almost immediately (Figure 4.5), which has been demonstrated in many studies using a variety of mechanical loading regimes. In rats, osteoblasts are visible within 2 days following four-point bending [51] and vertebral pinning [51, 52]. Indices of formation increased within one week following ulnar compression [53] and vertebral pinning [52, 54]. In C57Bl/6 mice, bone formation was evident just 2 days following ulnar compression [55]. In the present study, the interaction between estrogen deficiency and mechanical loading became evident after 6 weeks, where the loaded limbs of our 6 Wk OVX group had the largest trabecular separation. Estrogen inhibits activation frequency of basic multicellular units through suppression of osteoblastogenesis and osteoclastogenesis and also inhibits osteoclast activity and lifespan [46]. Estrogen deficiency, therefore, may be permissive for osteoclasts to remove trabeculae under low or insufficient mechanical stimulus while the remaining ones thicken under applied mechanical loading [24, 25, 56]. Whether the differences between OVX and Sham would become more prominent given a longer experimental duration remains to be determined.

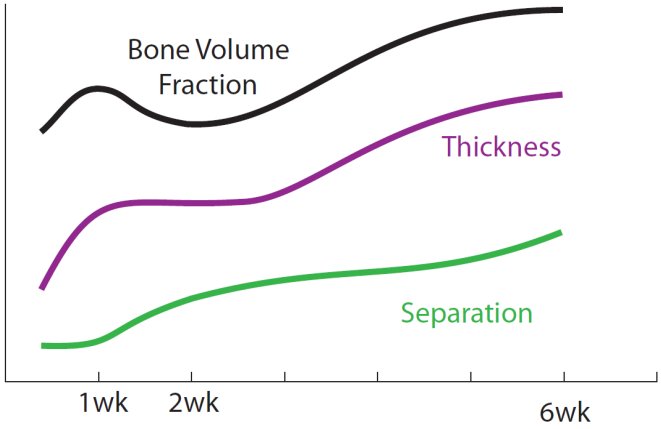

Figure 4.5 Schematic of relative effects of trabecular thickness (purple-middle) and separation (green-bottom) on cancellous bone volume fraction (black-top) in ovariectomized adult mice over the course of 1, 2 and 6 weeks of tibial compression.

Several in vivo studies have demonstrated that diaphyseal bone of Sham and OVX groups respond similarly to mechanical stimuli. Repetitive jumping in adult and growing rats increased cortical area and moment of inertia similarly between Sham and OVX groups [57, 58]. Under four-point bending, adult OVX and Sham rats increased cortical area similarly through equivalent periosteal bone formation rates, mineral apposition rates, and formation surfaces [59]. One other study has incorporated in vivo tibial compression and hormone deficiency in 10-week old male mice. Orchidectomized and Sham mice increased I_{MAX} similarly after 6 weeks of loading, but only the ORX group increased I_{MIN} [42]. However, those male mice were growing while our females are adult. In addition, steroid hormones may play different roles on the periosteum in males and females [60]. Estrogen deficiency did not affect cortical geometry in the control limbs of our OVX mice. In the C57Bl/6 mouse, changes in the mid-diaphyseal tibial cortex did not emerge until 16 weeks post-ovariectomy [49], therefore no changes would be expected during the 6 week time frame used here [42, 50].

In summary, we demonstrated that in vivo tibial compression increased cancellous bone mass in the metaphysis through trabecular thickening for up to 6 weeks following estrogen deficiency. Estrogen deficiency did not affect the adaptive response in the tibial diaphysis. Estrogen deficiency and tibial compression altered cancellous architecture through different mechanisms and at different rates. Tibial loading primarily increased trabecular thickness whereas estrogen deficiency increased trabecular separation. The interactive effect of these two mechanisms on cancellous mass was evident after 6 weeks. Whether these trends would continue after 6 weeks, when OVX-induced bone loss becomes evident in C57Bl/6 mice, remains to be determined. In the future, initiating tibial compression 6 or more weeks following OVX, after bone loss has been established, will demonstrate whether tibial compression can be used to recover bone loss in an osteoporotic, estrogen-deficient adult population.

REFERENCES

1. Burge, R., Dawson-Hughes, B., Solomon, D. H., Wong, J. B., King, A., and Tosteson, A. Incidence and economic burden of osteoporosis-related fractures in the United States, 2005-2025. J Bone Miner Res 22*:*465-75; 2007.
2. Fuchs, R. K., Bauer, J. J., and Snow, C. M. Jumping improves hip and lumbar spine bone mass in prepubescent children: a randomized controlled trial. J Bone Miner Res 16*:*148-56; 2001.
3. Kontulainen, S., Sievanen, H., Kannus, P., Pasanen, M., and Vuori, I. Effect of long-term impact-loading on mass, size, and estimated strength of humerus and radius of female racquet-sports players: a peripheral quantitative computed tomography study between young and old starters and controls. J Bone Miner Res 18*:*352-9; 2003.
4. Nikander, R., Sievanen, H., Uusi-Rasi, K., Heinonen, A., and Kannus, P. Loading modalities and bone structures at nonweight-bearing upper extremity and weight-bearing lower extremity: a pQCT study of adult female athletes. Bone 39*:*886-94; 2006.
5. Winters-Stone, K. M., and Snow, C. M. Site-specific response of bone to exercise in premenopausal women. Bone 39*:*1203-9; 2006.
6. Vainionpaa, A., Korpelainen, R., Leppaluoto, J., and Jamsa, T. Effects of high-impact exercise on bone mineral density: a randomized controlled trial in premenopausal women. Osteoporos Int 16*:*191-7; 2005.
7. Ehrlich, P. J., and Lanyon, L. E. Mechanical strain and bone cell function: a review. Osteoporos Int 13*:*688-700; 2002.
8. Turner, R. T. Mechanical signaling in the development of postmenopausal osteoporosis. Lupus 8*:*388-92; 1999.

9. Kerr, D., Ackland, T., Maslen, B., Morton, A., and Prince, R. Resistance training over 2 years increases bone mass in calcium-replete postmenopausal women. J Bone Miner Res 16*:*175-81; 2001.

10. Kohrt, W. M., Ehsani, A. A., and Birge, S. J., Jr. Effects of exercise involving predominantly either joint-reaction or ground-reaction forces on bone mineral density in older women. J Bone Miner Res 12*:*1253-61; 1997.

11. Kerr, D., Morton, A., Dick, I., and Prince, R. Exercise effects on bone mass in postmenopausal women are site-specific and load-dependent. J Bone Miner Res 11*:*218-25; 1996.

12. Kohrt, W. M., Snead, D. B., Slatopolsky, E., and Birge SJ, J. r. Additive effects of weight-bearing exercise and estrogen on bone mineral density in older women. J Bone Miner Res 10*:*1303-1311; 1995.

13. Engelke, K., Kemmler, W., Lauber, D., Beeskow, C., Pintag, R., and Kalender, W. A. Exercise maintains bone density at spine and hip EFOPS: a 3-year longitudinal study in early postmenopausal women. Osteoporos Int 17*:*133-42; 2006.

14. von Stengel, S., Kemmler, W., Kalender, W. A., Engelke, K., and Lauber, D. Differential effects of strength versus power training on bone mineral density in postmenopausal women: a 2-year longitudinal study. Br J Sports Med 41*:*649-55; discussion 655; 2007.

15. Snow, C. M., Shaw, J. M., Winters, K. M., and Witzke, K. A. Long-term exercise using weighted vests prevents hip bone loss in postmenopausal women. J Gerontol A Biol Sci Med Sci 55*:*M489-91; 2000.

16. Pruitt, L. A., Taaffe, D. R., and Marcus, R. Effects of a one-year high-intensity versus low-intensity resistance training program on bone mineral density in older women. J Bone Miner Res 10*:*1788-95; 1995.

17. Wronski, T. J., Cintron, M., and Dann, L. M. Temporal relationship between bone loss and increased bone turnover in overiectomized rats. Calcif. Tissue Int. 43*:*179-183; 1988.

18. Wronski, T. J., Dann, L. M., Scott, K. S., and Cintron, M. Long-term effects of ovariectomy and aging on the rat skeleton. Calcif. Tissue Int. 45*:*360-366; 1989.

19. Parfitt, A. M. Age-related structural changes in trabecular and cortical bone: cellular mechanisms and biomechanical consequences. Calcif Tissue Int 36 Suppl 1*:*S123-8; 1984.

20. Parfitt, A. M., Mathews, C. H., Villanueva, A. R., Kleerekoper, M., Frame, B., and Rao, D. S. Relationships between surface, volume, and thickness of iliac trabecular bone in aging and in osteoporosis. Implications for the microanatomic and cellular mechanisms of bone loss. J Clin Invest 72*:*1396-409; 1983.

21. Waarsing, J. H., Day, J. S., Verhaar, J. A., Ederveen, A. G., and Weinans, H. Bone loss dynamics result in trabecular alignment in aging and ovariectomized rats. J Orthop Res 24*:*926-35; 2006.

22. Baldock, P. A., Need, A. G., Moore, R. J., Durbridge, T. C., and Morris, H. A. Discordance between bone turnover and bone loss: effects of aging and ovariectomy in the rat. J Bone Miner Res 14*:*1442-8; 1999.

23. Abe, T., Chow, J. W., Lean, J. M., and Chambers, T. J. Estrogen does not restore bone lost after ovariectomy in the rat. J Bone Miner Res 8*:*831-8; 1993.

24. Ito, M., Nishida, A., Nakamura, T., Uetani, M., and Hayashi, K. Differences of three-dimensional trabecular microstructure in osteopenic rat models caused by ovariectomy and neurectomy. Bone 30*:*594-8; 2002.

25. Westerlind, K. C., Wronski, T. J., Ritman, E. L., Luo, Z. P., An, K. N., Bell, N. H., and Turner, R. T. Estrogen regulates the rate of bone turnover but bone balance in ovariectomized rats is modulated by prevailing mechanical strain. Proc Natl Acad Sci U S A 94*:*4199-204; 1997.

26. Wright, L. E., Christian, P. J., Rivera, Z., Van Alstine, W. G., Funk, J. L., Bouxsein, M. L., and Hoyer, P. B. Comparison of Skeletal Effects of Ovariectomy Versus Chemically-Induced Ovarian Failure in Mice. J Bone Miner Res; 2008.

27. Bouxsein, M. L., Myers, K. S., Shultz, K. L., Donahue, L. R., Rosen, C. J., and Beamer, W. G. Ovariectomy-induced bone loss varies among inbred strains of mice. J Bone Miner Res 20*:*1085-92; 2005.

28. Zhou, H., Iida-Klein, A., Lu, S. S., Ducayen-Knowles, M., Levine, L. R., Dempster, D. W., and Lindsay, R. Anabolic action of parathyroid hormone on cortical and cancellous bone differs between axial and appendicular skeletal sites in mice. Bone 32*:*513-20; 2003.

29. Iwaniec, U. T., Yuan, D., Power, R. A., and Wronski, T. J. Strain-dependent variations in the response of cancellous bone to ovariectomy in mice. J Bone Miner Res 21*:*1068-74; 2006.

30. Cano, A., Dapia, S., Noguera, I., Pineda, B., Hermenegildo, C., del Val, R., Caeiro, J. R., and Garcia-Perez, M. A. Comparative effects of 17beta-estradiol, raloxifene and genistein on bone 3D microarchitecture and volumetric bone mineral density in the ovariectomized mice. Osteoporos Int 19*:*793-800; 2008.

31. Emerton, K. B., Hu, B., Woo, A. A., Sinofsky, A., Hernandez, C., Majeska, R. J., Jepsen, K. J., and Schaffler, M. B. Osteocyte apoptosis and control of bone resorption following ovariectomy in mice. Bone 46*:*577-83; 2010.

32. Notomi, T., Okimoto, N., Okazaki, Y., Nakamura, T., and Suzuki, M. Tower climbing exercise started 3 months after ovariectomy recovers bone strength of the femur and lumbar vertebrae in aged osteopenic rats. J Bone Miner Res 18*:*140-9; 2003.

33. Peng, Z. Q., Vaananen, H. K., and Tuukkanen, J. Ovariectomy-induced bone loss can be affected by different intensities of treadmill running exercise in rats. Calcif Tissue Int 60*:*441-8; 1997.

34. Yeh, J. K., Liu, C. C., and Aloia, J. F. Additive effect of treadmill exercise and 17 beta-estradiol replacement on prevention of tibial bone loss in adult ovariectomized rat. J Bone Miner Res 8*:*677-83; 1993.

35. Iwamoto, J., Takeda, T., and Ichimura, S. Effects of moderate intensity exercise on tibial bone mass in mature ovariectomized rats: bone histomorphometry study. Keio J Med 47*:*162-7; 1998.

36. Marenzana, M., De Souza, R. L., and Chenu, C. Blockade of beta-adrenergic signaling does not influence the bone mechano-adaptive response in mice. Bone 41*:*206-15; 2007.

37. Fritton, J. C., Myers, E. R., Wright, T. M., and van der Meulen, M. C. Loading induces site-specific increases in mineral content assessed by microcomputed tomography of the mouse tibia. Bone 36*:*1030-8; 2005.

38. Lynch, M. E., Main, R. P., Xu, Q., Walsh, D. J., Schaffler, M. B., Wright, T. M., and van der Meulen, M. C. H. Cancellous bone adaptation to tibial compression is not sex-dependent in growing mice. Journal of Applied Physiology; 2010.

39. De Souza, R. L., Matsuura, M., Eckstein, F., Rawlinson, S. C., Lanyon, L. E., and Pitsillides, A. A. Non-invasive axial loading of mouse tibiae increases cortical bone formation and modifies trabecular organization: a new model to

study cortical and cancellous compartments in a single loaded element. Bone 37:810-8; 2005.

40. Brodt, M. D., and Silva, M. J. Aged mice have enhanced endocortical response and normal periosteal response compared to young-adult mice following 1 week of axial tibial compression. J Bone Miner Res; 2010.

41. Sugiyama, T., Price, J. S., and Lanyon, L. E. Functional adaptation to mechanical loading in both cortical and cancellous bone is controlled locally and is confined to the loaded bones. Bone 46:314-21; 2010.

42. Fritton, J. C., Myers, E. R., Wright, T. M., and van der Meulen, M. C. Bone mass is preserved and cancellous architecture altered due to cyclic loading of the mouse tibia after orchidectomy. J Bone Miner Res 23:663-71; 2008.

43. Lynch, M. E., Main, R. P., Xu, Q., Schmicker, T. L., Schaffler, M. B., Wright, T. M., and van der Meulen, M. C. H. The Adaptive Response to Tibial Compression in Adult Female Mice Varies with Applied Load Magnitude. JBMR; 2010.

44. Bourne, B. C., and van der Meulen, M. C. Finite element models predict cancellous apparent modulus when tissue modulus is scaled from specimen CT-attenuation. J Biomech 37:613-21; 2004.

45. Lanyon, L. E. Using functional loading to influence bone mass and architecture: objectives, mechanisms, and relationship with estrogen of the mechanically adaptive process in bone. Bone 18:37S-43S; 1996.

46. Riggs, B. L., Khosla, S., and Melton, L. J., 3rd Sex steroids and the construction and conservation of the adult skeleton. Endocr Rev 23:279-302; 2002.

47. Turner, R. T., Maran, A., Lotinun, S., Hefferan, T., Evans, G. L., Zhang, M., and Sibonga, J. D. Animal models for osteoporosis. Rev Endocr Metab Disord 2*:*117-27; 2001.

48. Glatt, V., Canalis, E., Stadmeyer, L., and Bouxsein, M. L. Age-related changes in trabecular architecture differ in female and male C57BL/6J mice. J Bone Miner Res 22*:*1197-207; 2007.

49. Li, C. Y., Schaffler, M. B., Wolde-Semait, H. T., Hernandez, C. J., and Jepsen, K. J. Genetic background influences cortical bone response to ovariectomy. J Bone Miner Res 20*:*2150-8; 2005.

50. Klinck, J., and Boyd, S. K. The Magnitude and Rate of Bone Loss in Ovariectomized Mice Differs Among Inbred Strains as Determined by Longitudinal In vivo Micro-Computed Tomography. Calcif Tissue Int 83*:*70-9; 2008.

51. Boppart, M. D., Kimmel, D. B., Yee, J. A., and Cullen, D. M. Time course of osteoblast appearance after in vivo mechanical loading. Bone 23*:*409-15; 1998.

52. Chow, J. W., Wilson, A. J., Chambers, T. J., and Fox, S. W. Mechanical loading stimulates bone formation by reactivation of bone lining cells in 13-week-old rats. J Bone Miner Res 13*:*1760-7; 1998.

53. Hillam, R. A., and Skerry, T. M. Inhibition of bone resorption and stimulation of formation by mechanical loading of the modeling rat ulna in vivo. J Bone Miner Res 10*:*683-689; 1995.

54. Kim, C. H., Takai, E., Zhou, H., von Stechow, D., Muller, R., Dempster, D. W., and Guo, X. E. Trabecular bone response to mechanical and parathyroid hormone stimulation: the role of mechanical microenvironment. J Bone Miner Res 18*:*2116-25; 2003.

55. Tanaka, S. M., Alam, I. M., and Turner, C. H. Stochastic resonance in osteogenic response to mechanical loading. Faseb J 17*:*313-4; 2003.

56. Weinans, H., and Prendergast, P. J. Tissue adaptation as a dynamical process far from equilibrium. Bone 19*:*143-149; 1996.

57. Honda, A., Sogo, N., Nagasawa, S., Shimizu, T., and Umemura, Y. High-impact exercise strengthens bone in osteopenic ovariectomized rats with the same outcome as Sham rats. J Appl Physiol 95*:*1032-7; 2003.

58. Honda, A., Umemura, Y., and Nagasawa, S. Effect of high-impact and low-repetition training on bones in ovariectomized rats. J Bone Miner Res 16*:*1688-93; 2001.

59. Hagino, H., Raab, D. M., Kimmel, D. B., Akhter, M. P., and Recker, R. R. Effect of ovariectomy on bone response to in vivo external loading. J Bone Miner Res 8*:*347-57; 1993.

60. Vanderschueren, D., Venken, K., Ophoff, J., Bouillon, R., and Boonen, S. Clinical Review: Sex steroids and the periosteum--reconsidering the roles of androgens and estrogens in periosteal expansion. J Clin Endocrinol Metab 91*:*378-82; 2006.

CHAPTER 5
CONCLUSIONS AND DISCUSSION

5.1 Summary

The objective of this work was to demonstrate that mechanical loading can stimulate bone formation at cancellous sites, which are most susceptible to osteoporotic fractures. Mechanical loading is a potential anabolic therapy for pathological bone loss, such as osteoporosis. Corticocancellous sites, such as the hip and spine, are at greatest risk for fracture due to bone loss. However, the adaptive response of cancellous bone is not well characterized. Understanding how mechanical loading and its parameters relate to bone formation in cancellous bone is fundamental to improving exercise strategies, both as preventative and therapeutic measures. Using tibial compression, the effects of sex, aging, and estrogen deficiency were assessed in cancellous bone. Cancellous mass increased similarly in growing male and female mice, and increased in osteopenic and estrogen-deficient adult female mice, thereby supporting the use of mechanical loading to increase bone mass at corticocancellous sites and reduce the risk of osteoporotic fractures.

Objective 1

Strategies designed to increase bone mass and alter architecture prior to the attainment of peak mass may be the most effective at reducing fracture risk when bone loss occurs [1-4]. Exercise studies in young adults suggest sexual dimorphism exists in the response to mechanical loading, but few comparisons have been made between female and male cohorts [5-8]. The effect of sex on the cancellous adaptive response to tibial loading was investigated in growing mice. The magnitude of peak applied loads that corresponded to +1200 με was determined in male and females from in vivo

strain gauging. Despite the larger size of male mice [9-12], the strains induced by loading were similar in males and females, and each sex required -11.5 N to engender +1200 με at tibial mid-shaft. This peak load resulted in similar peak compressive cancellous tissue strains of 2400 με in females and 2100 με in males. Following 2 weeks of tibial compression, male and female mice increased cancellous bone mass similarly in the proximal tibia, primarily through increased trabecular thickening. Tissue mineral density increased, and trabecular separation decreased. As a result of this architectural adaptation, the proportion of the applied load carried by the cancellous compartment, rather than by the cortical shell, increased. In addition, the metaphyseal stiffness of the loaded limbs was greater than in control limbs. None of these loading-induced changes differed by sex in the cancellous compartment.

Objective 2

The adaptive response of the skeleton is reduced with aging in both humans and in animal models [13-16]. In animal models, however, the response to loading has been primarily characterized in the cortex of long bones of animals. Therefore, we sought to demonstrate that cancellous bone in adult, osteopenic female mice would increase with loading as in cortical bone. Then, we determined whether the response in adult mice was reduced relative to that observed previously in growing mice. To determine appropriate loading parameters that account for possible reduced responsiveness, we utilized two protocols based on the one used previously in growing female mice. We applied the same peak compressive loads to one group of adult female mice (Load-Matched) and the same peak mid-diaphyseal strains to a second group of adult female mice (Strain-Matched). The Load-Matched (LM) group received -11.3 N peak applied load, which corresponded to +2200 με mid-diaphyseal strains, and the Strain-Matched (SM) group received +1200 με mid-diaphyseal strains,

engendered by -5.9 N peak applied load. These protocols resulted in peak cancellous tissue strains of -2130 με and -1178 με in the LM and SM groups, respectively. In the LM group only, cancellous bone mass increased through trabecular thickening, and cortical mass increased through medullary contraction and periosteal expansion. These adaptive changes increased the metaphyseal stiffness of loaded limbs relative to control limbs. The response in the cancellous compartment was reduced relative to that observed in growing mice. However, tibial loading recovered age-related loss of bone mass to reach levels equivalent to the control limbs of young animals, supporting the use of mechanical loading as a therapeutic intervention against osteoporotic bone loss. In contrast, the response in the cortical compartment was enhanced relative to that in young mice. While both young and adult mice similarly increased I_{MAX} and cortical area, adult mice underwent enhanced medullary contraction while young mice underwent enhanced periosteal deposition.

Objective 3

In women, aging is accompanied by estrogen deficiency at menopause. Following estrogen deficiency, the skeleton's ability to respond appropriately to mechanical signals is inhibited [17]. Estrogen deficiency may increase the level of mechanical stimuli that the skeleton requires to maintain 'normal' homeostasis, thereby triggering bone loss, or may impair the ability of bone cells to appropriately respond to mechanical loading [18, 19]. Tibial compression was applied to osteopenic, estrogen-deficient adult female mice to demonstrate that mechanical loading can stimulate cancellous bone formation following estrogen withdrawal. Estrogen deficiency was established in adult female mice through ovariectomy (OVX), and a Sham surgery group served as controls. To prevent OVX-induced bone loss, loading was applied immediately following surgery and lasted 1, 2, and 6 weeks to

characterize the adaptive response over time. Estrogen deficiency did not inhibit the adaptive response of cancellous bone in adult females. After 6 weeks of loading, cancellous bone mass increased similarly in Sham and OVX groups. Cancellous bone mass exhibited a bimodal response due to the differing effects of loading and estrogen deficiency, acting at different rates, on cancellous architecture. Loading primarily increased trabecular thickness while estrogen deficiency primarily increased trabecular separation. No differences in the control limbs between Sham and OVX groups were observed within the 6 week time period. The cortical compartment responded differently, showing no effects of OVX and increasing mass with loading in a dose-dependent fashion with longer experimental duration.

Strengths

The primary strength of our tibial compression model is that the adaptive response of cancellous bone can be characterized. The applied loads are directed in a physiological direction and their application does not require invasive surgery. The strains (as determined by strain gauging of the diaphysis) engendered by peak loads are also within the physiological range of moderate to intense activities [20, 21]. Based on our studies, an osteogenic, physiological loading model exists for studying cancellous and cortical adaptation in female mice, which can be used to investigate many other factors that modulate adaptation, as discussed in the Introduction.

Tibial compression elicited a robust, anabolic signal in cancellous bone of the proximal tibia, even in osteopenic and estrogen deficient adult mice. Cancellous bone mass increases occurred through trabecular thickening, and the resulting metaphyseal structure became stiffer. These results demonstrate that mechanical loading can be targeted to corticocancellous sites to increase bone mass, improve structural integrity, and reduce risk for fracture. Based on our data, mechanical loading can be

implemented as a preventative measure, either in growing children or pre- and peri-menopausal women, to increase peak bone mass and reduce risk of fracture.

Limitations

The primary limitation with our model, as with any cancellous model, is that the mechanical environment is difficult to characterize in the cancellous compartment. Cancellous bone cannot undergo strain gauging because the cortical shell limits access and the tissue is highly porous. While our FE models give a first-order approximation of the cancellous strain environment during tibial compression, those models are limited in that they are voxel-based, partial models undergoing a uniformly applied displacement with homogeneous material properties. We reported longitudinal strains, but they are likely not the only stimulus that bone cells perceive [22, 23]. The mid-diaphyseal region was selected for gauging in many other studies [21, 24-27], so the functional strains are known, and thus is a reasonable location for gauging. Therefore, we selected our applied load magnitudes based on in vivo strain gauging at the mid-diaphysis. We are limited to attachment of a single gauge due to the small size of the mouse tibia. Therefore, we have strain data in a single direction, for a single point, on the surface of the tibia.

An additional limitation is that microCT measurable outcomes serve as proxy for mechanical strength, and reflect only changes within the metaphyseal cortex rather than the entire metaphysis (see ***Future Works***). In our loading studies, cancellous bone mass increased primarily through increased trabecular thickness, but other factors such as trabecular orientation and the cortical contribution to load transmission likely play a role in overall strength. Whether or not increased trabecular thickness, or another microCT parameter, translates to stronger cancellous tissue has not been verified by mechanical testing. Based on virtual mechanical testing (FE analysis), the

metaphysis became stiffer with tibial compression. As stated previously, our FE models have limitations. Mechanical testing in the laboratory would help determine the relationship between microCT parameters and strength; however, the murine skeleton is difficult to test in the lab due to its small size. The morphology of the tibia is non-uniform, irregular, and curved, making traditional methods of mechanical testing (i.e., compression and three-point bending) difficult. In addition, mechanical testing would necessarily require inclusion of the cortical shell, so isolation of cancellous bone is not possible. Therefore, these results of such mechanical tests would likely reflect the strength of the cortex, rather than the cancellous bone.

Finally, we reported the mean value of each microCT parameter and do not have information about the spatial distribution of values within the proximal metaphysis. For example, changes in mean trabecular thickness could be driven by the thickening of a few individual trabeculae while the remaining ones do not change or perhaps even become thinner. Where those particular trabeculae are located within the cancellous structure would provide more detailed information about load transmission throughout the metaphysis.

5.1 Future Works

The studies of this thesis provide the foundation for examining additional questions that relate to the preventative and therapeutic potential of mechanical loading. Whether or not the benefits of mechanical loading will persist after cessation of loading needs to be demonstrated. Furthermore, the efficacy of mechanical loading as a therapeutic strategy for bone loss associated with estrogen withdrawal requires further exploration. Will mechanical loading prevent bone loss due to estrogen withdrawal in an adult, whose skeleton is less responsive to mechanical signals? Can mechanical loading recover bone loss that has already occurred due to aging and

estrogen deficiency? What is the relative contribution to strength of the metaphyseal cortex and the cancellous tissue within, and what role does load-sharing play?

Effects of Detraining

The focus of Chapter 2 was to determine if sex-specific adaptive responses existed in the cancellous compartment of growing mice with an eye toward developing exercise interventions in children and young adults to enhance peak bone mass. During this time of accelerated growth, mechanical loading can improve structural integrity by inducing architectural changes in the skeleton. In animal models, architectural changes in the cortices of the femoral neck and the tibial diaphysis, and the resulting improved mechanical properties, remained for a time (4 to 14 weeks) after cessation of treadmill running [28-30], and the changes in the ulnar diaphysis remained into senescence after compression [31]. Only one study explicitly investigated the effects of detraining on cancellous bone following treadmill running, an activity for which the mechanical environment is more complex and uncontrolled [30]. Following cessation of running, the metaphyseal cortical shell maintained its loading-induced increase in geometry whereas cancellous bone mass declined back to control levels, likely because running was initiated while the rodents were still in a bone modeling period. A detraining study could be undertaken to test the hypothesis that loading-induced architectural changes at corticocancellous sites persist after cessation of loading. Additionally, reduced loading levels were sufficient to maintain loading-induced architectural enhancements for 4 weeks [32], which could be investigated using tibial compression as well. Only two detraining studies were carried out into adulthood or into senescence [29, 31]. Therefore, the detraining study should last until the mice are adult or aged, to determine if the loading-induced architectural

changes that occur during growth indeed persist into adulthood and senescence, when they provide additional fracture resistance.

Similarly, in Chapter 3, tibial compression increased cancellous mass in adult mice to levels equivalent to the control limbs of young mice, effectively recovering age-related bone loss. No studies have investigated the effects of detraining on cancellous bone, especially when loading was initiated in adulthood. Whether or not the higher mass will be maintained if loading is stopped should be determined because the results will elucidate whether a brief interval of mechanical stimuli is sufficient to address age-related bone loss or whether mechanical loading should be considered a more permanent intervention for adults.

Characterization of the Dose-dependent Response of Tibial Compression

Osteogenesis in the cortex is enhanced with increasing applied load magnitude [24, 33, 34]. Over time, however, the skeleton accommodates repetitive mechanical signals [35, 36]. The response to ulnar compression was greatest if high peak loads were applied first followed by lower peak loads, rather than the other way around [36, 37]. After 15 to 16 weeks of loading, the adaptive response of the loaded limbs decreased to levels observed in control, non-loaded limbs. A similar pattern of accommodation occurred using four-point bending [37]. In addition, the skeleton desensitizes to repeated loading within a single loading session. The adaptive response to ulnar compression and four-point bending was improved when loading sessions were broken up into shorter, more frequent sessions with at least 8 hours between sessions [38-41]. During this refractory period, increasing the load magnitude further did not improve the adaptive response [36]. However, inserting periods of rest between single loading cycles enhanced the cortical response under four-point and cantilever bending [15, 39, 42, 43] and can transform a non-osteogenic protocol into

an osteogenic one [15, 43]. Inserting rests during tibial compression has not improved the adaptive response of cancellous bone [44, 45], though the reason for this result is unclear.

These studies all reveal that the response to loading can be saturated. Our peak applied load of approximately -11 N during tibial compression resulted in peak cancellous tissue strains of -2100 to -2400 με, which may be relatively high strains for a mouse, based on diaphyseal strain gauging [24]. Therefore, we could be maximizing our response to tibial compression and potentially masking the effects of sex or estrogen deficiency. Based on the results from Chapter 3, we have determined that the threshold for osteogenesis in adult female B6 mice undergoing tibial compression lies somewhere between -6 and -11 N peak applied loads. A dose-response study could be conducted using peak loads within that range to determine the threshold for osteogenesis and determine if the magnitude of the response varies linearly with applied load, peak cancellous tissue strain, or peak mid-diaphyseal strain. In addition, ascertaining a lower peak load that will still induce bone formation would improve the well-being of the mice.

An alternative source of response saturation may be the total number of applied cycles. Currently, we apply 1200 loading cycles each day, 5 days per week. The osteogenic responses observed in other tibial loading studies that employ loading with rests inserted, described above, were not as robust as that described in this thesis [44, 45]. In these studies, 60 cycles per day were applied at a frequency of 3 days per week. Overall, we applied 6000 total cycles while 180 cycles were applied in a given week. These two additional parameters could also be investigated to determine if the osteogenic response could have been saturated based on cycle number.

Recovering Bone Mass Lost Due to Estrogen Deficiency

Tibial loading studies were carried out for 1, 2, and 6 weeks. These time points were selected based on previous studies with growing male mice, which determined that steady-state adaptive response occurs at 6 weeks [46, 47], at which time cancellous bone mass peaked. Based on the results from Chapter 4, however, the effect of estrogen deficiency is still in a transient phase after 6 weeks. In the B6 mouse strain, 6 weeks was insufficient for OVX-induced reductions in cancellous bone to occur in the control limbs. In addition, estrogen deficiency did not interact with mechanical loading until after 6 weeks. A longer loading period would allow the combined effects of estrogen deficiency and mechanical loading to be better characterized.

Only two studies characterized the tibia of C57Bl/6 mice following OVX for more than 5 weeks [48, 49]. In the diaphysis, changes in cortical geometry were not detected until after 16 weeks. In the proximal tibia, reductions in cancellous bone mass were detected after 4 weeks, disappeared after 7 weeks, and then reappeared again after 11 weeks. Based on these results and our own, extending the loading period to 11 to 16 weeks should allow sufficient time for the effects of estrogen withdrawal to take place. Initiating tibial compression immediately following OVX investigates the preventative potential of mechanical loading to avoid or attenuate lost cancellous mass. Allowing bone loss to occur first, then initiate tibial compression investigates the therapeutic potential of mechanical loading to recover cancellous bone mass. The latter study is particularly relevant for the elderly post-menopausal population for whom pathological bone loss has already occurred.

Characterization of Tibial Compression on the Metaphyseal Cortical Shell

In the current studies, we limited our analysis to cancellous tissue, rather than the entire corticocancellous site. While the loading-induced changes to the cortical tissue are well-documented, most studies have been limited to diaphyseal bone. Focus on the mid-shaft is due to the loading modality of the majority of in vivo models. Four-point bending, for example, limits analysis to the region between the applied loading points, which occurs at the mid-shaft. Similarly, strain gauging is limited to the mid-diaphyseal region because sufficient bone surface and limited tendon attachment are required for gauge attachment. Yet, the response to loading varies along the length of the bone [46, 50-52], suggesting that the cortical response in the proximal tibia will likely be different than at the mid-shaft as the induced loads vary along the length of the tibia. Strain gauging at the metaphysis would help understand how diaphyseal strain under tibial compression changes along the length of the tibia, then these site-specific changes could be related to the adaptive response. Because geometric changes in the cortical shell also confer increased strength to corticocancellous sites, limiting analysis to only cancellous tissue may be underestimating the benefits of mechanical loading in reducing fracture risk.

Load-Sharing between the Metaphyseal Cortex and Cancellous Tissue

Load-sharing between the cortical shell and cancellous tissue in the proximal metaphysis was examined in Chapters 2 and 3 through finite element models. In growing mice, 56 to 66% (male to female control limbs) of the applied load was carried by the cortical shell. Following 2 weeks of tibial compression and its associated adaptation, the cortical shell transmitted less load, 50 to 59% (male to female loaded limbs). Therefore, the cancellous tissue itself became stiffer and more mechanically competent with adaptation. The mid-diaphyseal cortex of adult mice is

larger than in young mice [9, 11], suggesting that the metaphyseal cortex is larger as well. Indeed, the cortical shell of controls limbs in adult female mice transmitted ~75% of the applied load. However, this proportion did not change with tibial compression, unlike that in young mice. Characterization of the site-specific relationship between cortical strain (through gauging) and resulting adaptation would help elucidate the role of load-sharing in adaptation.

Contributing to the relative load-sharing arrangement between young and adult mice is the location of cortical adaptation within the cross-section and the size of the cortices. For example, in growing mice, 85% of the loading-induced increases in cortical area occurred on the periosteum while in adult mice, only 66% occurred at the periosteum. Therefore, bone formation in the growing animals was more 'strategic' in increasing over mechanical integrity. However, adult mice also have greater I_{MAX} and I_{MIN}, which could counteract the need for cortical bone formation in adult mice to be strategic. Clearly, load-sharing between the cortical shell and cancellous tissue is affected by several parameters and these relationships could be explored to better understand the mechanical integrity of the overall metaphysis.

REFERENCES

1. Karlsson, M. K. Does exercise during growth prevent fractures in later life? Med Sport Sci 51*:*121-36; 2007.
2. Borer, K. T. Physical activity in the prevention and amelioration of osteoporosis in women : interaction of mechanical, hormonal and dietary factors. Sports Med 35*:*779-830; 2005.
3. Daly, R. M. The effect of exercise on bone mass and structural geometry during growth. Med Sport Sci 51*:*33-49; 2007.
4. Tabensky, A., Duan, Y., Edmonds, J., and Seeman, E. The contribution of reduced peak accrual of bone and age-related bone loss to osteoporosis at the spine and hip: insights from the daughters of women with vertebral or hip fractures. J Bone Miner Res 16*:*1101-7; 2001.
5. Ryan, A. S., Ivey, F. M., Hurlbut, D. E., Martel, G. F., Lemmer, J. T., Sorkin, J. D., Metter, E. J., Fleg, J. L., and Hurley, B. F. Regional bone mineral density after resistive training in young and older men and women. Scand J Med Sci Sports 14*:*16-23; 2004.
6. Ballard, T. L., Specker, B. L., Binkley, T. L., and Vukovich, M. D. Effect of protein supplementation during a 6-month strength and conditioning program on areal and volumetric bone parameters. Bone 38*:*898-904; 2006.
7. Ducher, G., Courteix, D., Meme, S., Magni, C., Viala, J. F., and Benhamou, C. L. Bone geometry in response to long-term tennis playing and its relationship with muscle volume: a quantitative magnetic resonance imaging study in tennis players. Bone 37*:*457-66; 2005.

8. Jones, H. H., Priest, J. D., Hayes, W. C., Tichenor, C. C., and Nagel, D. A. Humeral hypertrophy in response to exercise. J Bone Joint Surg Am 59*:*204-8; 1977.

9. Brodt, M. D., Ellis, C. B., and Silva, M. J. Growing C57Bl/6 mice increase whole bone mechanical properties by increasing geometric and material properties. J Bone Miner Res 14*:*2159-66; 1999.

10. Ferguson, V. L., Ayers, R. A., Bateman, T. A., and Simske, S. J. Bone development and age-related bone loss in male C57BL/6J mice. Bone 33*:*387-98; 2003.

11. Price, C., Herman, B. C., Lufkin, T., Goldman, H. M., and Jepsen, K. J. Genetic variation in bone growth patterns defines adult mouse bone fragility. J Bone Miner Res 20*:*1983-91; 2005.

12. Somerville, J. M., Aspden, R. M., Armour, K. E., Armour, K. J., and Reid, D. M. Growth of C57BL/6 mice and the material and mechanical properties of cortical bone from the tibia. Calcif Tissue Int 74*:*469-75; 2004.

13. Rubin, C. T., Bain, S. D., and McLeod, K. J. Suppression of the osteogenic response in the aging skeleton. Calcif Tissue Int 50*:*306-13; 1992.

14. Turner, C. H., Takano, Y., and Owan, I. Aging changes mechanical loading thresholds for bone formation in rats. J Bone Miner Res 10*:*1544-9; 1995.

15. Srinivasan, S., Agans, S. C., King, K. A., Moy, N. Y., Poliachik, S. L., and Gross, T. S. Enabling bone formation in the aged skeleton via rest-inserted mechanical loading. Bone 33*:*946-55; 2003.

16. Bassey, E. J., Rothwell, M. C., Littlewood, J. J., and Pye, D. W. Pre- and postmenopausal women have different bone mineral density responses to the same high-impact exercise. J Bone Miner Res 13*:*1805-13; 1998.

17. Lanyon, L., and Skerry, T. Postmenopausal osteoporosis as a failure of bone's adaptation to functional loading: a hypothesis. J Bone Miner Res 16*:*1937-47; 2001.

18. Turner, R. T. Mechanical signaling in the development of postmenopausal osteoporosis. Lupus 8*:*388-92; 1999.

19. Ehrlich, P. J., and Lanyon, L. E. Mechanical strain and bone cell function: a review. Osteoporos Int 13*:*688-700; 2002.

20. Lee, K. C., Maxwell, A., and Lanyon, L. E. Validation of a technique for studying functional adaptation of the mouse ulna in response to mechanical loading. Bone 31*:*407-12; 2002.

21. Rubin, C. T., and Lanyon, L. E. Dynamic strain similarity in vertebrates; an alternative to allometric limb bone scaling. J Theor Biol 107*:*321-7; 1984.

22. Turner, C. H., and Robling, A. G. Exercise as an anabolic stimulus for bone. Curr Pharm Des 10*:*2629-41; 2004.

23. Skerry, T. M. One mechanostat or many? Modifications of the site-specific response of bone to mechanical loading by nature and nurture. J Musculoskelet Neuronal Interact 6*:*122-7; 2006.

24. Mosley, J. R., March, B. M., Lynch, J., and Lanyon, L. E. Strain magnitude related changes in whole bone architecture in growing rats. Bone 20*:*191-8; 1997.

25. Biewener, A. A., Dial, K. P., and Goslow, G. E. J. Pectoralis muscle force and power output during flight in the starling. J. exp. Biol. 164*:*1-18; 1992.

26. Hillam, R. A., and Skerry, T. M. Inhibition of bone resorption and stimulation of formation by mechanical loading of the modeling rat ulna in vivo. J Bone Miner Res 10*:*683-689; 1995.

27. Rubin, C. T., and Lanyon, L. E. Limb mechanics as a function of speed and gait: a study of functional strains in the radius and tibia of horse and dog. J Exp Biol 101*:*187-211; 1982.

28. Jarvinen, T. L., Pajamaki, I., Sievanen, H., Vuohelainen, T., Tuukkanen, J., Jarvinen, M., and Kannus, P. Femoral neck response to exercise and subsequent deconditioning in young and adult rats. J Bone Miner Res 18*:*1292-9; 2003.

29. Pajamaki, I., Kannus, P., Vuohelainen, T., Sievanen, H., Tuukkanen, J., Jarvinen, M., and Jarvinen, T. L. The bone gain induced by exercise in puberty is not preserved through a virtually life-long deconditioning: a randomized controlled experimental study in male rats. J Bone Miner Res 18*:*544-52; 2003.

30. Fujie, H., Miyagaki, J., Terrier, A., Rakotomanana, L., Leyvraz, P. F., and Hayashi, K. Detraining effects on the mechanical properties and morphology of rat tibiae. Biomed Mater Eng 14*:*219-33; 2004.

31. Warden, S. J., Fuchs, R. K., Castillo, A. B., Nelson, I. R., and Turner, C. H. Exercise when young provides lifelong benefits to bone structure and strength. J Bone Miner Res 22*:*251-9; 2007.

32. Wu, J., Wang, X. X., Higuchi, M., Yamada, K., and Ishimi, Y. High bone mass gained by exercise in growing male mice is increased by subsequent reduced exercise. J Appl Physiol 97*:*806-10; 2004.

33. Cullen, D. M., Smith, R. T., and Akhter, M. P. Bone-loading response varies with strain magnitude and cycle number. J Appl Physiol 91*:*1971-6; 2001.

34. Kesavan, C., Mohan, S., Oberholtzer, S., Wergedal, J. E., and Baylink, D. J. Mechanical loading-induced gene expression and BMD changes are different in two inbred mouse strains. J Appl Physiol 99*:*1951-7; 2005.

35. Turner, C. H. Toward a mathematical description of bone biology: the principle of cellular accommodation. Calcif Tissue Int 65*:*466-71.; 1999.

36. Schriefer, J. L., Warden, S. J., Saxon, L. K., Robling, A. G., and Turner, C. H. Cellular accommodation and the response of bone to mechanical loading. J Biomech 38*:*1838-45; 2005.

37. Saxon, L. K., Robling, A. G., Alam, I., and Turner, C. H. Mechanosensitivity of the rat skeleton decreases after a long period of loading, but is improved with time off. Bone 36*:*454-64; 2005.

38. Robling, A. G., Burr, D. B., and Turner, C. H. Partitioning a daily mechanical stimulus into discrete loading bouts improves the osteogenic response to loading. J Bone Miner Res 15*:*1596-602; 2000.

39. Robling, A. G., Burr, D. B., and Turner, C. H. Recovery periods restore mechanosensitivity to dynamically loaded bone. J Exp Biol 204*:*3389-99; 2001.

40. Robling, A. G., Hinant, F. M., Burr, D. B., and Turner, C. H. Shorter, more frequent mechanical loading sessions enhance bone mass. Med Sci Sports Exerc 34*:*196-202; 2002.

41. Robling, A. G., Hinant, F. M., Burr, D. B., and Turner, C. H. Improved bone structure and strength after long-term mechanical loading is greatest if loading is separated into short bouts. J. Bone Miner. Res. 17*:*1545-1554; 2002.

42. Srinivasan, S., Weimer, D. A., Agans, S. C., Bain, S. D., and Gross, T. S. Low-magnitude mechanical loading becomes osteogenic when rest is inserted between each load cycle. J Bone Miner Res 17*:*1613-20; 2002.

43. Srinivasan, S., Ausk, B. J., Poliachik, S. L., Warner, S. E., Richardson, T. S., and Gross, T. Rest-Inserted Loading Rapidly Amplifies the Response of Bone to Small Increases in Strain and Load Cycles. J Appl Physiol; 2007.

44. De Souza, R. L., Matsuura, M., Eckstein, F., Rawlinson, S. C., Lanyon, L. E., and Pitsillides, A. A. Non-invasive axial loading of mouse tibiae increases cortical bone formation and modifies trabecular organization: a new model to study cortical and cancellous compartments in a single loaded element. Bone 37*:*810-8; 2005.

45. Brodt, M. D., and Silva, M. J. Aged mice have enhanced endocortical response and normal periosteal response compared to young-adult mice following 1 week of axial tibial compression. J Bone Miner Res; 2010.

46. Fritton, J. C., Myers, E. R., Wright, T. M., and van der Meulen, M. C. Loading induces site-specific increases in mineral content assessed by microcomputed tomography of the mouse tibia. Bone 36*:*1030-8; 2005.

47. Fritton, J. C., Myers, E. R., Wright, T. M., and van der Meulen, M. C. Bone mass is preserved and cancellous architecture altered due to cyclic loading of the mouse tibia after orchidectomy. J Bone Miner Res 23*:*663-71; 2008.

48. Zhou, H., Iida-Klein, A., Lu, S. S., Ducayen-Knowles, M., Levine, L. R., Dempster, D. W., and Lindsay, R. Anabolic action of parathyroid hormone on cortical and cancellous bone differs between axial and appendicular skeletal sites in mice. Bone 32*:*513-20; 2003.

49. Li, C. Y., Schaffler, M. B., Wolde-Semait, H. T., Hernandez, C. J., and Jepsen, K. J. Genetic background influences cortical bone response to ovariectomy. J Bone Miner Res 20*:*2150-8; 2005.

50. Hsieh, Y. F., Robling, A. G., Ambrosius, W. T., Burr, D. B., and Turner, C. H. Mechanical loading of diaphyseal bone in vivo: the strain threshold for an osteogenic response varies with location. J Bone Miner Res 16*:*2291-7; 2001.

51. Torrance, A. G., Mosley, J. R., Suswillo, R. F., and Lanyon, L. E. Noninvasive loading of the rat ulna in vivo induces a strain-related modeling response

uncomplicated by trauma or periostal pressure. Calcif Tissue Int 54*:*241-7; 1994.

52. Mosley, J. R., and Lanyon, L. E. Strain rate as a controlling influence on adaptive modeling in response to dynamic loading of the ulna in growing male rats. Bone 23*:*313-8; 1998.

APPENDIX A: Chapter 2 Data

Table A.1: Indices of cancellous adaptation determined by microCT analysis of VOIs from the proximal metaphysis of loaded and control tibiae from female and male mice after 2 weeks of loading.

Mouse	Sex	tBMD (mg/cc)				BV/TV			
		L	R	L-R	%diff	L	R	L-R	%diff
A01	Female	563.1	467.1	96.0	20.6	0.222	0.120	0.102	84.4
A02	Female	574.7	470.5	104.1	22.1	0.246	0.119	0.126	105.8
A04	Female	578.3	479.6	98.7	20.6	0.246	0.111	0.135	121.2
B05	Female	559.5	496.5	63.1	12.7	0.215	0.143	0.073	51.0
B06	Female	576.8	478.2	98.6	20.6	0.234	0.111	0.122	109.6
B07	Female	565.1	482.8	82.3	17.0	0.242	0.104	0.138	133.1
C09	Female	563.7	464.9	98.8	21.3	0.247	0.116	0.131	113.5
C11	Female	562.2	475.0	87.1	18.3	0.189	0.091	0.098	107.6
C12	Female	583.3	484.5	98.8	20.4	0.238	0.122	0.116	95.2
D14	Female	588.5	484.2	104.3	21.5	0.230	0.110	0.119	108.0
D15	Female	555.7	473.1	82.6	17.5	0.209	0.106	0.103	97.1
D16	Female	536.2	465.5	70.7	15.2	0.218	0.155	0.063	40.6
E17	Female	588.8	492.5	96.3	19.6	0.225	0.113	0.112	99.0
E18	Female	572.0	495.4	76.6	15.5	0.181	0.109	0.072	66.2
	MEAN	**569.1**	**479.3**	**89.9**	**18.8**	**0.224**	**0.116**	**0.108**	**95.2**
	SD	**14.2**	**10.6**	**13.0**	**2.8**	**0.021**	**0.016**	**0.024**	**26.3**
		L	**R**	**L-R**	**%diff**	**L**	**R**	**L-R**	**%diff**
F01	Male	569.7	503.6	66.1	13.1	0.319	0.217	0.102	47.1
F02	Male	600.4	498.7	101.7	20.4	0.302	0.177	0.125	70.7
F04	Male	593.7	510.5	83.3	16.3	0.288	0.215	0.073	33.9
G05	Male	564.8	520.5	44.3	8.5	0.303	0.220	0.083	37.9
G06	Male	622.2	479.8	142.4	29.7	0.317	0.142	0.175	122.9
G08	Male	590.0	512.2	77.8	15.2	0.306	0.209	0.097	46.2
H09	Male	574.9	483.3	91.6	19.0	0.342	0.190	0.151	79.5
H11	Male	591.6	478.5	113.1	23.6	0.367	0.201	0.166	82.5
H12	Male	555.6	502.0	53.5	10.7	0.270	0.207	0.063	30.3
I13	Male	586.2	475.9	110.3	23.2	0.380	0.188	0.192	102.5
I14	Male	551.0	472.1	79.0	16.7	0.299	0.180	0.118	65.5
I16	Male	554.5	535.5	18.9	3.5	0.304	0.276	0.028	10.2
J17	Male	583.3	501.5	81.8	16.3	0.326	0.176	0.150	85.5
J19	Male	591.3	495.2	96.1	19.4	0.370	0.193	0.177	92.2
	MEAN	**580.7**	**497.8**	**82.9**	**16.8**	**0.321**	**0.199**	**0.121**	**64.8**
	SD	**20.1**	**18.5**	**31.1**	**6.7**	**0.033**	**0.030**	**0.049**	**31.7**

Table A.1 continued:

Mouse	Sex	Tb.Th. (µm)				Tb.Sp. (µm)			
		L	R	L-R	%diff	L	R	L-R	%diff
A01	Female	40.7	23.2	17.5	75.6	130.4	146.8	-16.4	-11.2
A02	Female	39.7	22.4	17.3	77.4	107.3	155.7	-48.4	-31.1
A04	Female	43.9	22.8	21.1	92.6	116.8	178.2	-61.4	-34.5
B05	Female	41.5	25.7	15.9	61.9	131.2	129.6	1.6	1.2
B06	Female	40.3	22.3	18.0	80.6	123.4	164.6	-41.2	-25.0
B07	Female	40.8	22.2	18.5	83.3	102.3	152.6	-50.3	-32.9
C09	Female	45.4	23.9	21.5	89.8	137.8	158.6	-20.8	-13.1
C11	Female	39.1	23.4	15.7	67.0	153.2	201.9	-48.7	-24.1
C12	Female	42.3	22.2	20.1	90.7	137.1	153.5	-16.5	-10.7
D14	Female	41.1	22.3	18.8	84.1	125.6	166.6	-41.0	-24.6
D15	Female	38.9	23.4	15.5	66.1	140.9	186.5	-45.6	-24.4
D16	Female	39.0	23.8	15.2	64.0	122.6	112.3	10.3	9.2
E17	Female	42.8	22.9	19.9	87.1	128.7	164.2	-35.5	-21.6
E18	Female	38.2	23.4	14.8	63.1	133.4	170.1	-36.7	-21.6
	MEAN	**41.0**	**23.1**	**17.8**	**77.4**	**127.9**	**160.1**	**-32.2**	**-18.9**
	SD	**2.1**	**0.9**	**2.2**	**11.1**	**13.3**	**22.3**	**20.9**	**12.7**
		L	**R**	**L-R**	**%diff**	**L**	**R**	**L-R**	**%diff**
F01	Male	42.5	25.0	17.5	69.9	70.4	88.7	-18.3	-20.6
F02	Male	47.9	25.9	22.0	85.1	87.7	110.6	-22.9	-20.7
F04	Male	41.3	27.8	13.5	48.5	88.2	104.3	-16.0	-15.4
G05	Male	39.2	28.2	11.0	39.2	88.2	95.2	-7.0	-7.4
G06	Male	47.9	20.7	27.1	130.9	91.9	126.9	-35.0	-27.6
G08	Male	43.8	25.7	18.1	70.5	92.4	104.0	-11.5	-11.1
H09	Male	44.6	23.0	21.5	93.4	72.4	94.0	-21.6	-23.0
H11	Male	47.4	22.9	24.5	107.3	71.8	96.3	-24.5	-25.5
H12	Male	38.7	26.7	12.0	44.9	89.3	100.6	-11.3	-11.2
I13	Male	50.0	22.8	27.2	119.5	70.6	99.5	-28.8	-29.0
I14	Male	41.5	24.0	17.5	73.1	77.2	107.6	-30.4	-28.3
I16	Male	41.9	37.5	4.4	11.6	92.2	91.9	0.3	0.4
J17	Male	45.2	24.1	21.0	87.2	78.9	114.6	-35.7	-31.1
J19	Male	48.8	23.7	25.2	106.5	75.2	88.7	-13.5	-15.3
	MEAN	**44.3**	**25.6**	**18.8**	**77.7**	**81.9**	**101.6**	**-19.7**	**-19.0**
	SD	**3.6**	**4.0**	**6.7**	**33.5**	**8.8**	**10.7**	**10.7**	**9.3**

Table A.2: Cancellous tissue longitudinal strains engendered by compressive 11.5 N determined by finite element analysis. Females required a 0.09% and males required a 0.07% uniformly applied displacement to get resultant 11.5 N.

Mouse	Sex	Max	Min	Mean	Std
B06	Female	-2519	284	-394	-399
B07	Female	-2564	431	-459	-486
D15	Female	-2200	414	-408	-399
D16	Female	-2360	313	-396	-351
E17	Female	-2543	835	-449	-416
	MEAN	**-2437**	**455**	**-421**	**-410**
	SD	**155**	**221**	**31**	**49**
G05	Male	-1529	247	-291	-245
G08	Male	-2627	253	-363	-288
J17	Male	-2453	452	-368	-362
H09	Male	-1972	253	-336	-329
F01	Male	-2086	225	-345	-284
	MEAN	**-2134**	**286**	**-341**	**-301**
	SD	**430**	**94**	**31**	**45**

Table A.3: Proximal metaphyseal stiffness determined by finite element analysis using 0.01% uniformly applied displacement.

Mouse	Sex	Reaction Force (N)					
		Corticocancellous		Cortical		Cortical : Corticocancellous	
		L	R	L	R	L	R
B06	Female	26.7	12.6	15.2	8.8	0.57	0.70
B07	Female	27.3	10.9	17.0	7.6	0.62	0.70
D15	Female	23.0	12.2	13.5	7.7	0.59	0.63
D16	Female	27.3	15.2	16.8	9.0	0.62	0.59
E17	Female	25.1	12.9	14.4	8.8	0.57	0.68
	MEAN	**25.9**	**12.8**	**15.4**	**8.4**	**0.59**	**0.66**
	SD	**1.8**	**1.6**	**1.5**	**0.7**	**0.02**	**0.05**
G05	Male	28.4	20.1	12.8	9.9	0.45	0.49
G08	Male	27.0	16.1	13.3	9.1	0.49	0.57
J17	Male	27.7	12.8	13.1	7.3	0.47	0.57
H09	Male	29.5	14.5	15.6	8.8	0.53	0.61
F01	Male	27.9	16.6	15.5	9.3	0.56	0.56
	MEAN	**28.1**	**16.0**	**14.1**	**8.9**	**0.50**	**0.56**
	SD	**0.9**	**2.7**	**1.4**	**1.0**	**0.04**	**0.04**

Table A.4: Indices of cortical adaptation determined by microCT analysis of VOIs centered at tibial mid-diaphysis of loaded and control tibiae from female and male mice after 2 weeks of loading.

Mouse	Sex	Marrow Area (mm^2)				Cortical Area (mm^2)			
		L	R	L-R	%diff	L	R	L-R	%diff
A01	Female	0.301	0.346	-0.045	-12.9	0.629	0.505	0.124	24.6
A02	Female	0.285	0.337	-0.052	-15.3	0.704	0.498	0.206	41.3
A04	Female	0.270	0.295	-0.024	-8.3	0.798	0.422	0.376	89.3
B05	Female	0.297	0.306	-0.009	-3.0	0.557	0.488	0.068	14.0
B06	Female	0.291	0.320	-0.029	-8.9	0.889	0.479	0.411	85.8
B07	Female	0.304	0.330	-0.026	-7.9	0.625	0.450	0.175	38.8
C09	Female	0.314	0.334	-0.020	-6.1	0.747	0.507	0.241	47.5
C11	Female	0.312	0.336	-0.025	-7.3	0.728	0.483	0.246	50.9
C12	Female	0.294	0.329	-0.035	-10.5	0.755	0.466	0.288	61.8
D14	Female	0.279	0.355	-0.075	-21.2	0.748	0.478	0.270	56.5
D15	Female	0.338	0.350	-0.013	-3.6	0.650	0.474	0.176	37.2
D16	Female	0.285	0.312	-0.027	-8.8	0.717	0.494	0.223	45.0
E17	Female	0.317	0.351	-0.034	-9.8	0.701	0.482	0.220	45.6
E18	Female	0.313	0.334	-0.021	-6.3	0.671	0.478	0.194	40.5
	MEAN	**0.300**	**0.331**	**-0.031**	**-9.3**	**0.708**	**0.479**	**0.230**	**48.5**
	SD	**0.018**	**0.018**	**0.017**	**4.7**	**0.082**	**0.022**	**0.090**	**20.4**
		L	**R**	**L-R**	**%diff**	**L**	**R**	**L-R**	**%diff**
F01	Male	0.370	0.374	-0.004	-1.1	0.695	0.616	0.080	13.0
F02	Male	0.335	0.349	-0.014	-4.0	0.706	0.620	0.086	13.9
F04	Male	0.432	0.485	-0.053	-10.9	0.706	0.689	0.017	2.4
G05	Male	0.390	0.432	-0.042	-9.8	0.723	0.700	0.023	3.3
G06	Male	0.283	0.340	-0.057	-16.8	0.798	0.507	0.292	57.5
G08	Male	0.360	0.361	-0.002	-0.4	0.717	0.568	0.149	26.2
H09	Male	0.386	0.371	0.015	4.0	0.707	0.594	0.113	19.0
H11	Male	0.368	0.389	-0.021	-5.4	0.757	0.620	0.137	22.2
H12	Male	0.425	0.434	-0.009	-2.0	0.714	0.638	0.076	11.8
I13	Male	0.331	0.397	-0.066	-16.6	0.757	0.581	0.176	30.4
I14	Male	0.317	0.352	-0.035	-10.0	0.798	0.585	0.214	36.5
I16	Male	0.446	0.404	0.042	10.3	0.779	0.765	0.014	1.8
J17	Male	0.383	0.398	-0.015	-3.8	0.683	0.613	0.069	11.3
J19	Male	0.295	0.338	-0.043	-12.8	0.739	0.523	0.217	41.4
	MEAN	**0.366**	**0.387**	**-0.022**	**-5.7**	**0.734**	**0.616**	**0.119**	**20.8**
	SD	**0.050**	**0.042**	**0.030**	**7.7**	**0.038**	**0.068**	**0.083**	**16.2**

Table A.4 continued:

Mouse	Sex	I_{max} (mm^4)				I_{min} (mm^4)			
		L	R	L-R	%diff	L	R	L-R	%diff
A01	Female	0.067	0.054	0.013	24.4	0.053	0.040	0.013	31.9
A02	Female	0.084	0.050	0.034	68.5	0.058	0.040	0.018	44.0
A04	Female	0.102	0.036	0.065	179.7	0.067	0.029	0.038	128.8
B05	Female	0.056	0.046	0.010	22.5	0.041	0.037	0.004	11.4
B06	Female	0.127	0.045	0.082	180.0	0.081	0.036	0.044	122.0
B07	Female	0.074	0.041	0.033	79.7	0.051	0.035	0.016	45.2
C09	Female	0.095	0.051	0.044	86.8	0.065	0.040	0.025	61.5
C11	Female	0.091	0.049	0.043	87.7	0.061	0.038	0.023	60.5
C12	Female	0.097	0.044	0.053	119.1	0.061	0.036	0.025	69.7
D14	Female	0.093	0.045	0.048	105.1	0.063	0.042	0.022	51.8
D15	Female	0.082	0.047	0.035	74.8	0.052	0.039	0.013	34.3
D16	Female	0.083	0.046	0.037	78.8	0.059	0.038	0.020	53.2
E17	Female	0.085	0.049	0.036	73.9	0.059	0.039	0.020	52.2
E18	Female	0.083	0.046	0.037	80.6	0.054	0.038	0.016	40.7
	MEAN	**0.087**	**0.046**	**0.041**	**90.1**	**0.059**	**0.038**	**0.021**	**57.7**
	SD	**0.017**	**0.004**	**0.018**	**45.9**	**0.009**	**0.003**	**0.010**	**32.1**
		L	**R**	**L-R**	**%diff**	**L**	**R**	**L-R**	**%diff**
F01	Male	0.094	0.075	0.019	25.4	0.065	0.056	0.008	14.8
F02	Male	0.092	0.078	0.015	18.8	0.062	0.051	0.011	21.4
F04	Male	0.102	0.108	-0.006	-5.8	0.074	0.075	-0.001	-1.4
G05	Male	0.104	0.103	0.000	0.2	0.069	0.069	0.000	-0.1
G06	Male	0.113	0.054	0.059	109.9	0.068	0.040	0.028	70.4
G08	Male	0.097	0.063	0.034	52.8	0.067	0.051	0.016	30.4
H09	Male	0.100	0.073	0.027	37.5	0.066	0.052	0.014	26.9
H11	Male	0.108	0.076	0.032	41.8	0.072	0.059	0.014	23.1
H12	Male	0.104	0.088	0.016	17.7	0.073	0.065	0.007	11.3
I13	Male	0.108	0.075	0.033	43.6	0.067	0.051	0.015	29.4
I14	Male	0.115	0.068	0.047	68.6	0.074	0.049	0.025	50.2
I16	Male	0.124	0.114	0.010	8.7	0.084	0.076	0.007	9.6
J17	Male	0.093	0.082	0.012	14.3	0.064	0.056	0.008	14.6
J19	Male	0.098	0.055	0.043	77.7	0.060	0.042	0.018	42.5
	MEAN	**0.104**	**0.079**	**0.024**	**36.5**	**0.069**	**0.057**	**0.012**	**24.5**
	SD	**0.009**	**0.018**	**0.018**	**32.4**	**0.006**	**0.011**	**0.008**	**19.7**

APPENDIX B: Chapter 3 Data

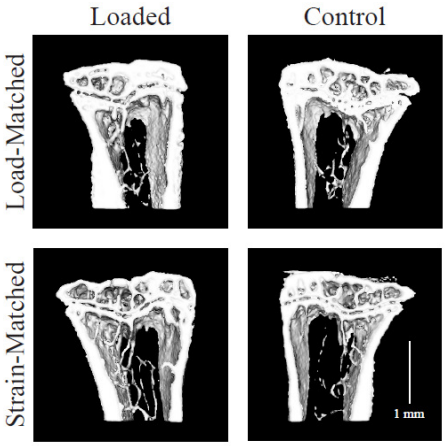

Figure B.1: Frontal sections (0.6 mm thick, extending 1.7 mm distal to the growth plate) through the proximal metaphysis from representative microCT scans. Representative loaded (left) and control (right) tibiae are shown from both Load-Matched (top) and Strain-Matched (bottom) groups.

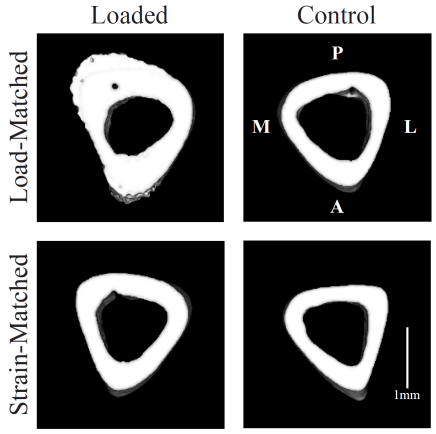

Figure B.2: Transverse sections (0.42 mm thick) centered at the tibial mid-diaphysis from representative microCT scans. Representative loaded (left) and control (right) tibiae are shown from both Load-Matched (top) and Strain-Matched (bottom) groups. M: Medial, P: Posterior, L: Lateral, A: Anterior.

Table B.1: Indices of cancellous adaptation determined by microCT analysis of VOIs from the proximal metaphysis of loaded and control tibiae from adult Load-Matched (Load) and Strain-Matched (Strain) female mice after 2 weeks of loading.

Mouse	Loading Protocol	tBMD (mg/cc)				BV/TV			
		L	R	L-R	%diff	L	R	L-R	%diff
C01	Load	603.0	522.5	80.5	15.4	0.095	0.051	0.044	84.6
C02	Load	591.1	508.9	82.2	16.1	0.137	0.062	0.076	122.7
C04	Load	557.1	525.5	31.6	6.0	0.094	0.091	0.003	3.0
D07	Load	565.6	528.6	37.0	7.0	0.116	0.086	0.030	34.3
E09	Load	590.2	507.4	82.8	16.3	0.149	0.080	0.068	85.1
E11	Load	572.4	493.3	79.1	16.0	0.088	0.065	0.022	33.9
E12	Load	598.2	516.9	81.3	15.7	0.106	0.069	0.038	55.3
E13	Load	570.1	516.4	53.7	10.4	0.077	0.061	0.016	26.2
F14	Load	499.2	497.7	1.5	0.3	0.076	0.062	0.015	23.6
F16	Load	578.0	531.9	46.1	8.7	0.125	0.089	0.037	41.1
F17	Load	549.3	491.7	57.6	11.7	0.104	0.072	0.032	43.9
F18	Load	562.7	478.3	84.4	17.6	0.119	0.085	0.034	39.9
	MEAN	**569.7**	**509.9**	**59.8**	**11.8**	**0.107**	**0.073**	**0.034**	**49.5**
	SD	**27.8**	**16.8**	**26.7**	**5.4**	**0.023**	**0.013**	**0.021**	**33.0**
		L	**R**	**L-R**	**%diff**	**L**	**R**	**L-R**	**%diff**
A01	Strain	483.8	458.8	25.1	5.5	0.069	0.052	0.017	33.5
A02	Strain	528.6	491.8	36.8	7.5	0.070	0.081	-0.011	-13.1
A03	Strain	529.6	513.9	15.6	3.0	0.064	0.077	-0.013	-16.5
A04	Strain	495.1	499.2	-4.1	-0.8	0.078	0.079	-0.001	-1.6
B06	Strain	528.0	529.3	-1.3	-0.3	0.111	0.111	0.000	0.2
B10	Strain	528.4	524.4	4.0	0.8	0.071	0.075	-0.004	-5.3
G11	Strain	471.1	526.0	-54.9	-10.4	0.059	0.063	-0.003	-5.4
G13	Strain	527.5	496.0	31.5	6.4	0.068	0.057	0.011	18.8
H15	Strain	499.2	518.9	-19.7	-3.8	0.067	0.077	-0.010	-12.8
H16	Strain	529.6	503.2	26.4	5.2	0.076	0.058	0.018	30.6
H18	Strain	526.7	532.9	-6.2	-1.2	0.114	0.094	0.021	22.0
	MEAN	**513.4**	**508.6**	**4.8**	**1.1**	**0.077**	**0.075**	**0.002**	**4.6**
	SD	**21.8**	**21.8**	**26.7**	**5.3**	**0.018**	**0.017**	**0.012**	**18.3**

Table B.1 continued:

Mouse	Loading Protocol	Tb.Th. (μm)				Tb.Sp. (μm)			
		L	R	L-R	%diff	L	R	L-R	%diff
C01	Load	50.6	28.0	22.6	80.6	202.1	222.8	-20.7	-9.3
C02	Load	48.1	25.5	22.7	89.2	145.4	194.9	-49.5	-25.4
C04	Load	53.7	29.2	24.4	83.6	174.9	202.5	-27.6	-13.6
D07	Load	41.5	27.9	13.6	48.9	159.9	169.7	-9.8	-5.8
E09	Load	50.5	29.0	21.4	73.8	159.0	170.3	-11.3	-6.6
E11	Load	43.3	25.5	17.8	69.9	203.7	207.1	-3.4	-1.6
E12	Load	49.2	30.6	18.6	60.6	193.6	210.9	-17.3	-8.2
E13	Load	43.7	27.2	16.5	60.6	174.3	244.7	-70.4	-28.8
F14	Load	30.0	23.6	6.3	26.8	166.9	183.2	-16.4	-8.9
F16	Load	45.0	29.2	15.7	53.8	143.6	163.7	-20.1	-12.3
F17	Load	43.8	29.0	14.8	51.2	152.2	204.5	-52.3	-25.6
F18	Load	44.0	25.7	18.3	71.1	167.6	214.3	-46.7	-21.8
	MEAN	**45.3**	**27.5**	**17.7**	**64.2**	**170.3**	**199.1**	**-28.8**	**-14.0**
	SD	**6.1**	**2.1**	**4.9**	**17.5**	**20.5**	**24.0**	**20.8**	**9.1**
		L	**R**	**L-R**	**%diff**	**L**	**R**	**L-R**	**%diff**
A01	Strain	25.7	21.2	4.5	21.3	167.9	184.1	-16.2	-8.8
A02	Strain	29.8	25.5	4.2	16.6	195.1	202.3	-7.2	-3.6
A03	Strain	31.4	27.0	4.3	16.0	212.7	177.9	34.9	19.6
A04	Strain	27.1	27.0	0.1	0.3	182.1	219.6	-37.5	-17.1
B06	Strain	29.4	29.6	-0.2	-0.7	157.2	163.6	-6.4	-3.9
B10	Strain	31.8	29.4	2.4	8.3	197.9	202.3	-4.3	-2.1
G11	Strain	28.1	28.6	-0.5	-1.7	193.6	182.7	10.9	6.0
G13	Strain	28.9	27.4	1.4	5.2	181.5	233.5	-52.0	-22.3
H15	Strain	26.8	28.2	-1.4	-4.9	186.6	172.4	14.2	8.2
H16	Strain	33.5	25.3	8.2	32.4	179.5	195.6	-16.1	-8.2
H18	Strain	30.7	28.7	2.0	6.9	165.6	201.4	-35.8	-17.8
	MEAN	**29.4**	**27.1**	**2.3**	**9.1**	**183.6**	**194.1**	**-10.5**	**-4.5**
	SD	**2.4**	**2.4**	**2.8**	**11.4**	**16.1**	**20.7**	**25.2**	**12.4**

Table B.2: Indices of cortical adaptation determined by microCT analysis of VOIs centered at tibial mid-diaphysis of loaded and control tibiae from adult Load-Matched (Load) and Strain-Matched (Strain) female mice after 2 weeks of loading.

Mouse	Loading Protocol	Marrow Area (mm^2)				Cortical Area (mm^2)			
		L	R	L-R	%diff	L	R	L-R	%diff
C01	Load	0.303	0.427	-0.124	-29.1	0.805	0.534	0.271	50.8
C02	Load	0.295	0.379	-0.084	-22.0	0.770	0.543	0.227	41.9
C04	Load	0.286	0.416	-0.129	-31.1	0.889	0.590	0.299	50.8
D07	Load	0.339	0.432	-0.093	-21.6	0.835	0.573	0.262	45.7
E09	Load	0.351	0.402	-0.051	-12.6	0.846	0.578	0.268	46.4
E11	Load	0.305	0.353	-0.048	-13.5	0.762	0.519	0.242	46.6
E12	Load	0.243	0.378	-0.135	-35.6	0.848	0.572	0.276	48.2
E13	Load	0.408	0.452	-0.044	-9.8	0.704	0.569	0.135	23.7
F14	Load	0.419	0.396	0.024	6.0	0.725	0.560	0.165	29.4
F16	Load	0.307	0.382	-0.075	-19.6	0.750	0.582	0.168	28.8
F17	Load	0.301	0.391	-0.090	-23.1	0.875	0.584	0.291	49.8
F18	Load	0.319	0.393	-0.074	-18.9	0.794	0.593	0.200	33.7
	MEAN	**0.323**	**0.400**	**-0.077**	**-19.3**	**0.800**	**0.566**	**0.234**	**41.3**
	SD	**0.050**	**0.028**	**0.044**	**11.0**	**0.060**	**0.023**	**0.055**	**9.7**
		L	**R**	**L-R**	**%diff**	**L**	**R**	**L-R**	**%diff**
A01	Strain	0.319	0.354	-0.035	-10.0	0.542	0.512	0.031	6.0
A02	Strain	0.349	0.389	-0.040	-10.3	0.565	0.524	0.041	7.9
A03	Strain	0.349	0.345	0.004	1.2	0.592	0.551	0.041	7.4
A04	Strain	0.323	0.337	-0.014	-4.2	0.562	0.538	0.024	4.5
B06	Strain	0.315	0.359	-0.044	-12.2	0.580	0.576	0.004	0.7
B10	Strain	0.433	0.461	-0.028	-6.1	0.557	0.568	-0.010	-1.8
G11	Strain	0.399	0.370	0.029	7.8	0.603	0.577	0.026	4.5
G13	Strain	0.416	0.398	0.019	4.7	0.606	0.573	0.033	5.8
H15	Strain	0.361	0.348	0.013	3.7	0.602	0.575	0.027	4.7
H16	Strain	0.334	0.352	-0.017	-4.9	0.570	0.534	0.036	6.7
H18	Strain	0.335	0.399	-0.064	-16.0	0.628	0.570	0.058	10.1
	MEAN	**0.358**	**0.374**	**-0.016**	**-4.2**	**0.583**	**0.554**	**0.028**	**5.1**
	SD	**0.041**	**0.036**	**0.029**	**7.7**	**0.026**	**0.024**	**0.018**	**3.3**

Table B.2 continued:

Mouse	Loading Protocol	I_{max} (mm^4)				I_{min} (mm^4)			
		L	R	L-R	%diff	L	R	L-R	%diff
C01	Load	0.134	0.064	0.070	110.7	0.091	0.052	0.039	75.4
C02	Load	0.117	0.060	0.057	95.6	0.068	0.050	0.018	36.5
C04	Load	0.146	0.074	0.072	96.8	0.088	0.058	0.031	53.5
D07	Load	0.132	0.073	0.059	81.6	0.084	0.057	0.027	48.1
E09	Load	0.140	0.072	0.067	93.3	0.091	0.054	0.037	68.7
E11	Load	0.112	0.061	0.051	83.2	0.063	0.040	0.023	58.4
E12	Load	0.142	0.074	0.067	91.1	0.090	0.047	0.043	90.0
E13	Load	0.105	0.074	0.032	43.2	0.073	0.059	0.014	23.6
F14	Load	0.110	0.067	0.044	65.9	0.076	0.053	0.023	44.1
F16	Load	0.137	0.066	0.071	108.0	0.080	0.057	0.024	41.6
F17	Load	0.143	0.068	0.075	110.6	0.094	0.057	0.037	64.5
F18	Load	0.122	0.071	0.051	71.9	0.084	0.058	0.026	45.0
	MEAN	**0.128**	**0.069**	**0.060**	**87.7**	**0.082**	**0.053**	**0.028**	**54.1**
	SD	**0.014**	**0.005**	**0.013**	**20.0**	**0.010**	**0.006**	**0.009**	**18.3**
		L	**R**	**L-R**	**%diff**	**L**	**R**	**L-R**	**%diff**
A01	Strain	0.055	0.051	0.004	8.8	0.044	0.046	-0.002	-3.5
A02	Strain	0.066	0.061	0.005	8.1	0.046	0.046	0.000	1.1
A03	Strain	0.064	0.055	0.009	16.6	0.054	0.051	0.004	7.0
A04	Strain	0.061	0.052	0.008	15.6	0.045	0.050	-0.005	-9.4
B06	Strain	0.063	0.070	-0.006	-9.3	0.047	0.048	-0.002	-3.3
B10	Strain	0.068	0.073	-0.005	-7.3	0.056	0.063	-0.007	-10.6
G11	Strain	0.070	0.068	0.002	2.7	0.061	0.056	0.006	10.0
G13	Strain	0.076	0.072	0.004	4.9	0.063	0.057	0.006	10.6
H15	Strain	0.069	0.065	0.004	6.7	0.056	0.051	0.005	9.6
H16	Strain	0.063	0.058	0.005	9.3	0.048	0.046	0.002	4.6
H18	Strain	0.073	0.066	0.007	10.5	0.055	0.056	0.000	-0.8
	MEAN	**0.066**	**0.063**	**0.003**	**6.1**	**0.052**	**0.052**	**0.001**	**1.4**
	SD	**0.006**	**0.008**	**0.005**	**8.2**	**0.007**	**0.006**	**0.004**	**7.6**

Table B.3: Cancellous tissue longitudinal strains engendered by compressive 11.3 N for the Load-Matched group (Load) and 5.9 N for the Strain-Matched group (Strain) determined by finite element analysis. The Load-Matched required an 0.08% and the Strain-Matched group required an 0.05% uniformly applied displacement to get their respective resultant reaction forces.

		Reaction Force (N)					
		Corticocancellous		Cortical		Cortical : Corticocancellous	
Mouse	Sex	L	R	L	R	L	R
D07	Load	17.2	8.8	13.2	6.5	0.77	0.74
E11	Load	16.9	8.7	12.4	7.0	0.73	0.80
E12	Load	21.0	9.5	15.2	6.6	0.73	0.70
F17	Load	18.7	10.1	13.8	7.8	0.74	0.78
F18	Load	17.8	10.3	12.6	7.3	0.71	0.71
	Mean	**18.3**	**9.5**	**13.4**	**7.1**	**0.73**	**0.75**
	SD	**1.6**	**0.7**	**1.1**	**0.5**	**0.02**	**0.04**
A02	Strain	9.3	8.8	7.2	6.8	0.77	0.77
A03	Strain	10.4	9.4	7.8	6.9	0.75	0.73
A04	Strain	9.4	8.5	7.3	6.3	0.78	0.74
B10	Strain	9.7	8.8	7.1	6.7	0.74	0.77
H15	Strain	10.8	9.7	8.5	7.6	0.78	0.79
	Mean	**9.9**	**9.0**	**7.6**	**6.9**	**0.76**	**0.76**
	SD	**0.7**	**0.5**	**0.6**	**0.5**	**0.02**	**0.02**

Table B.4: Dynamic histomorphometry for the proximal metaphysis of Load-Matched and Strain-Matched mice after 2 weeks of *in vivo* tibial compression.

Variable[a]	Group	Loaded (Left)	Control (Right)	Δ (Left - Right)
aBV/TV (%)	Load-Matched	3.8±0.7	5.3±0.7	-1.5±3.3
	Strain-Matched	4.1±0.5	4.5±2.0	-1.6±3.3
ES/BS (%)	Load-Matched	0.37±0.4	1.5±2.9	-1.1±3.2
	Strain-Matched	0.00±0.0	0.16±0.3	-0.16±0.3
MS (%)	Load-Matched	14.5±4.7	15.2±4.4	-0.68±8.9
	Strain-Matched	11.8±3.9	14.6±5.8	-4.4±9.9
MAR (μm)	Load-Matched	3.8±2.8	3.0±3.5	0.80±5.9
	Strain-Matched	4.0±3.0	3.6±4.1	-0.28±3.9
BFR (%/yr)	Load-Matched[b]	231±190	200±240	31±420
	Strain-Matched	194±140	235±290	-64±300

[a]Loading did not affect any histomorphometric measure. Data represented as mean ± SD.

APPENDIX C: Chapter 4 Data

Table C.1: Indices of cancellous adaptation determined by microCT analysis of VOIs from the proximal metaphysis of loaded and control tibiae from adult Sham-ovariectomy (Sham) and ovariectomy (OVX) female mice after 1 week of loading.

Mouse	Estrogen	tBMD (mg/cc)				BV/TV			
		L	R	L-R	%diff	L	R	L-R	%diff
A01	Sham	707.4	728.4	-21.0	-2.9	0.070	0.048	0.022	45.2
A03	Sham	730.6	726.5	4.2	0.6	0.071	0.080	-0.009	-11.6
A04	Sham	729.9	748.1	-18.2	-2.4	0.085	0.042	0.043	103.6
B05	Sham	747.6	717.6	29.9	4.2	0.055	0.063	-0.008	-12.0
B06	Sham	730.4	701.7	28.7	4.1	0.098	0.060	0.038	62.6
D13	Sham	734.7	693.6	41.1	5.9	0.064	0.043	0.020	46.9
D14	Sham	701.9	714.8	-12.9	-1.8	0.062	0.056	0.006	11.1
D15	Sham	756.4	728.2	28.2	3.9	0.082	0.073	0.008	11.3
D16	Sham	754.5	729.1	25.3	3.5	0.067	0.061	0.006	10.0
E20	Sham	691.4	687.8	3.6	0.5	0.058	0.043	0.015	34.5
F21	Sham	696.2	729.5	-33.3	-4.6	0.089	0.069	0.020	29.2
F23	Sham	745.2	699.6	45.6	6.5	0.073	0.063	0.010	15.2
	MEAN	**727.2**	**717.1**	**10.1**	**1.5**	**0.073**	**0.058**	**0.014**	**28.8**
	SD	**22.7**	**18.0**	**26.6**	**3.7**	**0.013**	**0.012**	**0.016**	**32.8**
		L	**R**	**L-R**	**%diff**	**L**	**R**	**L-R**	**%diff**
A02	OVX	734.4	687.5	46.8	6.8	0.055	0.046	0.008	17.9
B07	OVX	752.3	740.8	11.6	1.6	0.097	0.070	0.028	39.9
B08	OVX	763.7	748.0	15.7	2.1	0.082	0.062	0.020	33.1
C09	OVX	739.1	731.8	7.2	1.0	0.097	0.082	0.016	18.9
C10	OVX	723.5	718.2	5.4	0.7	0.087	0.068	0.019	27.5
C11	OVX	746.6	704.4	42.2	6.0	0.097	0.069	0.028	39.9
C12	OVX	744.2	724.2	20.0	2.8	0.070	0.047	0.022	47.0
E17	OVX	735.8	744.2	-8.4	-1.1	0.073	0.045	0.028	62.2
E18	OVX	703.0	698.3	4.6	0.7	0.068	0.040	0.028	69.0
E19	OVX	665.6	684.3	-18.7	-2.7	0.054	0.049	0.005	9.9
F22	OVX	776.0	742.8	33.2	4.5	0.059	0.065	-0.006	-9.0
F24	OVX	738.7	708.0	30.6	4.3	0.120	0.071	0.049	68.7
	MEAN	**735.2**	**719.4**	**15.9**	**2.2**	**0.080**	**0.060**	**0.020**	**35.4**
	SD	**28.7**	**22.7**	**19.8**	**2.8**	**0.020**	**0.013**	**0.014**	**24.1**

Table C.1 continued:

Mouse	Estrogen	Tb.Th. (μm)				Tb.Sp. (μm)			
		L	R	L-R	%diff	L	R	L-R	%diff
A01	Sham	59.2	56.7	2.5	4.4	400.4	405.7	-5.3	-1.3
A03	Sham	58.8	56.0	2.8	5.0	353.5	353.2	0.3	0.1
A04	Sham	64.5	57.7	6.8	11.8	336.3	365.2	-28.9	-7.9
B05	Sham	67.3	54.2	13.1	24.2	447.8	378.8	69.0	18.2
B06	Sham	66.6	50.8	15.8	31.1	404.2	388.6	15.6	4.0
D13	Sham	64.8	54.8	10.0	18.2	380.9	477.5	-96.6	-20.2
D14	Sham	58.7	54.5	4.2	7.7	376.4	376.8	-0.4	-0.1
D15	Sham	64.7	60.7	4.0	6.6	458.9	405.8	53.1	13.1
D16	Sham	73.8	56.4	17.4	30.9	423.9	337.0	86.9	25.8
E20	Sham	68.6	53.7	14.9	27.7	420.9	417.9	3.0	0.7
F21	Sham	59.9	57.2	2.7	4.7	402.8	370.2	32.6	8.8
F23	Sham	62.4	49.3	13.1	26.6	386.2	387.5	-1.3	-0.3
	MEAN	**64.1**	**55.2**	**8.9**	**16.6**	**399.4**	**388.7**	**10.7**	**3.4**
	SD	**4.6**	**3.1**	**5.7**	**11.0**	**35.8**	**36.2**	**47.9**	**12.0**
		L	**R**	**L-R**	**%diff**	**L**	**R**	**L-R**	**%diff**
A02	OVX	64.7	57.8	6.9	11.9	435.5	420.4	15.1	3.6
B07	OVX	71.5	58.2	13.3	22.9	304.4	343.5	-39.1	-11.4
B08	OVX	70.0	58.7	11.3	19.3	376.6	365.3	11.3	3.1
C09	OVX	73.5	55.4	18.1	32.7	407.9	358.8	49.1	13.7
C10	OVX	66.7	53.5	13.2	24.7	357.9	323.5	34.4	10.6
C11	OVX	72.1	57.9	14.2	24.5	391.7	432.1	-40.4	-9.3
C12	OVX	66.8	51.8	15.0	29.0	372.0	403.0	-31.0	-7.7
E17	OVX	67.9	58.7	9.2	15.7	321.4	373.2	-51.8	-13.9
E18	OVX	62.8	46.7	16.1	34.5	461.2	411.4	49.8	12.1
E19	OVX	57.1	54.5	2.6	4.8	419.8	493.8	-74.0	-15.0
F22	OVX	68.4	60.3	8.1	13.4	438.9	376.1	62.8	16.7
F24	OVX	72.4	53.0	19.4	36.6	385.9	374.9	11.0	2.9
	MEAN	**67.8**	**55.5**	**12.3**	**22.5**	**389.4**	**389.7**	**-0.2**	**0.5**
	SD	**4.7**	**3.9**	**4.9**	**9.8**	**47.0**	**45.7**	**45.5**	**11.5**

Table C.2: Indices of cancellous adaptation determined by microCT analysis of VOIs from the proximal metaphysis of loaded and control tibiae from adult Sham-ovariectomy (Sham) and ovariectomy (OVX) female mice after 2 weeks of loading.

Mouse	Estrogen	tBMD (mg/cc)				BV/TV			
		L	R	L-R	%diff	L	R	L-R	%diff
B06	Sham	751.9	711.4	40.5	5.7	0.067	0.034	0.033	95.9
B07	Sham	742.0	700.1	41.9	6.0	0.068	0.032	0.036	114.2
B08	Sham	775.9	727.7	48.2	6.6	0.042	0.063	-0.021	-33.4
D13	Sham	751.3	704.3	47.1	6.7	0.062	0.063	-0.002	-2.7
D14	Sham	790.3	721.8	68.6	9.5	0.054	0.029	0.025	87.2
D15	Sham	715.8	751.3	-35.5	-4.7	0.049	0.049	0.000	0.4
D16	Sham	760.7	732.9	27.8	3.8	0.113	0.063	0.051	81.4
F21	Sham	773.9	690.2	83.7	12.1	0.053	0.034	0.019	55.6
F22	Sham	779.4	719.0	60.4	8.4	0.052	0.039	0.013	32.4
F23	Sham	760.4	695.9	64.5	9.3	0.032	0.037	-0.005	-12.3
F24	Sham	741.4	709.3	32.1	4.5	0.077	0.036	0.041	112.7
	MEAN	**758.5**	**714.9**	**43.6**	**6.2**	**0.061**	**0.043**	**0.017**	**48.3**
	SD	**21.2**	**18.0**	**31.0**	**4.3**	**0.022**	**0.013**	**0.022**	**53.8**
		L	**R**	**L-R**	**%diff**	**L**	**R**	**L-R**	**%diff**
A01	OVX	743.2	690.4	52.8	7.7	0.046	0.043	0.004	8.4
A02	OVX	740.8	676.7	64.1	9.5	0.036	0.060	-0.024	-40.4
A04	OVX	798.6	684.2	114.4	16.7	0.035	0.043	-0.008	-17.8
B05	OVX	729.3	712.6	16.7	2.3	0.044	0.039	0.004	11.2
C09	OVX	735.6	711.6	24.0	3.4	0.060	0.043	0.017	39.2
C10	OVX	783.1	752.8	30.4	4.0	0.082	0.052	0.030	56.9
C11	OVX	753.7	722.5	31.1	4.3	0.056	0.040	0.016	39.6
C12	OVX	725.8	723.7	2.2	0.3	0.054	0.040	0.014	35.0
E17	OVX	767.4	745.3	22.1	3.0	0.060	0.046	0.014	29.3
E18	OVX	757.7	730.6	27.2	3.7	0.044	0.037	0.007	18.6
E19	OVX	773.9	741.6	32.3	4.3	0.045	0.054	-0.009	-16.5
E20	OVX	741.5	730.4	11.1	1.5	0.085	0.060	0.025	41.1
	MEAN	**754.2**	**718.5**	**35.7**	**5.1**	**0.054**	**0.046**	**0.007**	**17.1**
	SD	**22.6**	**24.4**	**29.9**	**4.4**	**0.016**	**0.008**	**0.015**	**29.2**

Table C.2 continued:

Mouse	Estrogen	Tb.Th. (μm)				Tb.Sp. (μm)			
		L	R	L-R	%diff	L	R	L-R	%diff
B06	Sham	62.1	46.1	16.0	34.7	375.9	490.7	-114.8	-23.4
B07	Sham	62.6	46.1	16.5	35.8	443.0	397.9	45.1	11.3
B08	Sham	69.3	53.1	16.2	30.5	393.6	370.3	23.3	6.3
D13	Sham	70.7	50.0	20.7	41.4	380.3	440.4	-60.1	-13.6
D14	Sham	80.4	53.1	27.3	51.4	518.5	448.7	69.8	15.6
D15	Sham	59.3	55.7	3.6	6.5	503.2	421.2	82.0	19.5
D16	Sham	72.9	52.2	20.7	39.7	353.4	352.8	0.6	0.2
F21	Sham	74.8	49.2	25.6	52.0	456.2	475.3	-19.1	-4.0
F22	Sham	76.2	45.3	30.9	68.2	493.0	372.7	120.3	32.3
F23	Sham	53.9	50.6	3.3	6.5	525.2	383.7	141.5	36.9
F24	Sham	65.9	52.1	13.8	26.5	465.9	449.2	16.7	3.7
	MEAN	**68.0**	**50.3**	**17.7**	**35.7**	**446.2**	**418.4**	**27.8**	**7.7**
	SD	**8.0**	**3.4**	**8.8**	**18.5**	**61.7**	**46.0**	**75.9**	**18.2**
		L	**R**	**L-R**	**%diff**	**L**	**R**	**L-R**	**%diff**
A01	OVX	67.3	51.2	16.1	31.4	593.6	444.4	149.2	33.6
A02	OVX	59.4	55.6	3.8	6.8	469.9	486.8	-16.9	-3.5
A04	OVX	68.7	51.0	17.7	34.7	463.1	413.9	49.2	11.9
B05	OVX	60.0	49.8	10.2	20.5	461.9	449.4	12.5	2.8
C09	OVX	63.8	49.8	14.0	28.1	421.8	405.4	16.4	4.0
C10	OVX	85.8	55.3	30.5	55.2	385.7	372.5	13.2	3.5
C11	OVX	59.1	48.4	10.7	22.1	432.7	403.0	29.7	7.4
C12	OVX	61.2	52.0	9.2	17.7	404.1	466.8	-62.7	-13.4
E17	OVX	78.7	62.9	15.8	25.1	431.7	438.7	-7.0	-1.6
E18	OVX	62.1	54.0	8.1	15.0	475.0	411.1	63.9	15.5
E19	OVX	64.7	58.5	6.2	10.6	427.1	413.6	13.5	3.3
E20	OVX	66.2	54.2	12.0	22.1	440.5	358.5	82.0	22.9
	MEAN	**66.4**	**53.6**	**12.9**	**24.1**	**450.6**	**422.0**	**28.6**	**7.2**
	SD	**8.2**	**4.1**	**6.9**	**12.7**	**52.4**	**37.1**	**53.6**	**12.5**

Table C.3: Indices of cancellous adaptation determined by microCT analysis of VOIs from the proximal metaphysis of loaded and control tibiae from adult Sham-ovariectomy (Sham) and ovariectomy (OVX) female mice after 6 weeks of loading.

Mouse	Estrogen	tBMD (mg/cc)				BV/TV			
		L	R	L-R	%diff	L	R	L-R	%diff
F01	Sham	806.1	721.2	84.9	11.8	0.104	0.046	0.058	125.8
F02	Sham	795.1	756.1	39.0	5.2	0.071	0.055	0.016	29.1
F03	Sham	730.3	689.2	41.0	5.9	0.212	0.172	0.039	22.7
F04	Sham	792.9	721.4	71.6	9.9	0.106	0.055	0.051	91.7
H10	Sham	771.5	706.2	65.3	9.2	0.078	0.048	0.030	63.3
H11	Sham	803.5	738.6	64.8	8.8	0.094	0.059	0.035	59.9
H12	Sham	768.1	701.1	67.0	9.6	0.102	0.029	0.073	254.4
J17	Sham	774.9	686.2	88.7	12.9	0.090	0.041	0.049	117.9
J18	Sham	777.4	766.7	10.7	1.4	0.116	0.062	0.054	87.7
J20	Sham	813.1	750.9	62.2	8.3	0.070	0.054	0.015	28.2
	MEAN	**783.3**	**723.8**	**59.5**	**8.3**	**0.104**	**0.062**	**0.042**	**88.1**
	SD	**24.3**	**28.4**	**23.4**	**3.4**	**0.041**	**0.040**	**0.018**	**68.9**
		L	**R**	**L-R**	**%diff**	**L**	**R**	**L-R**	**%diff**
G05	OVX	756.6	701.4	55.2	7.9	0.131	0.041	0.090	216.7
G07	OVX	746.4	660.3	86.1	13.0	0.125	0.062	0.063	101.1
G08	OVX	782.6	692.8	89.7	13.0	0.114	0.044	0.070	159.9
I13	OVX	753.7	702.8	50.9	7.2	0.107	0.052	0.055	105.6
I14	OVX	745.4	776.0	-30.6	-3.9	0.130	0.034	0.096	284.6
I15	OVX	737.1	733.3	3.8	0.5	0.090	0.041	0.049	121.2
I16	OVX	782.4	723.4	59.0	8.2	0.084	0.036	0.048	132.2
K21	OVX	790.5	756.5	34.0	4.5	0.107	0.036	0.071	196.1
K22	OVX	801.6	685.7	116.0	16.9	0.077	0.040	0.037	94.0
K23	OVX	759.1	709.7	49.4	7.0	0.113	0.033	0.081	244.7
K24	OVX	786.0	707.3	78.7	11.1	0.097	0.050	0.047	93.2
	MEAN	**767.4**	**713.6**	**53.8**	**7.8**	**0.107**	**0.043**	**0.064**	**159.0**
	SD	**21.7**	**32.5**	**41.1**	**5.9**	**0.018**	**0.009**	**0.019**	**66.9**

Table C.3 continued:

Mouse	Estrogen	Tb.Th. (μm)				Tb.Sp. (μm)			
		L	R	L-R	%diff	L	R	L-R	%diff
F01	Sham	89.9	54.0	35.9	66.5	421.2	486.8	-65.6	-13.5
F02	Sham	89.6	62.2	27.4	44.1	475.1	573.4	-98.3	-17.1
F03	Sham	89.2	71.6	17.6	24.6	291.5	272.8	18.7	6.9
F04	Sham	91.3	53.0	38.3	72.3	416.0	430.8	-14.8	-3.4
H10	Sham	70.9	49.4	21.5	43.5	404.0	370.3	33.7	9.1
H11	Sham	94.4	56.2	38.2	68.0	439.1	389.0	50.1	12.9
H12	Sham	86.1	45.6	40.5	88.8	434.2	419.7	14.5	3.5
J17	Sham	90.7	51.6	39.1	75.8	505.5	448.5	57.0	12.7
J18	Sham	87.6	60.4	27.2	45.0	536.8	415.2	121.6	29.3
J20	Sham	91.3	54.1	37.2	68.8	400.0	451.4	-51.4	-11.4
	MEAN	**88.1**	**55.8**	**32.3**	**59.7**	**432.3**	**425.8**	**6.6**	**2.9**
	SD	**6.4**	**7.4**	**8.2**	**19.5**	**66.8**	**78.0**	**65.5**	**14.4**
		L	**R**	**L-R**	**%diff**	**L**	**R**	**L-R**	**%diff**
G05	OVX	91.4	52.4	39.0	74.4	409.5	405.5	4.0	1.0
G07	OVX	88.9	53.5	35.4	66.2	421.2	404.9	16.3	4.0
G08	OVX	86.8	46.8	40.0	85.5	484.4	446.1	38.3	8.6
I13	OVX	81.5	55.3	26.2	47.4	515.5	488.7	26.8	5.5
I14	OVX	83.9	55.8	28.1	50.4	514.4	504.9	9.5	1.9
I15	OVX	85.1	49.5	35.6	71.9	500.8	511.6	-10.8	-2.1
I16	OVX	93.7	52.8	40.9	77.5	641.7	590.5	51.2	8.7
K21	OVX	87.9	64.7	23.2	35.9	697.7	574.0	123.7	21.6
K22	OVX	92.9	56.5	36.4	64.4	668.3	571.6	96.7	16.9
K23	OVX	83.7	50.2	33.5	66.7	566.9	497.8	69.1	13.9
K24	OVX	90.6	47.9	42.7	89.1	459.2	429.7	29.5	6.9
	MEAN	**87.9**	**53.2**	**34.6**	**66.3**	**534.5**	**493.2**	**41.3**	**7.9**
	SD	**4.0**	**5.0**	**6.3**	**16.3**	**97.8**	**66.6**	**41.0**	**7.1**

Table C.4: Indices of cortical adaptation determined by microCT analysis of VOIs centered at the mid-diaphysis of loaded and control tibiae from adult Sham-ovariectomy (Sham) and ovariectomy (OVX) female mice after 1 week of loading.

Mouse	Estrogen	I_{max} (mm^4)				I_{min} (mm^4)				Cortical Area (mm^2)			
		L	R	L-R	%diff	L	R	L-R	%diff	L	R	L-R	%diff
A01	Sham	0.087	0.089	-0.002	-2.1	0.064	0.060	0.004	6.3	0.695	0.656	0.039	6.0
A03	Sham	0.077	0.084	-0.006	-7.5	0.069	0.067	0.002	2.5	0.681	0.659	0.023	3.4
A04	Sham	0.094	0.086	0.008	9.5	0.069	0.067	0.002	3.6	0.711	0.658	0.053	8.0
B05	Sham	0.068	0.070	-0.001	-2.0	0.051	0.049	0.002	3.5	0.628	0.606	0.022	3.6
B06	Sham	0.083	0.073	0.010	13.1	0.064	0.057	0.008	13.6	0.682	0.636	0.046	7.2
D13	Sham	0.095	0.088	0.007	8.3	0.078	0.063	0.015	23.5	0.705	0.637	0.068	10.6
D14	Sham	0.076	0.062	0.014	22.1	0.052	0.047	0.005	10.2	0.608	0.557	0.051	9.2
D15	Sham	0.097	0.077	0.020	26.0	0.072	0.065	0.007	10.4	0.717	0.639	0.078	12.1
D16	Sham	0.071	0.077	-0.006	-8.2	0.058	0.060	-0.002	-3.5	0.626	0.623	0.003	0.5
E20	Sham	0.093	0.073	0.020	27.2	0.072	0.065	0.008	11.9	0.679	0.614	0.065	10.6
F21	Sham	0.086	0.077	0.009	11.6	0.063	0.062	0.001	1.6	0.673	0.631	0.042	6.7
F23	Sham	0.100	0.086	0.014	16.6	0.081	0.072	0.009	12.1	0.705	0.666	0.039	5.8
	MEAN	**0.086**	**0.078**	**0.007**	**9.5**	**0.066**	**0.061**	**0.005**	**8.0**	**0.676**	**0.632**	**0.044**	**7.0**
	SD	**0.011**	**0.008**	**0.009**	**12.4**	**0.009**	**0.007**	**0.005**	**7.1**	**0.036**	**0.030**	**0.021**	**3.4**

Table C.4 Continued:

Mouse	Estrogen	I_{max} (mm^4)				I_{min} (mm^4)				Cortical Area (mm^2)			
		L	R	L-R	%diff	L	R	L-R	%diff	L	R	L-R	%diff
A02	OVX	0.102	0.085	0.017	19.5	0.077	0.069	0.008	11.3	0.724	0.675	0.049	7.3
B07	OVX	0.076	0.067	0.009	13.7	0.058	0.051	0.007	14.3	0.660	0.601	0.059	9.8
B08	OVX	0.092	0.074	0.018	24.7	0.060	0.058	0.001	2.6	0.705	0.649	0.055	8.5
C09	OVX	0.077	0.072	0.005	7.5	0.058	0.057	0.001	2.3	0.662	0.619	0.043	6.9
C10	OVX	0.085	0.085	0.001	0.6	0.066	0.066	0.000	-0.3	0.675	0.650	0.026	4.0
C11	OVX	0.093	0.073	0.021	28.5	0.063	0.056	0.008	13.5	0.711	0.653	0.057	8.8
C12	OVX	0.075	0.071	0.004	5.3	0.059	0.056	0.003	5.5	0.647	0.604	0.043	7.1
E17	OVX	0.101	0.076	0.025	32.6	0.073	0.058	0.015	26.6	0.763	0.651	0.112	17.2
E18	OVX	0.078	0.070	0.008	10.7	0.058	0.057	0.001	1.0	0.668	0.623	0.045	7.2
E19	OVX	0.092	0.076	0.016	21.3	0.065	0.067	-0.003	-3.7	0.670	0.614	0.056	9.1
F22	OVX	0.090	0.112	-0.022	-19.5	0.073	0.080	-0.007	-8.6	0.720	0.754	-0.034	-4.5
F24	OVX	0.073	0.060	0.013	21.8	0.062	0.050	0.012	25.1	0.669	0.612	0.057	9.3
	MEAN	**0.086**	**0.077**	**0.010**	**13.9**	**0.064**	**0.060**	**0.004**	**7.5**	**0.690**	**0.642**	**0.047**	**7.6**
	SD	**0.010**	**0.013**	**0.012**	**14.3**	**0.007**	**0.009**	**0.006**	**10.9**	**0.035**	**0.042**	**0.033**	**4.9**

Table C.5: Indices of cortical adaptation determined by microCT analysis of VOIs centered at the mid-diaphysis of loaded and control tibiae from adult Sham-ovariectomy (Sham) and ovariectomy (OVX) female mice after 2 weeks of loading.

Mouse	Estrogen	I_{max} (mm^4)				I_{min} (mm^4)				Cortical Area (mm^2)			
		L	R	L-R	%diff	L	R	L-R	%diff	L	R	L-R	%diff
B06	Sham	0.096	0.081	0.015	18.3	0.072	0.063	0.009	14.4	0.703	0.642	0.061	9.5
B07	Sham	0.096	0.072	0.023	32.0	0.063	0.059	0.004	5.9	0.711	0.617	0.094	15.2
B08	Sham	0.108	0.085	0.023	27.6	0.077	0.066	0.010	15.6	0.761	0.666	0.095	14.3
D13	Sham	0.110	0.093	0.018	19.1	0.076	0.069	0.007	10.5	0.735	0.745	-0.010	-1.3
D14	Sham	0.123	0.074	0.049	65.3	0.075	0.060	0.015	25.6	0.807	0.617	0.190	30.8
D15	Sham	0.095	0.098	-0.003	-3.6	0.072	0.074	-0.002	-3.1	0.677	0.705	-0.028	-3.9
D16	Sham	0.104	0.065	0.039	60.5	0.071	0.050	0.021	42.0	0.805	0.620	0.185	29.9
F21	Sham	0.123	0.079	0.044	55.4	0.077	0.059	0.018	30.7	0.814	0.621	0.193	31.1
F22	Sham	0.118	0.078	0.040	50.8	0.073	0.060	0.012	20.2	0.789	0.651	0.138	21.2
F23	Sham	0.091	0.092	-0.001	-1.0	0.070	0.068	0.002	3.2	0.702	0.652	0.049	7.6
F24	Sham	0.093	0.077	0.016	20.5	0.072	0.063	0.009	14.7	0.710	0.627	0.083	13.1
	MEAN	**0.105**	**0.081**	**0.024**	**31.4**	**0.072**	**0.063**	**0.010**	**16.3**	**0.747**	**0.651**	**0.096**	**15.2**
	SD	**0.012**	**0.010**	**0.017**	**23.8**	**0.004**	**0.006**	**0.007**	**12.9**	**0.050**	**0.041**	**0.076**	**12.2**

Table C.5 Continued:

Mouse	Estrogen	I_{max} (mm^4)				I_{min} (mm^4)				Cortical Area (mm^2)			
		L	R	L-R	%diff	L	R	L-R	%diff	L	R	L-R	%diff
A01	OVX	0.094	0.083	0.011	13.0	0.072	0.072	0.000	0.3	0.707	0.665	0.042	6.2
A02	OVX	0.107	0.095	0.012	12.6	0.081	0.069	0.012	16.8	0.752	0.723	0.029	4.0
A04	OVX	0.096	0.087	0.009	10.8	0.071	0.062	0.009	14.9	0.700	0.670	0.030	4.5
B05	OVX	0.120	0.086	0.034	40.2	0.085	0.068	0.017	25.3	0.816	0.683	0.133	19.5
C09	OVX	0.092	0.076	0.016	21.3	0.067	0.058	0.009	15.7	0.701	0.608	0.093	15.3
C10	OVX	0.154	0.073	0.081	110.8	0.097	0.056	0.041	73.6	0.991	0.653	0.339	51.9
C11	OVX	0.106	0.099	0.007	7.3	0.077	0.077	0.001	0.7	0.758	0.728	0.030	4.1
C12	OVX	0.093	0.078	0.015	18.7	0.077	0.062	0.016	25.2	0.721	0.634	0.087	13.8
E17	OVX	0.148	0.077	0.071	91.7	0.094	0.065	0.029	44.6	0.936	0.662	0.275	41.5
E18	OVX	0.111	0.084	0.027	31.9	0.082	0.069	0.013	19.1	0.786	0.661	0.126	19.0
E19	OVX	0.095	0.097	-0.002	-2.1	0.076	0.080	-0.003	-4.1	0.743	0.717	0.026	3.6
E20	OVX	0.089	0.074	0.015	20.2	0.069	0.059	0.011	18.1	0.705	0.624	0.081	13.0
	MEAN	**0.109**	**0.084**	**0.025**	**31.4**	**0.079**	**0.066**	**0.013**	**20.8**	**0.776**	**0.669**	**0.108**	**16.4**
	SD	**0.022**	**0.009**	**0.026**	**34.7**	**0.009**	**0.007**	**0.012**	**21.2**	**0.095**	**0.038**	**0.101**	**15.5**

Table C.6: Indices of cortical adaptation determined by microCT analysis of VOIs centered at the mid-diaphysis of loaded and control tibiae from adult Sham-ovariectomy (Sham) and ovariectomy (OVX) female mice after 6 weeks of loading.

Mouse	Estrogen	I_{max} (mm^4)				I_{min} (mm^4)				Cortical Area (mm^2)			
		L	R	L-R	%diff	L	R	L-R	%diff	L	R	L-R	%diff
F01	Sham	0.094	0.063	0.031	48.3	0.067	0.050	0.017	33.6	0.755	0.584	0.171	29.3
F02	Sham	0.113	0.092	0.021	23.0	0.087	0.064	0.023	35.0	0.820	0.686	0.134	19.5
F03	Sham	0.115	0.072	0.044	60.8	0.081	0.052	0.030	57.4	0.800	0.637	0.163	25.5
F04	Sham	0.171	0.065	0.107	164.6	0.083	0.043	0.040	92.1	0.992	0.559	0.433	77.5
H10	Sham	0.156	0.104	0.052	49.7	0.097	0.069	0.028	39.6	0.928	0.725	0.203	27.9
H11	Sham	0.097	0.092	0.005	5.4	0.078	0.067	0.011	16.7	0.705	0.650	0.055	8.5
H12	Sham	0.109	0.085	0.024	28.1	0.078	0.067	0.011	16.8	0.750	0.611	0.140	22.9
J17	Sham	0.137	0.088	0.049	55.0	0.098	0.065	0.032	49.5	0.856	0.643	0.213	33.2
J18	Sham	0.119	0.092	0.027	29.5	0.078	0.065	0.013	20.3	0.803	0.630	0.173	27.4
J20	Sham	0.122	0.088	0.035	39.6	0.083	0.070	0.014	19.3	0.790	0.660	0.130	19.6
	MEAN	**0.123**	**0.084**	**0.039**	**50.4**	**0.083**	**0.061**	**0.022**	**38.0**	**0.820**	**0.638**	**0.181**	**29.1**
	SD	**0.025**	**0.013**	**0.027**	**43.5**	**0.009**	**0.009**	**0.010**	**23.6**	**0.086**	**0.048**	**0.099**	**18.3**

Table C.6 Continued:

Mouse	Estrogen	I_{max} (mm^4)				I_{min} (mm^4)				Cortical Area (mm^2)			
		L	R	L-R	%diff	L	R	L-R	%diff	L	R	L-R	%diff
G05	OVX	0.117	0.095	0.023	23.7	0.086	0.073	0.013	18.4	0.777	0.645	0.132	20.5
G07	OVX	0.129	0.097	0.032	33.3	0.088	0.074	0.014	18.8	0.836	0.694	0.142	20.5
G08	OVX	0.121	0.086	0.035	40.3	0.082	0.066	0.016	24.4	0.772	0.638	0.134	21.1
I13	OVX	0.132	0.084	0.048	57.6	0.083	0.063	0.020	31.4	0.813	0.630	0.183	29.1
I14	OVX	0.126	0.070	0.056	79.0	0.072	0.064	0.008	12.6	0.757	0.586	0.172	29.3
I15	OVX	0.137	0.105	0.032	30.6	0.088	0.073	0.015	20.0	0.814	0.683	0.132	19.3
I16	OVX	0.139	0.085	0.054	63.3	0.093	0.072	0.022	30.0	0.839	0.617	0.222	36.0
K21	OVX	0.102	0.076	0.026	33.7	0.071	0.060	0.011	18.3	0.724	0.620	0.104	16.9
K22	OVX	0.160	0.104	0.056	53.5	0.100	0.078	0.022	27.9	0.860	0.682	0.177	26.0
K23	OVX	0.122	0.095	0.027	28.6	0.087	0.075	0.012	16.1	0.772	0.687	0.085	12.4
K24	OVX	0.112	0.095	0.017	17.6	0.075	0.072	0.003	3.7	0.739	0.661	0.077	11.7
	MEAN	**0.127**	**0.090**	**0.037**	**41.9**	**0.084**	**0.070**	**0.014**	**20.2**	**0.791**	**0.649**	**0.142**	**22.1**
	SD	**0.015**	**0.011**	**0.014**	**18.9**	**0.009**	**0.006**	**0.006**	**8.1**	**0.044**	**0.035**	**0.044**	**7.4**

APPENDIX D: *10 week old intact females*

1wk Loading (e114)

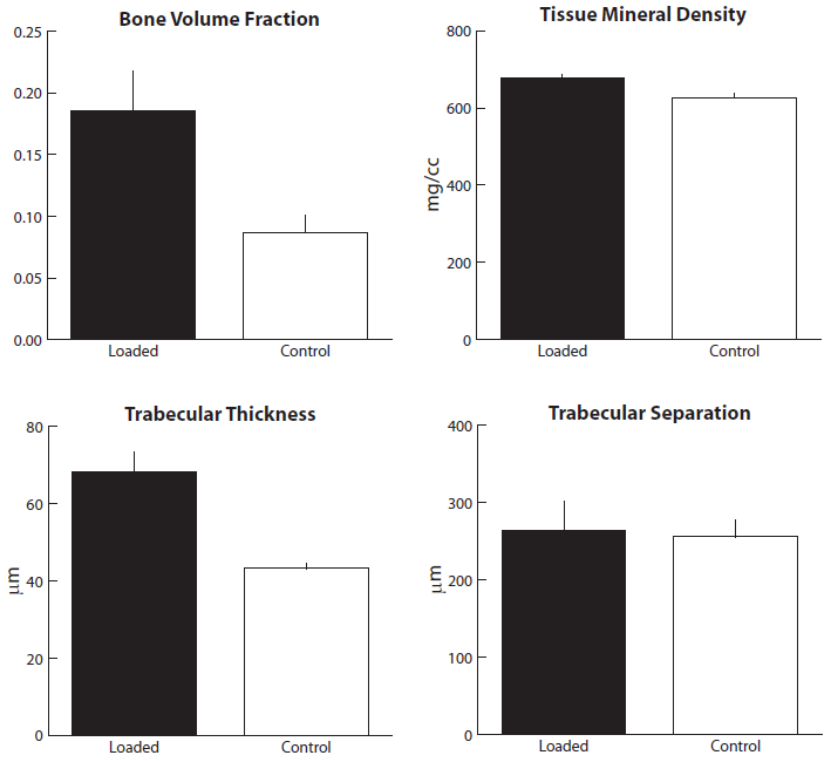

Figure D.1: Cancellous parameters of growing female mice after 1 week of loading, analyzed by microCT from a purely cancellous VOI in the proximal metaphysis.

Table D.1: Summary of cancellous indices determined by microCT analysis of VOIs from the proximal metaphysis of loaded and control tibiae from growing female mice after 1 week of loading.

Variable	Loaded (Left)	Control (Right)	Δ (Left - Right)	Difference (%)
BV/TV	0.19±0.03	0.09±0.01	0.10±0.03	115±39
tBMD (mg/cc)	679±5	627±10	52±8	8±1.4
Tb.Th (µm)	68±5.2	43±1.3	25±4.7	58±10
Tb.Sp (µm)	264±38	256±23	8±25	3.1±9.4

Table D.2: Indices of cancellous adaptation for each mouse, determined by microCT analysis of VOIs from the proximal metaphysis of loaded and control tibiae from growing female mice after 1 week of loading.

Mouse	tBMD (mg/cc)				BV/TV			
	L	R	L-R	%diff	L	R	L-R	%diff
A01	679.8	631.8	48.0	7.6	0.187	0.087	0.100	114.9
A02	676.2	622.5	53.7	8.6	0.172	0.076	0.096	127.5
A03	674.6	631.8	42.8	6.8	0.134	0.062	0.072	117.5
A04	675.9	609.6	66.3	10.9	0.197	0.102	0.095	93.5
A05	681.6	638.7	42.9	6.7	0.229	0.078	0.150	192.0
B06	687.0	636.7	50.3	7.9	0.212	0.084	0.128	152.6
B07	676.5	613.8	62.8	10.2	0.176	0.098	0.078	79.0
B08	686.6	639.0	47.5	7.4	0.209	0.093	0.117	126.0
B09	673.7	621.5	52.2	8.4	0.205	0.107	0.098	90.9
B10	678.1	620.5	57.6	9.3	0.126	0.082	0.044	54.0
MEAN	**679.0**	**626.6**	**52.4**	**8.4**	**0.185**	**0.087**	**0.098**	**114.8**
SD	**4.7**	**10.5**	**7.9**	**1.4**	**0.033**	**0.014**	**0.030**	**39.0**

Mouse	Tb.Th. (µm)				Tb.Sp. (µm)			
	L	R	L-R	%diff	L	R	L-R	%diff
A01	69.7	44.1	25.6	58.0	253.1	259.2	-6.1	-2.4
A02	70.8	42.5	28.3	66.6	299.8	296.7	3.1	1.0
A03	66.0	40.8	25.2	61.8	340.8	286.2	54.6	19.1
A04	77.5	44.1	33.4	75.7	269.8	251.4	18.4	7.3
A05	66.2	42.6	23.6	55.4	211.4	251.9	-40.5	-16.1
B06	71.6	44.5	27.1	60.9	275.5	243.9	31.6	13.0
B07	64.7	42.9	21.8	50.8	249.0	241.2	7.8	3.2
B08	72.9	44.7	28.2	63.1	244.7	249.8	-5.1	-2.0
B09	60.9	43.8	17.1	39.0	219.6	214.4	5.2	2.4
B10	61.9	41.8	20.1	48.1	275.6	262.6	13.0	5.0
MEAN	**68.2**	**43.2**	**25.0**	**57.9**	**263.9**	**255.7**	**8.2**	**3.1**
SD	**5.2**	**1.3**	**4.7**	**10.3**	**37.9**	**23.1**	**25.0**	**9.4**

Table D.3: Cancellous dynamic histomorphometry for each mouse, measured within the tibial proximal metaphysis of loaded and control tibiae from growing female mice after 1 week of loading.

Mouse	Limb	BV/TV (%)	Er.S (%)	MS (%)	MAR (um/d)	BFRs
A02	Left	11.6	13.2	11.1	5.4	219.2
A04	Left	13.8	10.2	13.7	4.7	235.9
B06	Left	12.8	4.1	14.1	5.1	263.6
B07	Left	7.6	4.2	21.1	6.4	496.4
B08	Left	9.7	2.9	13.1	6.6	316.7
A02	Right	11.0	7.0	8.3	3.7	111.8
A04	Right	9.1	1.9	8.4	4.5	137.5
B06	Right	10.0	1.8	15.1	5.7	315.9
B07	Right	8.2	2.7	9.5	5.9	204.7
B08	Right	9.9	1.5	17.1	2.3	145.5

Table D.4: Cancellous static histomorphometry for each mouse, measured within the tibial proximal metaphysis of loaded and control tibiae from growing female mice after 1 week of loading.

Mouse	Limb	T.Ar (mm^2)	B.Ar (mm^2)	Ma.Ar (mm^2)	B.Pm (mm)	E.Pm (mm)	dL.Pm (mm)	sL.Pm (mm)	Ir.L.Wi (um)
A02	Left	0.85	0.10	0.75	4.16	0.55	0.01	0.91	16
A04	Left	0.64	0.09	0.55	4.43	0.45	0.16	0.89	14
B06	Left	0.64	0.08	0.56	3.37	0.14	0.13	0.69	15
B07	Left	0.21	0.02	0.20	1.24	0.05	0.17	0.18	19
B08	Left	0.74	0.07	0.67	3.75	0.11	0.01	0.96	20
A02	Right	0.96	0.11	0.85	5.15	0.36	0.16	0.85	11
A04	Right	0.85	0.08	0.77	4.86	0.09	0.01	0.81	14
B06	Right	0.74	0.07	0.67	4.21	0.08	0.28	0.71	17
B07	Right	0.74	0.06	0.68	3.40	0.09	0.21	0.22	18
B08	Right	0.85	0.08	0.77	4.10	0.06	0.01	1.40	7

APPENDIX E: *10 week old OVX females*

1wk Loading (e141)

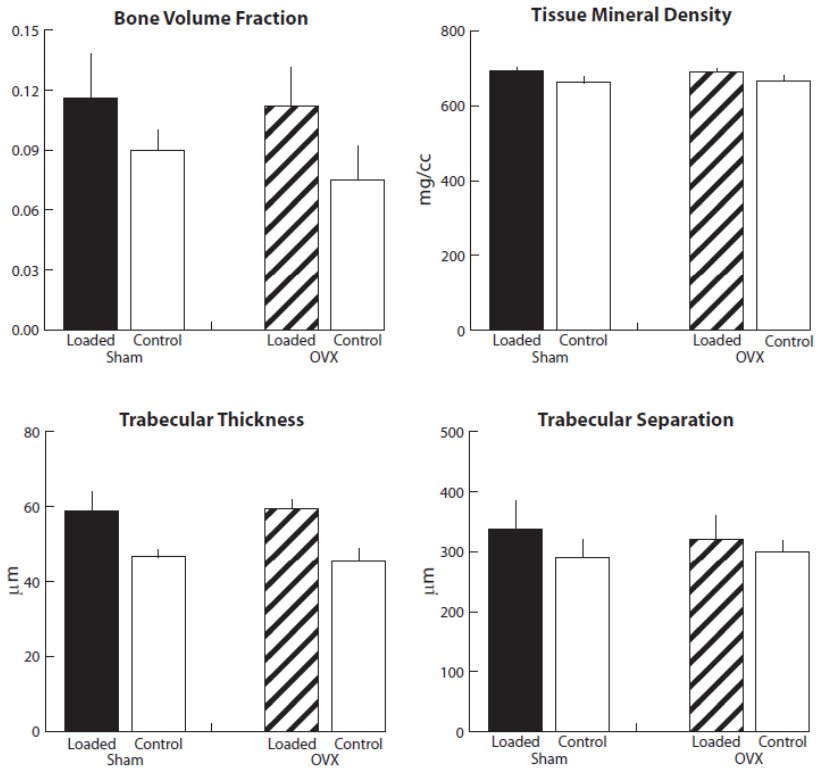

Figure E.1: Cancellous parameters of growing Sham-surgery (Sham) and ovariectomized (OVX) female mice after 1 week of loading, analyzed by microCT from a purely cancellous VOI in the proximal metaphysis.

Table E.1: Summary of cancellous indices determined by microCT analysis of VOIs from the proximal metaphysis of loaded and control tibiae from growing Sham-surgery (Sham) and ovariectomized (OVX) female mice after 1 week of loading.

Variable	Estrogen Status	Loaded (Left)	Control (Right)	Δ (Left - Right)	Difference (%)
BV/TV	Sham	0.12±0.02	0.09±0.01	0.03±0.02	30±25
	OVX	0.11±0.02	0.08±0.02	0.04±0.02	54±32
tBMD (mg/cc)	Sham	694±8.7	662±17	32±20	5.0±3.1
	OVX	690±8.8	666±17	24±19	3.7±2.8
Tb.Th (µm)	Sham	59±5.3	47±2.0	12±4.2	26±8.8
	OVX	59±2.6	46±3.3	14±4.7	31±13
Tb.Sp (µm)	Sham	338±48	291±30	47±32	16±10
	OVX	320±41	300±21	20±39	6.9±12

Table E.2: Indices of cancellous adaptation for each mouse, determined by microCT analysis of VOIs from the proximal metaphysis of loaded and control tibiae from growing Sham-surgery (Sham) and ovariectomized (OVX) female mice after 1 week of loading.

Mouse	Estrogen	tBMD (mg/cc)				BV/TV			
		L	R	L-R	%diff	L	R	L-R	%diff
A01	Sham	682.8	655.7	27.1	4.1	0.087	0.084	0.003	3.5
A04	Sham	688.4	645.8	42.6	6.6	0.121	0.076	0.045	59.8
B07	Sham	710.1	677.4	32.7	4.8	0.114	0.083	0.031	36.9
B08	Sham	691.6	654.2	37.4	5.7	0.099	0.090	0.009	10.0
C09	Sham	697.0	668.2	28.8	4.3	0.128	0.100	0.028	28.2
C10	Sham	690.2	681.0	9.1	1.3	0.106	0.094	0.012	12.8
D15	Sham	686.2	678.8	7.4	1.1	0.137	0.085	0.053	61.8
D16	Sham	698.3	631.6	66.6	10.5	0.110	0.111	-0.001	-0.5
E19	Sham	688.7	675.7	13.1	1.9	0.160	0.096	0.065	67.5
E20	Sham	705.4	647.1	58.3	9.0	0.099	0.083	0.017	20.0
	MEAN	**693.9**	**661.5**	**32.3**	**5.0**	**0.116**	**0.090**	**0.026**	**30.0**
	SD	**8.7**	**17.0**	**19.9**	**3.1**	**0.022**	**0.010**	**0.022**	**25.4**
		L	**R**	**L-R**	**%diff**	**L**	**R**	**L-R**	**%diff**
A02	OVX	697.6	661.5	36.1	5.5	0.100	0.103	-0.004	-3.7
A03	OVX	687.0	664.1	22.9	3.5	0.125	0.064	0.062	97.2
B05	OVX	683.1	647.3	35.8	5.5	0.109	0.076	0.033	43.3
B06	OVX	686.4	664.7	21.7	3.3	0.122	0.097	0.025	25.6
C11	OVX	678.0	701.0	-23.0	-3.3	0.096	0.050	0.046	90.5
C12	OVX	701.5	662.4	39.1	5.9	0.134	0.082	0.052	62.9
D13	OVX	705.2	690.5	14.7	2.1	0.105	0.079	0.025	31.7
D14	OVX	692.7	653.9	38.8	5.9	0.109	0.072	0.037	52.1
E17	OVX	682.5	661.9	20.5	3.1	0.143	0.075	0.068	90.4
E18	OVX	689.6	652.7	37.0	5.7	0.079	0.054	0.025	46.6
	MEAN	**690.4**	**666.0**	**24.4**	**3.7**	**0.112**	**0.075**	**0.037**	**53.7**
	SD	**8.8**	**16.8**	**18.9**	**2.8**	**0.019**	**0.017**	**0.021**	**32.3**

Table E.2 Continued:

Mouse	Estrogen	Tb.Th. (μm)				Tb.Sp. (μm)			
		L	R	L-R	%diff	L	R	L-R	%diff
A01	Sham	52.3	45.7	6.6	14.4	360.5	313.5	47.0	15.0
A04	Sham	64.3	45.9	18.4	40.1	411	322.3	88.7	27.5
B07	Sham	62.2	46.8	15.4	32.9	379.1	310.4	68.7	22.1
B08	Sham	51.7	43.3	8.4	19.4	283.6	268.1	15.5	5.8
C09	Sham	59.9	46.5	13.4	28.8	320.9	261	59.9	23.0
C10	Sham	58.4	49.3	9.1	18.5	377.3	307.9	69.4	22.5
D15	Sham	64.1	47	17.1	36.4	329.2	317.1	12.1	3.8
D16	Sham	54.7	45.3	9.4	20.8	266.4	228.1	38.3	16.8
E19	Sham	65.4	49.9	15.5	31.1	364.7	288.1	76.6	26.6
E20	Sham	53.6	45	8.6	19.1	287.9	294.4	-6.5	-2.2
	MEAN	**58.7**	**46.5**	**12.2**	**26.1**	**338.1**	**291.1**	**47.0**	**16.1**
	SD	**5.3**	**2.0**	**4.2**	**8.8**	**48.0**	**30.2**	**31.5**	**10.3**
		L	**R**	**L-R**	**%diff**	**L**	**R**	**L-R**	**%diff**
A02	OVX	56.4	49.7	6.7	13.5	293.7	273.6	20.1	7.3
A03	OVX	61.1	41.9	19.2	45.8	299.7	310.1	-10.4	-3.4
B05	OVX	55.8	45.1	10.7	23.7	311.3	288.5	22.8	7.9
B06	OVX	60.1	47.7	12.4	26.0	278.4	269.4	9.0	3.3
C11	OVX	59.2	41.1	18.1	44.0	403.3	322.9	80.4	24.9
C12	OVX	63.3	46.2	17.1	37.0	314.3	313.6	0.7	0.2
D13	OVX	57	49.6	7.4	14.9	300.3	328.7	-28.4	-8.6
D14	OVX	57.3	45.6	11.7	25.7	286.9	305.7	-18.8	-6.1
E17	OVX	62.7	47.1	15.6	33.1	326.2	281.5	44.7	15.9
E18	OVX	60	40.5	19.5	48.1	382.9	301	81.9	27.2
	MEAN	**59.3**	**45.5**	**13.8**	**31.2**	**319.7**	**299.5**	**20.2**	**6.9**
	SD	**2.6**	**3.3**	**4.7**	**12.5**	**41.3**	**20.5**	**38.5**	**12.4**

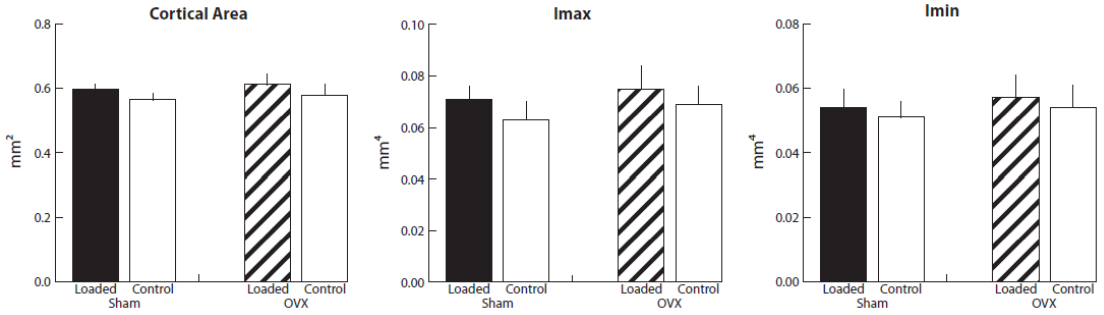

Figure E.2: Cortical parameters of growing Sham-surgery (Sham) and ovariectomized (OVX) female mice after 1 week of loading, analyzed by microCT from a cortical VOI centered at the tibial mid-diaphysis.

Table E.3: Summary of cortical indices determined by microCT analysis of VOIs centered at the mid-diaphysis of loaded and control tibiae from growing ovariectomy (OVX) and Sham-ovariectomy (Sham) female mice after 1 week of loading.

Variable	Estrogen Status	Loaded (Left)	Control (Right)	Δ (Left - Right)	Difference (%)
I_{max} (mm^4)	Sham	0.071±0.01	0.063±0.01	0.008±0.00	14±7.8
	OVX	0.075+0.01	0.069±0.01	0.006±0.01	9.2±11
I_{min} (mm^4)	Sham	0.054±0.01	0.051±0.01	0.004±0.00	7.3±5.2
	OVX	0.057±0.1	0.054±0.1	0.004±0.01	7.3±8.6
Ct.Ar (mm^2)	Sham	0.597±0.02	0.564±0.02	0.034±0.02	6.0±2.9
	OVX	0.611±0.04	0.579±0.03	0.033±0.02	5.7±4.1

Table E.4: Indices of cortical adaptation determined by microCT analysis of VOIs centered at the mid-diaphysis of loaded and control tibiae from growing ovariectomy (OVX) and Sham-ovariectomy (Sham) female mice after 1 week of loading.

Mouse	Estrogen	I_{max} (mm^4)				I_{min} (mm^4)				Cortical Area (mm^2)			
		L	R	L-R	%diff	L	R	L-R	%diff	L	R	L-R	%diff
A01	Sham	0.070	0.064	0.007	10.4	0.054	0.050	0.004	8.6	0.586	0.559	0.028	4.9
A04	Sham	0.070	0.058	0.013	22.3	0.052	0.047	0.005	11.5	0.596	0.544	0.052	9.6
B07	Sham	0.081	0.070	0.011	15.6	0.063	0.060	0.003	5.5	0.626	0.597	0.029	4.9
B08	Sham	0.071	0.063	0.007	11.7	0.054	0.052	0.002	4.0	0.575	0.563	0.012	2.1
C09	Sham	0.070	0.071	-0.001	-1.7	0.057	0.057	0.000	-0.2	0.589	0.572	0.018	3.1
C10	Sham	0.070	0.066	0.004	6.4	0.055	0.052	0.003	6.4	0.598	0.572	0.026	4.5
D15	Sham	0.072	0.061	0.011	17.8	0.056	0.047	0.008	17.5	0.620	0.564	0.056	10.0
D16	Sham	0.076	0.068	0.009	12.7	0.061	0.055	0.006	11.2	0.608	0.583	0.026	4.4
E19	Sham	0.060	0.052	0.009	16.8	0.042	0.042	0.001	1.2	0.583	0.531	0.051	9.6
E20	Sham	0.068	0.054	0.014	25.6	0.050	0.047	0.003	6.8	0.593	0.554	0.039	7.1
	MEAN	**0.071**	**0.063**	**0.008**	**13.8**	**0.054**	**0.051**	**0.004**	**7.3**	**0.597**	**0.564**	**0.034**	**6.0**
	SD	**0.005**	**0.007**	**0.004**	**7.8**	**0.006**	**0.005**	**0.003**	**5.2**	**0.016**	**0.019**	**0.015**	**2.9**
		L	**R**	**L-R**	**%diff**	**L**	**R**	**L-R**	**%diff**	**L**	**R**	**L-R**	**%diff**
A02	OVX	0.067	0.072	-0.006	-7.9	0.051	0.057	-0.006	-10.3	0.584	0.601	-0.018	-3.0
A03	OVX	0.075	0.070	0.006	8.5	0.059	0.058	0.001	1.6	0.614	0.587	0.027	4.6
B05	OVX	0.082	0.076	0.005	7.0	0.059	0.059	0.000	0.7	0.639	0.600	0.040	6.6
B06	OVX	0.080	0.068	0.012	18.2	0.060	0.052	0.008	15.8	0.613	0.592	0.021	3.5
C11	OVX	0.078	0.067	0.011	15.9	0.060	0.054	0.007	12.1	0.623	0.566	0.057	10.1
C12	OVX	0.081	0.064	0.017	27.2	0.062	0.053	0.009	16.9	0.631	0.574	0.057	10.0
D13	OVX	0.081	0.077	0.004	5.5	0.066	0.060	0.006	10.5	0.638	0.603	0.035	5.8
D14	OVX	0.055	0.053	0.002	3.2	0.040	0.035	0.004	11.9	0.533	0.494	0.039	8.0
E17	OVX	0.083	0.070	0.013	18.1	0.061	0.054	0.007	12.3	0.651	0.595	0.056	9.5
E18	OVX	0.071	0.074	-0.003	-3.5	0.056	0.055	0.001	2.0	0.587	0.574	0.013	2.3
	MEAN	**0.075**	**0.069**	**0.006**	**9.2**	**0.057**	**0.054**	**0.004**	**7.3**	**0.611**	**0.579**	**0.033**	**5.7**
	SD	**0.009**	**0.007**	**0.007**	**10.7**	**0.007**	**0.007**	**0.005**	**8.6**	**0.035**	**0.032**	**0.023**	**4.1**

Table E.5: Estrogen blood concentration by radio-immunoassay after 1 week.

Mouse	Estrogen	[E2] pg/mL
A01	Sham	9.8
A04	Sham	14.2
B07	Sham	12.4
B08	Sham	14.7
C09	Sham	14.3
C10	Sham	12.8
D15	Sham	11.9
D16	Sham	16.8
E19	Sham	27.2
E20	Sham	11.3
	MEAN	**14.5**
	SD	**4.9**
A02	OVX	12.3
A03	OVX	13.8
B05	OVX	10.5
B06	OVX	11.3
C11	OVX	14.4
C12	OVX	16.9
D13	OVX	13.3
D14	OVX	8.9
E17	OVX	15.8
E18	OVX	65.8
	MEAN	**18.3**
	SD	**16.9**

2 weeks loading (e106)

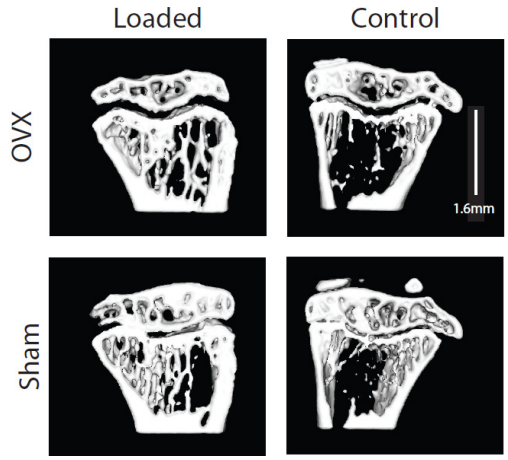

Figure E.3: Frontal sections (0.6 mm thick, extending 1.7 mm distal to the growth plate) through the proximal metaphysis from representative microCT scans. Representative loaded (left) and control (right) tibiae are shown from both ovariectomized (OVX) (top) and Sham-ovariectomy (Sham) (bottom) groups.

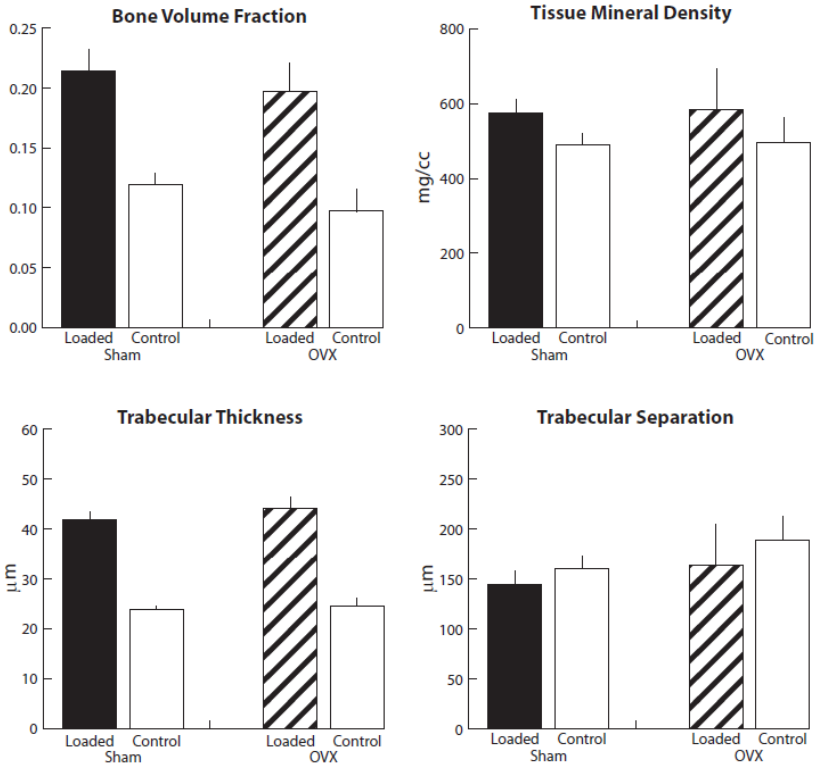

Figure E.4: Cancellous parameters of growing Sham-surgery (Sham) and ovariectomized (OVX) female mice after 2 weeks of loading, analyzed by microCT from a purely cancellous VOI in the proximal metaphysis.

Table E.6: Summary of cancellous indices determined by microCT analysis of VOIs from the proximal metaphysis of loaded and control tibiae from growing Sham-surgery (Sham) and ovariectomized (OVX) female mice after 2 weeks of loading.

Variable	Estrogen Status	Loaded (Left)	Control (Right)	Δ (Left - Right)	Difference (%)
BV/TV	Sham	0.21±0.02	0.12±0.01	0.09±0.02	80±14
	OVX	0.20±0.02	0.10±0.02	0.10±0.02	108±37
tBMD (mg/cc)	Sham	573±12	488±15	94±11	17±3
	OVX	585±24	497±19	88±23	18±5
Tb.Th (μm)	Sham	42±2	24±1	18±2	75±7
	OVX	44±2	24±2	20±3	82±18
Tb.Sp (μm)	Sham	144±14	161±12	-17±20	-10±11
	OVX	164±41	189±25	-25±35	-13±18

Table E.7: Indices of cancellous adaptation for each mouse, determined by microCT analysis of VOIs from the proximal metaphysis of loaded and control tibiae from growing Sham-surgery (Sham) and ovariectomized (OVX) female mice after 2 weeks of loading.

Mouse	Estrogen	tBMD (mg/cc)				BV/TV			
		L	R	L-R	%diff	L	R	L-R	%diff
A01	Sham	588.1	507.7	80.4	15.8	0.189	0.112	0.077	68.4
A02	Sham	579.4	500.6	78.8	15.7	0.223	0.133	0.090	67.8
A03	Sham	573.5	502.8	70.7	14.1	0.218	0.130	0.087	67.1
A04	Sham	582.0	505.7	76.3	15.1	0.198	0.116	0.082	70.5
D16	Sham	578.5	475.9	102.6	21.6	0.225	0.108	0.117	107.8
D17	Sham	546.5	472.6	73.9	15.6	0.228	0.119	0.109	91.7
D18	Sham	564.6	475.3	89.3	18.8	0.244	0.132	0.111	84.2
D19	Sham	578.9	478.6	100.2	20.9	0.194	0.109	0.085	78.6
D20	Sham	567.7	480.7	87.0	18.1	0.204	0.111	0.093	84.4
	MEAN	**573.3**	**488.9**	**84.4**	**17.3**	**0.214**	**0.119**	**0.095**	**80.1**
	STDEV	**12.3**	**14.8**	**11.3**	**2.7**	**0.018**	**0.010**	**0.014**	**13.6**
		L	R	L-R	%diff	L	R	L-R	%diff
B06	OVX	614.5	489.3	125.3	25.6	0.195	0.075	0.120	161.0
B07	OVX	612.4	520.0	92.4	17.8	0.206	0.075	0.131	174.2
B08	OVX	617.6	533.0	84.6	15.9	0.170	0.097	0.073	75.2
B09	OVX	577.8	503.0	74.8	14.9	0.239	0.107	0.132	123.3
B10	OVX	559.2	497.5	61.7	12.4	0.220	0.133	0.088	66.3
C11	OVX	555.4	492.7	62.7	12.7	0.186	0.106	0.080	74.8
C12	OVX	570.6	475.2	95.4	20.1	0.195	0.100	0.095	94.9
C15	OVX	562.9	494.0	68.9	13.9	0.156	0.078	0.078	99.5
C13	OVX	586.1	491.2	94.8	19.3	0.193	0.103	0.091	88.6
C14	OVX	592.9	470.7	122.2	26.0	0.206	0.092	0.113	122.7
	MEAN	**584.9**	**496.7**	**88.3**	**17.9**	**0.197**	**0.097**	**0.100**	**108.0**
	STDEV	**23.7**	**18.7**	**22.5**	**4.9**	**0.024**	**0.018**	**0.022**	**36.8**

Table E.7 Continued:

Mouse	Estrogen	Tb.Th. (μm)				Tb.Sp. (μm)			
		L	R	L-R	%diff	L	R	L-R	%diff
A01	Sham	42.5	24.1	18.4	76.1	146.7	166.7	-20.0	-12.0
A02	Sham	40.8	24.2	16.5	68.3	136.0	146.5	-10.5	-7.2
A03	Sham	39.3	23.6	15.6	66.2	151.8	150.4	1.3	0.9
A04	Sham	39.9	23.3	16.6	71.2	161.8	171.2	-9.3	-5.5
D16	Sham	44.6	24.3	20.3	83.7	128.8	180.7	-52.0	-28.8
D17	Sham	41.2	24.2	17.0	70.0	135.5	170.8	-35.3	-20.6
D18	Sham	41.7	24.5	17.3	70.6	122.4	152.9	-30.5	-20.0
D19	Sham	43.3	23.4	19.8	84.5	160.1	154.0	6.1	3.9
D20	Sham	42.4	22.9	19.4	84.9	154.1	152.8	1.3	0.9
	MEAN	**41.7**	**23.8**	**17.9**	**75.1**	**144.1**	**160.7**	**-16.5**	**-9.8**
	STDEV	**1.7**	**0.5**	**1.7**	**7.5**	**14.1**	**11.9**	**19.5**	**11.3**
		L	**R**	**L-R**	**%diff**	**L**	**R**	**L-R**	**%diff**
B06	OVX	44.1	21.7	22.3	102.8	164.4	207.6	-43.2	-20.8
B07	OVX	42.2	23.3	18.9	81.4	173.0	221.9	-48.9	-22.0
B08	OVX	43.8	25.3	18.5	73.2	253.7	195.2	58.5	30.0
B09	OVX	49.1	25.3	23.8	94.1	127.9	204.1	-76.3	-37.4
B10	OVX	40.7	26.6	14.1	53.1	127.4	155.3	-27.9	-18.0
C11	OVX	42.1	26.3	15.9	60.3	141.9	163.7	-21.8	-13.3
C12	OVX	44.3	24.7	19.6	79.6	143.0	173.4	-30.4	-17.5
C15	OVX	43.5	25.5	18.0	70.4	215.1	223.1	-8.0	-3.6
C13	OVX	46.5	23.2	23.3	100.2	151.8	168.0	-16.1	-9.6
C14	OVX	44.5	22.0	22.4	101.9	141.4	173.8	-32.4	-18.6
	MEAN	**44.1**	**24.4**	**19.7**	**81.7**	**164.0**	**188.6**	**-24.6**	**-13.1**
	STDEV	**2.4**	**1.7**	**3.3**	**17.7**	**40.8**	**24.8**	**34.9**	**17.5**

6 weeks loading (e137)

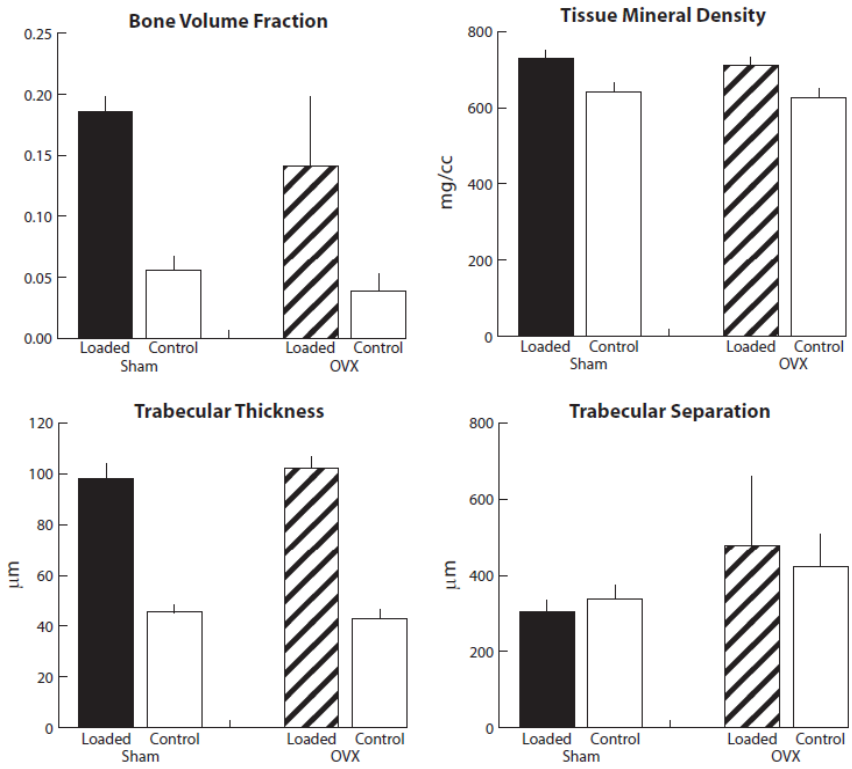

Figure E.5: Cancellous parameters of growing Sham-surgery (Sham) and ovariectomized (OVX) female mice after 6 weeks of loading, analyzed by microCT from a purely cancellous VOI in the proximal metaphysis.

Table E.8: Summary of cancellous indices determined by microCT analysis of VOIs from the proximal metaphysis of loaded and control tibiae from growing Sham-surgery (Sham) and ovariectomized (OVX) female mice after 6 weeks of loading

Variable	Estrogen Status	Loaded (Left)	Control (Right)	Δ (Left - Right)	Difference (%)
BV/TV	Sham	0.19±0.01	0.05±0.01	0.13±0.02	240±63
	OVX	0.14±0.06	0.04±0.01	0.10±0.05	277±162
tBMD (mg/cc)	Sham	728±24	642±22	86±29	13±4.7
	OVX	711±24	625±27	86±40	14±6.9
Tb.Th (µm)	Sham	98±5.7	45±2.9	53±5.7	116±16
	OVX	102±4.6	43±3.5	59±4.8	139±20
Tb.Sp (µm)	Sham	305±30	339±36	-34±38	-9.3±11
	OVX	476±183	424±84	53±165	13±40

Table E.9: Indices of cancellous adaptation for each mouse, determined by microCT analysis of VOIs from the proximal metaphysis of loaded and control tibiae from growing Sham-surgery (Sham) and ovariectomized (OVX) female mice after 6 weeks of loading.

Mouse	Estrogen	tBMD (mg/cc)				BV/TV			
		L	R	L-R	%diff	L	R	L-R	%diff
A01	Sham	699.3	632.6	66.7	10.5	0.180	0.045	0.134	296.7
A04	Sham	745.7	616.8	128.8	20.9	0.174	0.043	0.131	305.1
B05	Sham	746.9	643.0	103.9	16.2	0.196	0.067	0.129	192.2
B06	Sham	697.5	637.7	59.8	9.4	0.199	0.052	0.147	286.2
C09	Sham	758.7	660.1	98.5	14.9	0.168	0.057	0.111	194.9
C10	Sham	728.1	688.0	40.1	5.8	0.181	0.063	0.117	184.7
C11	Sham	754.9	644.0	111.0	17.2	0.180	0.077	0.104	134.9
D16	Sham	709.7	613.9	95.9	15.6	0.197	0.053	0.144	271.3
E20	Sham	712.2	646.3	66.0	10.2	0.202	0.052	0.150	291.7
	MEAN	**728.1**	**642.5**	**85.6**	**13.4**	**0.186**	**0.056**	**0.130**	**239.8**
	SD	**24.2**	**22.4**	**28.7**	**4.7**	**0.012**	**0.011**	**0.016**	**62.9**
		L	**R**	**L-R**	**%diff**	**L**	**R**	**L-R**	**%diff**
A03	OVX	676.9	598.6	78.3	13.1	0.136	0.022	0.114	522.4
B07	OVX	728.4	611.1	117.3	19.2	0.058	0.027	0.032	118.4
B08	OVX	712.2	661.0	51.2	7.7	0.195	0.036	0.160	445.5
D13	OVX	723.8	613.9	110.0	17.9	0.164	0.040	0.124	309.0
D14	OVX	736.7	594.8	141.8	23.8	0.204	0.066	0.137	207.6
D15	OVX	721.7	643.0	78.6	12.2	0.066	0.036	0.030	81.5
E17	OVX	679.9	653.8	26.1	4.0	0.164	0.046	0.118	255.5
	MEAN	**711.4**	**625.2**	**86.2**	**14.0**	**0.141**	**0.039**	**0.102**	**277.1**
	SD	**23.7**	**27.0**	**40.0**	**6.9**	**0.058**	**0.014**	**0.051**	**162.4**

Table E.9 Continued:

Mouse	Estrogen	Tb.Th. (μm)				Tb.Sp. (μm)			
		L	R	L-R	%diff	L	R	L-R	%diff
A01	Sham	100.7	43.2	57.5	133.1	353.6	337.2	16.4	4.9
A04	Sham	103.7	43.8	59.9	136.8	306.7	360.3	-53.6	-14.9
B05	Sham	97.6	46.9	50.7	108.1	275.8	321.6	-45.8	-14.2
B06	Sham	100.4	45.8	54.6	119.2	352.6	389.2	-36.6	-9.4
C09	Sham	103.0	49.7	53.3	107.2	274.4	371.3	-96.9	-26.1
C10	Sham	89.6	47.5	42.1	88.6	284.3	306.9	-22.6	-7.4
C11	Sham	100.9	48.6	52.3	107.6	293.9	305.5	-11.6	-3.8
D16	Sham	99.7	42.4	57.3	135.1	300.0	371.8	-71.8	-19.3
E20	Sham	87.8	41.5	46.3	111.6	306.4	288.2	18.2	6.3
	MEAN	**98.2**	**45.5**	**52.7**	**116.4**	**305.3**	**339.1**	**-33.8**	**-9.3**
	SD	**5.7**	**2.9**	**5.7**	**16.1**	**29.6**	**35.6**	**38.4**	**10.7**
		L	**R**	**L-R**	**%diff**	**L**	**R**	**L-R**	**%diff**
A03	OVX	98.6	36.0	62.6	173.9	414.7	446.5	-31.8	-7.1
B07	OVX	105.9	46.5	59.4	127.7	717.0	555.2	161.8	29.1
B08	OVX	104.8	43.3	61.5	142.0	343.1	485.4	-142.3	-29.3
D13	OVX	108.6	44.4	64.2	144.6	351.9	415.0	-63.1	-15.2
D14	OVX	101.9	41.2	60.7	147.3	273.8	291.2	-17.4	-6.0
D15	OVX	101.1	45.1	56.0	124.2	732.1	390.4	341.7	87.5
E17	OVX	94.9	44.9	50.0	111.4	501.0	381.4	119.6	31.4
	MEAN	**102.3**	**43.1**	**59.2**	**138.7**	**476.2**	**423.6**	**52.6**	**12.9**
	SD	**4.6**	**3.5**	**4.8**	**20.2**	**183.5**	**83.8**	**165.0**	**39.8**

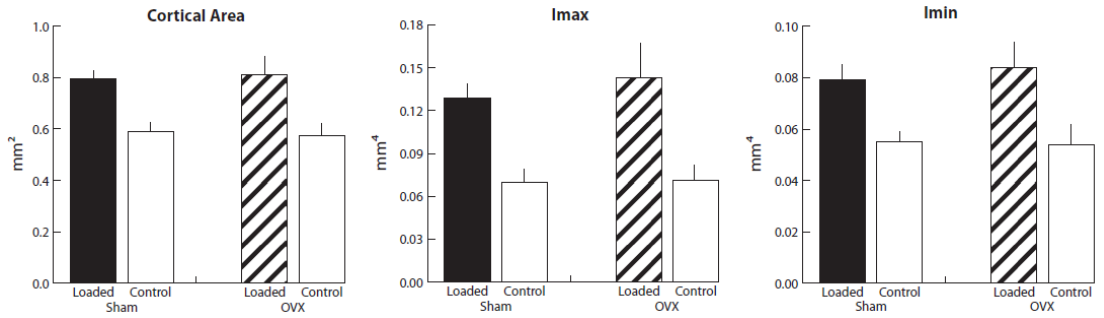

Figure E.6: Cortical parameters of growing Sham-surgery (Sham) and ovariectomized (OVX) female mice after 6 weeks of loading, analyzed by microCT from a cortical VOI centered at the tibial mid-diaphysis.

Table E.10: Summary of cortical indices determined by microCT analysis of VOIs centered at the mid-diaphysis of loaded and control tibiae from growing ovariectomy (OVX) and Sham-ovariectomy (Sham) female mice after 6 weeks of loading

Variable	Estrogen Status	Loaded (Left)	Control (Right)	Δ (Left - Right)	Difference (%)
I_{max} (mm^4)	Sham	0.129±0.01	0.070±0.01	0.058±0.01	85±23
	OVX	0.143±0.02	0.071±0.01	0.072±0.02	104±35
I_{min} (mm^4)	Sham	0.079±0.01	0.055±0.00	0.023±0.01	43±9.6
	OVX	0.084±0.1	0.054±0.1	0.029±0.01	55±14
Ct.Ar (mm^2)	Sham	0.796±0.03	0.590±0.04	0.206±0.03	35±6.3
	OVX	0.813±0.01	0.575±0.05	0.238±0.06	42±11

Table E.11: Indices of cortical adaptation determined by microCT analysis of VOIs centered at the mid-diaphysis of loaded and control tibiae from growing ovariectomy (OVX) and Sham-ovariectomy (Sham) female mice after 6 weeks of loading.

Mouse	Estrogen	I_{max} (mm^4)				I_{min} (mm^4)				Cortical Area (mm^2)			
		L	R	L-R	%diff	L	R	L-R	%diff	L	R	L-R	%diff
A01	Sham	0.122	0.066	0.056	84.4	0.072	0.055	0.017	30.9	0.777	0.571	0.206	36.1
A04	Sham	0.120	0.077	0.044	56.8	0.078	0.057	0.021	37.6	0.758	0.602	0.156	25.8
B05	Sham	0.130	0.083	0.047	56.0	0.082	0.053	0.028	53.1	0.807	0.604	0.203	33.7
B06	Sham	0.119	0.064	0.056	87.9	0.076	0.051	0.025	49.5	0.783	0.581	0.202	34.7
C09	Sham	0.127	0.068	0.058	85.5	0.078	0.060	0.018	30.6	0.794	0.608	0.186	30.7
C10	Sham	0.140	0.079	0.061	77.5	0.086	0.064	0.022	34.3	0.836	0.639	0.197	30.9
C11	Sham	0.143	0.079	0.064	80.8	0.089	0.057	0.032	56.4	0.849	0.628	0.220	35.0
D16	Sham	0.124	0.057	0.068	118.6	0.074	0.051	0.023	46.1	0.794	0.547	0.247	45.2
E20	Sham	0.134	0.061	0.073	120.6	0.076	0.052	0.023	44.3	0.769	0.531	0.238	44.7
	MEAN	**0.129**	**0.070**	**0.058**	**85.3**	**0.079**	**0.055**	**0.023**	**42.5**	**0.796**	**0.590**	**0.206**	**35.2**
	SD	**0.009**	**0.009**	**0.009**	**22.7**	**0.006**	**0.004**	**0.005**	**9.6**	**0.030**	**0.036**	**0.027**	**6.3**
		L	**R**	**L-R**	**%diff**	**L**	**R**	**L-R**	**%diff**	**L**	**R**	**L-R**	**%diff**
A03	OVX	0.150	0.059	0.091	154.7	0.078	0.050	0.027	54.0	0.811	0.519	0.292	56.2
B07	OVX	0.117	0.082	0.036	43.6	0.083	0.058	0.025	42.7	0.735	0.590	0.146	24.7
B08	OVX	0.153	0.067	0.086	128.8	0.085	0.049	0.036	72.7	0.864	0.562	0.302	53.7
D13	OVX	0.163	0.075	0.088	118.5	0.092	0.063	0.029	45.5	0.842	0.611	0.231	37.9
D14	OVX	0.163	0.081	0.082	102.2	0.084	0.061	0.023	37.8	0.865	0.632	0.233	36.9
D15	OVX	0.102	0.055	0.047	86.7	0.068	0.042	0.027	63.9	0.700	0.511	0.189	36.9
E17	OVX	0.152	0.078	0.075	95.9	0.099	0.059	0.040	68.5	0.875	0.600	0.275	45.9
	MEAN	**0.143**	**0.071**	**0.072**	**104.3**	**0.084**	**0.054**	**0.029**	**55.0**	**0.813**	**0.575**	**0.238**	**41.7**
	SD	**0.024**	**0.011**	**0.022**	**35.2**	**0.010**	**0.008**	**0.006**	**13.6**	**0.069**	**0.046**	**0.057**	**11.0**

Table E.12: Estrogen blood concentration by radio-immunoassay after 6 weeks.

Mouse	Estrogen	[E2]pg/mL
A01	Sham	23.1
A04	Sham	8.3
B05	Sham	17.8
C09	Sham	30.7
C10	Sham	23.9
C11	Sham	18.8
D16	Sham	14.8
E20	Sham	50.3
	MEAN	**23.5**
	SD	**12.7**

A03	OVX	12.7
B07	OVX	27.0
B08	OVX	14.2
D13	OVX	27.4
D14	OVX	22.4
D15	OVX	8.7
E17	OVX	13.8
	MEAN	**18.0**
	SD	**7.5**

APPENDIX F: *26 week old intact females*

1wk Loading (e134)

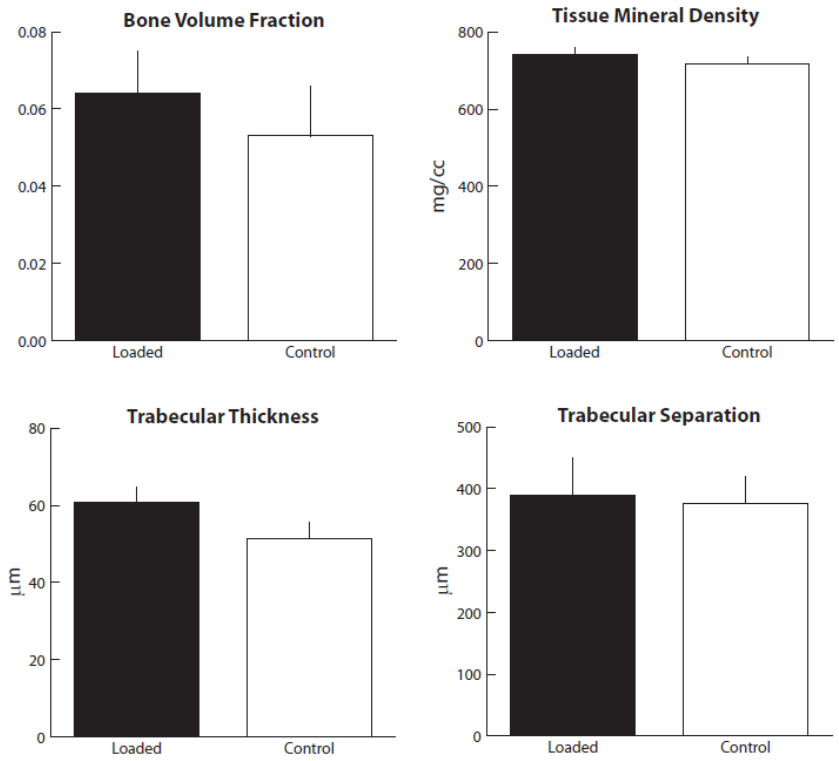

Figure F.1: Cancellous parameters of adult female mice after 1 week of loading, analyzed by microCT from a purely cancellous VOI in the proximal metaphysis.

Table F.1: Summary of cancellous indices determined by microCT analysis of VOIs from the proximal metaphysis of loaded and control tibiae from adult female mice after 1 week of loading.

Variable	Loaded (Left)	Control (Right)	Δ (Left - Right)	Difference (%)
BV/TV	0.06±0.01	0.05±0.01	0.01±0.02	28±39
tBMD (mg/cc)	741±20	718±17	23±20	3.2±2.9
Tb.Th (µm)	61±3.9	51±4.3	9.5±5.4	19±13
Tb.Sp (µm)	389±61	377±43	12±41	3.4±11

Table F.2: Indices of cancellous adaptation for each mouse, determined by microCT analysis of VOIs from the proximal metaphysis of loaded and control tibiae from adult female mice after 1 week of loading.

Mouse	tBMD (mg/cc)				BV/TV			
	L	R	L-R	%diff	L	R	L-R	%diff
A01	724.1	739.1	-15.0	-2.0	0.072	0.065	0.007	10.4
A02	725.9	729.5	-3.7	-0.5	0.064	0.058	0.006	10.5
A03	758.7	720.5	38.2	5.3	0.065	0.047	0.018	37.5
A04	752.4	718.4	34.0	4.7	0.067	0.056	0.011	19.9
B05	740.2	707.1	33.1	4.7	0.051	0.031	0.020	64.7
B06	753.8	738.3	15.5	2.1	0.067	0.079	-0.013	-15.9
B07	741.5	690.7	50.8	7.4	0.069	0.048	0.021	44.6
B08	762.1	715.4	46.7	6.5	0.070	0.060	0.010	17.1
C09	714.4	695.1	19.3	2.8	0.086	0.038	0.048	124.8
C10	743.9	733.8	10.1	1.4	0.061	0.043	0.018	41.3
C11	705.6	699.2	6.5	0.9	0.054	0.051	0.003	5.9
C12	766.6	730.8	35.8	4.9	0.045	0.057	-0.012	-20.4
MEAN	**740.8**	**718.2**	**22.6**	**3.2**	**0.064**	**0.053**	**0.011**	**28.4**
SD	**19.5**	**17.0**	**20.5**	**2.9**	**0.011**	**0.013**	**0.016**	**39.1**

Mouse	Tb.Th. (µm)				Tb.Sp. (µm)			
	L	R	L-R	%diff	L	R	L-R	%diff
A01	57.6	53.4	4.2	7.9	388.5	389.0	-0.5	-0.1
A02	55.3	53.1	2.2	4.1	396.0	321.1	74.9	23.3
A03	65.1	49.6	15.5	31.3	441.6	427.9	13.7	3.2
A04	61.0	50.3	10.7	21.3	354.1	367.8	-13.7	-3.7
B05	66.8	49.3	17.5	35.5	549.5	471.7	77.8	16.5
B06	65.0	54.3	10.7	19.7	336.5	336.9	-0.4	-0.1
B07	59.3	49.6	9.7	19.6	375.5	376.3	-0.8	-0.2
B08	56.1	51.7	4.4	8.5	404.3	337.3	67.0	19.9
C09	59.6	40.9	18.7	45.7	322.2	377.4	-55.2	-14.6
C10	59.0	53.2	5.8	10.9	334.2	352.4	-18.2	-5.2
C11	59.9	52.0	7.9	15.2	375.2	354.8	20.4	5.7
C12	65.6	59.1	6.5	11.0	390.4	406.1	-15.7	-3.9
MEAN	**60.9**	**51.4**	**9.5**	**19.2**	**389.0**	**376.6**	**12.4**	**3.4**
SD	**3.9**	**4.3**	**5.4**	**12.6**	**60.8**	**42.7**	**41.2**	**11.2**

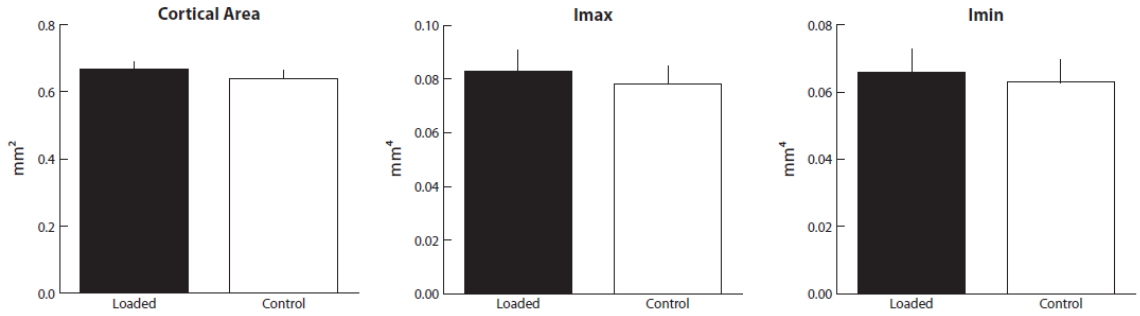

Figure F.2: Cortical parameters of adult female mice after 1 week of loading, analyzed by microCT from a cortical VOI centered at the tibial mid-diaphysis.

Table F.3: Summary of cortical indices determined by microCT analysis of VOIs centered at the mid-diaphysis of loaded and control tibiae from adult female mice after 1 week of loading.

Variable	Loaded (Left)	Control (Right)	Δ (Left - Right)	Difference (%)
I_{max} (mm^4)	0.083±0.01	0.078±0.01	0.005±0.01	6.5±6.7
I_{min} (mm^4)	0.066±0.01	0.063±0.01	0.003±0.01	5.0±9.1
Ct.Ar (mm^2)	0.669±0.02	0.639±0.03	0.030±0.02	4.8±3.3

Table F.4: Indices of cortical adaptation determined by microCT analysis of VOIs centered at the mid-diaphysis of loaded and control tibiae from adult female mice after 1 week of loading.

Mouse	I_{max} (mm^4)				I_{min} (mm^4)				Cortical Area (mm^2)			
	L	R	L-R	%diff	L	R	L-R	%diff	L	R	L-R	%diff
A01	0.096	0.094	0.002	1.8	0.079	0.075	0.004	5.8	0.702	0.678	0.025	3.7
A02	0.086	0.078	0.008	10.3	0.065	0.067	-0.003	-4.2	0.659	0.638	0.021	3.3
A03	0.072	0.074	-0.002	-2.6	0.065	0.058	0.007	11.1	0.668	0.629	0.039	6.3
A04	0.074	0.069	0.005	7.3	0.063	0.057	0.006	11.0	0.670	0.607	0.063	10.4
B05	0.092	0.080	0.012	14.6	0.073	0.067	0.007	9.9	0.696	0.637	0.059	9.3
B06	0.088	0.075	0.013	17.1	0.062	0.064	-0.002	-3.4	0.680	0.636	0.044	6.9
B07	0.073	0.070	0.003	4.7	0.056	0.058	-0.002	-2.9	0.640	0.624	0.016	2.5
B08	0.080	0.084	-0.004	-4.9	0.065	0.072	-0.008	-10.6	0.672	0.684	-0.011	-1.6
C09	0.093	0.087	0.006	6.7	0.074	0.065	0.009	13.6	0.697	0.678	0.019	2.8
C10	0.082	0.077	0.005	6.2	0.071	0.058	0.012	21.2	0.657	0.634	0.023	3.5
C11	0.078	0.076	0.002	2.8	0.061	0.060	0.001	1.3	0.652	0.627	0.026	4.1
C12	0.082	0.072	0.010	13.7	0.058	0.054	0.004	7.8	0.641	0.598	0.042	7.0
MEAN	**0.083**	**0.078**	**0.005**	**6.5**	**0.066**	**0.063**	**0.003**	**5.0**	**0.669**	**0.639**	**0.030**	**4.8**
SD	**0.008**	**0.007**	**0.005**	**6.7**	**0.007**	**0.007**	**0.006**	**9.1**	**0.021**	**0.027**	**0.020**	**3.3**

6 weeks loading (e125)

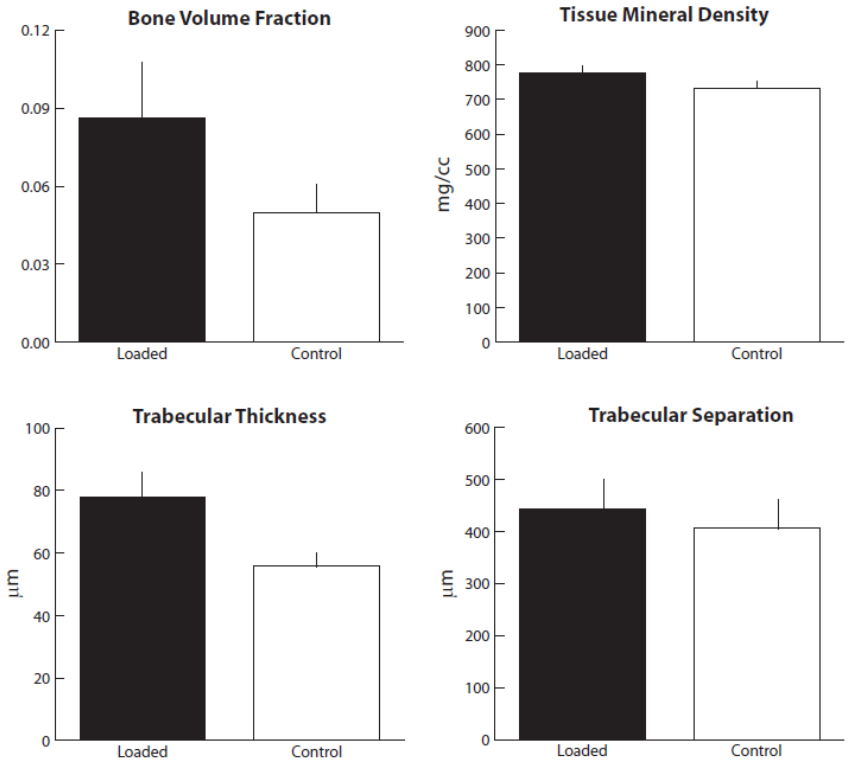

Figure F.3: Cancellous parameters of adult female mice after 6 weeks of loading, analyzed by microCT from a purely cancellous VOI in the proximal metaphysis

Table F.5: Summary of cancellous indices determined by microCT analysis of VOIs from the proximal metaphysis of loaded and control tibiae from adult female mice after 6 weeks of loading.

Variable	Loaded (Left)	Control (Right)	Δ (Left - Right)	Difference (%)
BV/TV	0.09±0.02	0.05±0.01	0.04±0.02	77±48
tBMD (mg/cc)	777±19	732±21	45±22	6.3±3.1
Tb.Th (µm)	78±7.8	56±4.6	22±6.9	40±13
Tb.Sp (µm)	443±59	406±56	37±88	11±21

Table F.6: Indices of cancellous adaptation for each mouse, determined by microCT analysis of VOIs from the proximal metaphysis of loaded and control tibiae from adult female mice after 6 weeks of loading.

Mouse	tBMD (mg/cc)				BV/TV			
	L	R	L-R	%diff	L	R	L-R	%diff
A01	791.6	714.8	76.7	10.7	0.092	0.033	0.059	179.0
A03	782.1	739.7	42.4	5.7	0.067	0.043	0.024	55.1
A04	789.6	751.9	37.7	5.0	0.061	0.054	0.007	12.6
A05	789.7	726.3	63.4	8.7	0.102	0.064	0.038	59.2
B06	738.3	731.0	7.2	1.0	0.098	0.051	0.047	92.5
B07	773.3	735.0	38.3	5.2	0.063	0.035	0.028	80.4
C11	772.7	721.8	50.9	7.0	0.066	0.041	0.025	60.2
C12	762.3	722.9	39.4	5.5	0.089	0.043	0.046	106.7
C14	790.2	714.1	76.1	10.7	0.071	0.061	0.010	17.0
D16	757.3	708.9	48.4	6.8	0.133	0.058	0.074	127.4
D17	802.3	783.9	18.4	2.3	0.101	0.065	0.036	55.2
MEAN	**777.2**	**731.8**	**45.4**	**6.3**	**0.086**	**0.050**	**0.036**	**76.8**
SD	**18.7**	**21.3**	**21.5**	**3.1**	**0.022**	**0.011**	**0.020**	**48.3**

Mouse	Tb.Th. (μm)				Tb.Sp. (μm)			
	L	R	L-R	%diff	L	R	L-R	%diff
A01	82.5	57.3	25.2	44.0	338.3	520.3	-182.0	-35.0
A03	78.3	51.9	26.4	50.9	420.3	360.0	60.3	16.8
A04	76.8	62.0	14.8	23.9	516.2	464.9	51.3	11.0
A05	81.2	54.4	26.8	49.3	473.5	329.9	143.6	43.5
B06	83.5	57.4	26.1	45.5	500.1	431.1	69.0	16.0
B07	81.8	50.9	30.9	60.7	520.4	385.4	135.0	35.0
C11	63.9	53.3	10.6	19.9	469.9	436.2	33.7	7.7
C12	74.0	50.5	23.5	46.5	406.5	386.9	19.6	5.1
C14	65.4	54.5	10.9	20.0	424.1	416.7	7.4	1.8
D16	79.8	55.7	24.1	43.3	370.3	390.1	-19.8	-5.1
D17	90.3	65.2	25.1	38.5	430.6	343.1	87.5	25.5
MEAN	**78.0**	**55.7**	**22.2**	**40.2**	**442.7**	**405.9**	**36.9**	**11.1**
SD	**7.8**	**4.6**	**6.9**	**13.4**	**59.0**	**55.8**	**88.1**	**21.0**

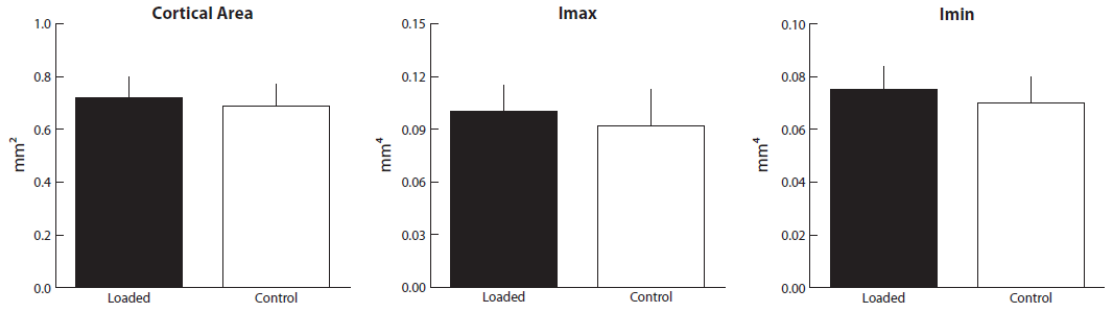

Figure F.4: Cortical parameters of adult female mice after 6 weeks of loading, analyzed by microCT from a cortical VOI centered at the tibial mid-diaphysis.

Table F.7: Summary of cortical indices determined by microCT analysis of VOIs centered at the mid-diaphysis of loaded and control tibiae from adult female mice after 6 weeks of loading.

Variable	Loaded (Left)	Control (Right)	Δ (Left - Right)	Difference (%)
I_{max} (mm^4)	0.100±0.02	0.092±0.02	0.009±0.03	16.8±36
I_{min} (mm^4)	0.075±0.01	0.070±0.01	0.005±0.02	10±25
Ct.Ar (mm^2)	0.721±0.08	0.689±0.16	0.032±0.16	7.1±22

Table F.8: Indices of cortical adaptation determined by microCT analysis of VOIs centered at the mid-diaphysis of loaded and control tibiae from adult female mice after 6 weeks of loading.

Mouse	I_{max} (mm^4)				I_{min} (mm^4)				Cortical Area (mm^2)			
	L	R	L-R	%diff	L	R	L-R	%diff	L	R	L-R	%diff
A01	0.120	0.089	0.031	34.3	0.085	0.069	0.016	22.4	0.819	0.650	0.168	25.9
A03	0.118	0.079	0.040	50.1	0.081	0.057	0.024	41.9	0.820	0.620	0.200	32.2
A04	0.103	0.075	0.029	38.2	0.080	0.062	0.018	29.6	0.751	0.620	0.131	21.2
A05	0.117	0.071	0.046	65.6	0.076	0.061	0.015	25.0	0.767	0.618	0.150	24.2
B06	0.094	0.076	0.018	23.2	0.076	0.063	0.013	20.8	0.713	0.635	0.078	12.2
B09	0.110	0.079	0.031	38.9	0.085	0.068	0.017	24.3	0.791	0.637	0.154	24.2
C11	0.084	0.106	-0.022	-21.2	0.067	0.082	-0.014	-17.4	0.631	0.727	-0.096	-13.2
C12	0.093	0.111	-0.018	-16.2	0.074	0.079	-0.005	-6.0	0.646	0.786	-0.140	-17.8
C14	0.105	0.076	0.030	39.2	0.082	0.065	0.017	26.1	0.751	0.634	0.117	18.4
D16	0.078	0.136	-0.059	-43.0	0.057	0.089	-0.032	-35.6	0.592	0.834	-0.242	-29.0
D17	0.084	0.111	-0.027	-24.5	0.062	0.079	-0.017	-21.4	0.652	0.815	-0.163	-20.0
MEAN	**0.100**	**0.092**	**0.009**	**16.8**	**0.075**	**0.070**	**0.005**	**10.0**	**0.721**	**0.689**	**0.032**	**7.1**
SD	**0.015**	**0.021**	**0.034**	**36.2**	**0.009**	**0.010**	**0.018**	**25.4**	**0.080**	**0.085**	**0.159**	**22.3**

APPENDIX G: *Micro-computed Tomography VOI Histograms*

10 week old intact females

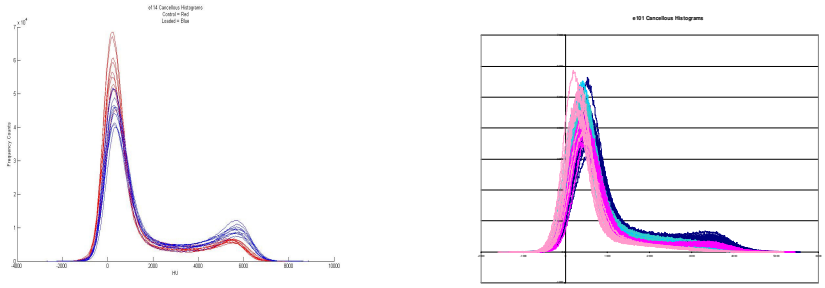

(a) (b)

Figure G.1: Histograms of all cancellous VOIs in the proximal metaphysis for growing mice after: (a) 1 week of loading (e114). All histograms are from female mice. Control limbs are in red, loaded limbs are in blue. (b) 2 weeks of loading (e101). Histograms from female mice are in pink, male mice are in blue.

10 week old OVX females

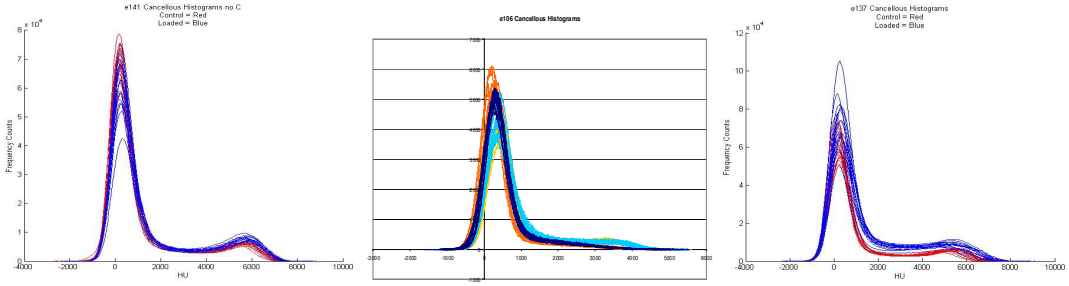

(a) (b) (c)

Figure G.2: Histograms of all cancellous VOIs in the proximal metaphysis for growing Sham and OVX female mice after: (a) 1 week of loading (e141). Control limbs are in red, loaded limbs are in blue. (b) 2 weeks of loading (e106). Histograms from Sham animals are in blue, OVX animals are in orange. (c) 6 weeks of loading (e137). Control limbs are in red, loaded limbs are in blue.

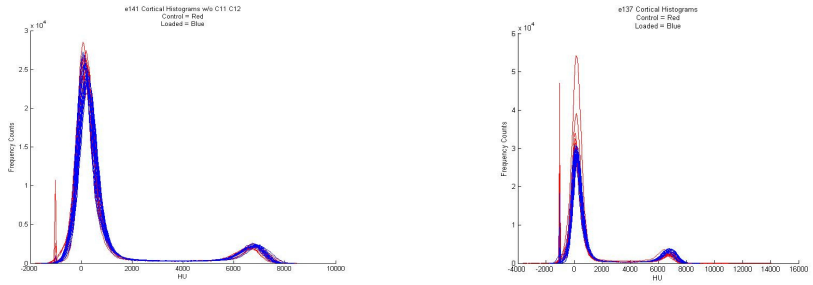

(a) (b)

Figure G.3: Histograms of all cortical VOIs centered at the tibial mid-diaphysis for growing Sham and OVX female mice after: (a) 1 week of loading (e141). (b) 6 weeks of loading (e137). Control limbs are in red, loaded limbs in blue, for all graphs.

26 week old intact females

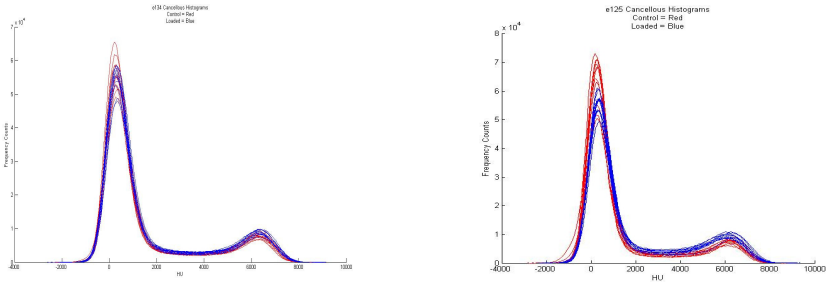

(a) (b)

Figure G.4: Histograms of all cancellous VOIs in the proximal metaphysis for adult female mice after: (a) 1 week of loading (e134). (b) 6 weeks of loading (e125). Control limbs are in red, loaded limbs in blue, for all graphs.

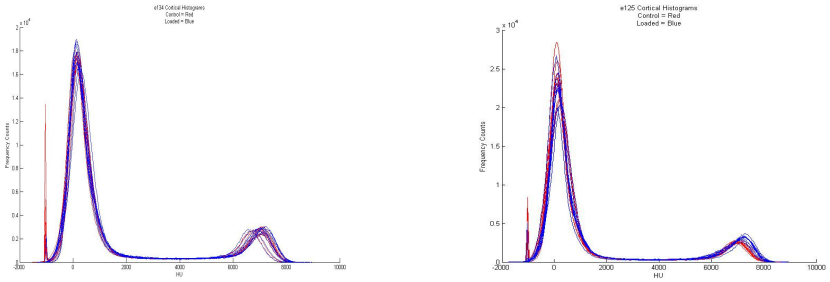

(a) (b)

Figure G.5: Histograms of all cortical VOIs centered at the tibial mid-diaphysis for adult female mice after: (a) 1 week of loading (e134). (b) 6 weeks of loading (e125). Control limbs are in red, loaded limbs in blue, for all graphs.

26 week old OVX females

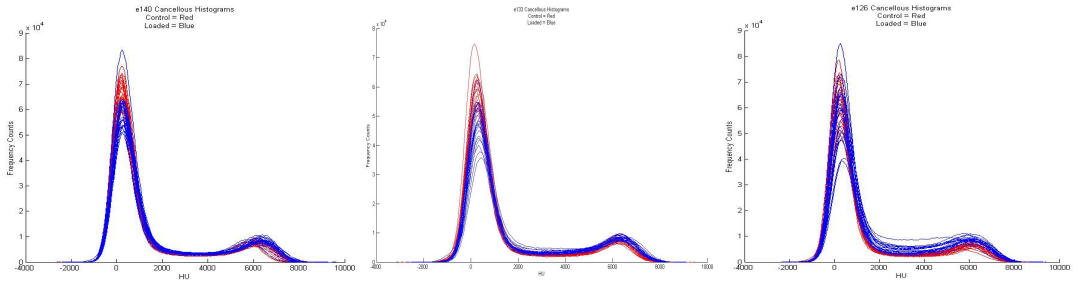

(a) (b) (c)

Figure G.6: Histograms of all cancellous VOIs in the proximal metaphysis for adult Sham and OVX female mice after: (a) 1 week of loading (e140). (b) 2 weeks of loading (e133). (c) 6 weeks of loading (e126). Control limbs are in red, loaded limbs in blue, for all graphs.

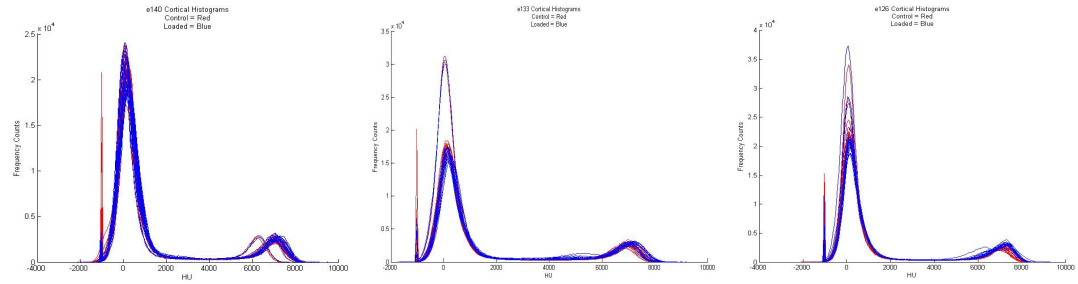

(a) (b) (c)

Figure G.7: Histograms of all cortical VOIs centered at the tibial mid-diaphysis for adult Sham and OVX female mice after: (a) 1 week of loading (e140). (b) 2 weeks of loading (e133). (c) 6 weeks of loading (e126). Control limbs are in red, loaded limbs in blue, for all graphs.